REPUBLIC OF TÜRKİYE

YILDIZ TECHNICAL UNIVERSITY

GRADUATE SCHOOL OF SCIENCE AND ENGINEERING

HYALURONIDASE-RESPONSIVE MSN–HA COATINGS FOR INFECTION-TRIGGERED ANTIBIOTIC DELIVERY ON TITANIUM SURFACES

Merve YOLUM

MASTER OF SCIENCE

Department of Biomedical Engineering

Program of Biomedical Engineering

Supervisor

Assoc. Prof. Dr. Sakip ÖNDER

June, 2026

REPUBLIC OF TÜRKİYE

YILDIZ TECHNICAL UNIVERSITY

GRADUATE SCHOOL OF SCIENCE AND ENGINEERING

HYALURONIDASE-RESPONSIVE MSN–HA COATINGS FOR INFECTION-TRIGGERED ANTIBIOTIC DELIVERY ON TITANIUM SURFACES

A thesis submitted by Merve YOLUM in partial fulfillment of the requirements for the degree of **MASTER OF SCIENCE** is approved by the committee on 12.06.2026 in Department of Biomedical Engineering, Program of Biomedical Engineering

Assoc. Prof. Dr. Sakip ÖNDER
Yildiz Technical University
Supervisor

Approved By the Examining Committee

Assoc. Prof. Dr. Sakip ÖNDER, Supervisor
Yildiz Technical University _____

Assist. Prof. Dr. Görke GÜREL PEKÖZER, Member
Yildiz Technical University _____

Assist. Prof. Dr. Abdulhalim KILIÇ, Member
İstanbul Technical University _____

I hereby declare that the study entitled “Development of Nanoparticle Based Functional Coating That Can Be Used for Local Drug Release and Determination Its Performance” that I prepared under the supervision of Assoc. Prof. Dr. Sakip ÖNDER was conducted in full compliance with the relevant legal requirements regarding data collection and data use; that all information obtained from other sources has been fully and properly acknowledged in the main text and references; that no fabrication and/or falsification has been made with respect to the research data or findings; and that throughout the study I have adhered to the principles of scientific research and academic ethics.

In the course of this thesis study, Generative Artificial Intelligence (GenAI) tools—specifically ChatGPT (OpenAI, GPT-5.4) were utilized under the author’s supervision for purposes such as enhancing linguistic clarity and coherence, supporting technical processes, and data visualization.

I declare that I am aware of the risk that GenAI tools may generate inaccurate or fabricated information (hallucinations), and that I have carefully reviewed and verified all outputs obtained from these tools in terms of accuracy, integrity, reliability, and compliance with ethical standards.

The use of GenAI tools has not, at any stage, replaced the author’s intellectual contribution, scientific judgment, or original idea generation. Full responsibility for the accuracy, currency, and scientific validity of all information, data, analyses, claims, and references presented in this thesis rests entirely with me.

I accept full administrative and legal responsibility for any consequences that may arise if this declaration is determined to be false.

Merve YOLUM

Signature

This work was supported by the the project no “FYL-2024-6341 of YTU Coordinatorship of Scientific Research Projects”

Dedicated to my family

and my best friends

ACKNOWLEDGEMENTS

First of all, I would like to sincerely thank my supervisor, Assoc. Prof. Dr. Sakip ÖNDER, for his continuous support, guidance, and encouragement throughout this thesis. His patience, understanding, and valuable feedback have meant a great deal to me during this process, and I am truly grateful for his contribution to this work.

I would like to offer my special thanks to Research Assistant Burcu DOYMUŞ for being by my side throughout all stages of my experiments. I am truly grateful for her support, encouragement, and for always being there for me.

I would like to acknowledge Assist. Prof. Dr. Abdulhalim KILIÇ and Yaşar YURTSEVER for granting access to the laboratory facilities at MOBGAM, ITU, and for their valuable technical assistance during the antibacterial activity experiments.

I would like to express my sincere gratitude to my lab mates, Berivan YURT and Fadi ELSHAKER ELKASSAR, as well as the other master's students, for their friendship and support, which made this process more enjoyable and meaningful. I also thank the interns who joined our lab, as guiding them was a valuable experience that contributed significantly to my personal and professional growth. I am especially grateful to my closest friends, Simge TORAMAN, Cansu GÖKÇE, and Ömer Mete BAŞKAN, for their constant support, understanding, and presence throughout this journey.

I gratefully acknowledge the financial support provided by YTU-BAP (Project No. FYL-2024-6341) and TÜBİTAK through the 2210/C Domestic Priority Areas Master's Scholarship Program.

I would like to sincerely thank my mother, Kezban YOLUM, my father, Ali YOLUM, and my sister, Buse YOLUM, for their endless love, support, and encouragement. Finally, I would like to thank myself for not giving up.

Merve YOLUM

TABLE OF CONTENTS

LIST OF SYMBOLS viii
LIST OF ABBREVIATIONS ix
LIST OF FIGURES x
LIST OF TABLES xii
ABSTRACT xiii
ÖZET xv
1 INTRODUCTION 1
1.1 Biomaterials 2
1.2 Metallic Biomaterials 5
1.3 Ti and Ti Alloys 6
1.4 Factors Affecting the Success of Metallic Biomaterials 6
1.4.1 Biocompatibility 7
1.4.2 Mechanical Properties 8
1.4.3 Corrosion Resistance and Wear Resistance 8
1.4.4 Osseointegration 8
1.5 Implant Associated Infection 9
1.5.1 Strategies to Prevent Implant Associated Infections 10
1.6 Drug Delivery Systems 11
1.7 Biomaterials for Drug Delivery Systems 12
1.7.1 Nanocarriers 13
1.7.2 Silica Nanoparticles 14
1.8 Mesoporous Silica Nanoparticles (MSNs) 14
1.8.1 Synthesis Methods for MSNs 16
1.8.2 Surface Modification of MSNs 18
1.9 Hyaluronic Acid (HA) 19
1.10 Drug Eluting Implant 20
1.10.1 Surface Coating Techniques 21
1.10.2 Electrophoretic Deposition (EPD) 23

2 MATERIALS AND METHODS **27**
2.1 Materials 27
2.2 Methods 28
2.2.1 Synthesis of MSNs 28
2.2.2 Synthesis of Amino-Modified MSNs (MSNs-NH_2) 28
2.2.3 Drug Loading and HA Coating 29
2.2.4 Characterization of MSNs 30
2.2.5 Coating of Ti Surfaces 31
2.2.6 Characterization of Coated Ti Plates 32
2.2.7 Drug Release Studies 33
2.2.8 Antibacterial Activity Test 34
2.2.9 Statistical Analysis 35
3 RESULTS AND DISCUSSIONS **36**
3.1 Characterization of MSNs 36
3.2 Characterization of Coated Ti Plates 41
3.3 Drug Loading and Drug Release Studies 46
3.4 Antibacterial Activity Test 53
4 CONCLUSION **57**
REFERENCES **59**
A PREPARATION OF BUFFER SOLUTIONS **76**
PUBLICATIONS FROM THE THESIS **77**

LIST OF SYMBOLS

cm	Centimeter
°C	Degree Celsius
H	Hour
µg	Microgram
µ	Microliter
µm	Micrometer
mg	Milligram
mL	Milliliter
mm	Millimeter
min	Minute
M	Molar
nm	Nanometer
%	Percent
p	Probability value
rpm	Revolutions per minute
U	Unit
V	Volt

LIST OF ABBREVIATIONS

ANOVA	Analysis of Variance
BET	Brunauer–Emmett–Teller
CFU	Colony-Forming Unit
CIP	Ciprofloxacin
DLE	Drug Loading Efficiency
EPD	Electrophoretic Deposition
FT-IR	Fourier Transform Infrared Spectroscopy
HA	Hyaluronic Acid
HAse	Hyaluronidase
MES	MES Hydrate
MSN	Mesoporous Silica Nanoparticle
MSN–CIP–HA	HA-coated and CIP-loaded MSN
MSN–NH_2	Amine-Functionalized Mesoporous Silica Nanoparticle
PBS	Phosphate-Buffered Saline
SD	Standard Deviation
SEM	Scanning Electron Microscopy
TEM	Transmission Electron Microscopy
Ti	Titanium
UV–Vis	Ultraviolet–Visible Spectroscopy

LIST OF FIGURES

Figure 1.1 A classification scheme for the functional requirements of biomaterials [28]. **5**

Figure 1.2 The foreign body reaction to an implanted material [38]. **7**

Figure 1.3 Schematic illustration of the implant bone osseointegration process [51]. **9**

Figure 1.4 Biofilm formation [56]. **10**

Figure 1.5 Conventional and controlled drug delivery systems [64]. **11**

Figure 1.6 List of representative biomaterials used in drug delivery systems [71]. **12**

Figure 1.7 Mechanism of controlled drug release via drug carrier [73]. **13**

Figure 1.8 Different classes of MSNs: hollow-type MSNPs (HMSNPs), organically modified silica (ORMOSIL), molecular sieves (M41S), Santa Barbara Amorphous (SBA), and periodic mesoporous organosilica (PMO) [82]. **15**

Figure 1.9 Representative M41S mesoporous silica materials, including Mobil Composition of Matter-41 (MCM-41), Mobil Composition of Matter-48 (MCM-48), and Mobil Composition of Matter-50 (MCM-50) [82]. **15**

Figure 1.10 MSN synthesis using sol-gel method [82]. **16**

Figure 1.11 Chemical structure of HA [103]. **19**

Figure 1.12 Illustration of a metallic implant-based drug delivery platform [106]. **20**

Figure 1.13 EPD process [134]. **24**

Figure 1.14 (a) Cathodic EPD and (b) anodic EPD [135]. **24**

Figure 2.1 Schematic illustration of MSN synthesis. **28**

Figure 2.2 Schematic illustration of amino modified MSNs (MSNs-NH_2) synthesis. **29**

Figure 2.3 Schematic illustration of (a) drug loading and (b) HA Coating. **30**

Figure 2.4 Schematic illustration of preparation of Ti plates. **31**

Figure 2.5 Schematic illustration of preparation of coating suspension. **31**

Figure 2.6 EPD Process. **32**

Figure 2.7 Schematic illustration of drug release studies. **.....33**

Figure 2.8 Schematic illustration of antibacterial activity test procedure. **.....34**

Figure 3.1 TEM images of a) MSN and b) MSN–CIP–HA. **.....36**

Figure 3.2 SEM images of a) MSN and b) MSN–CIP–HA, where arrows indicate block like structures formed due to nanoparticle agglomeration. **.....37**

Figure 3.3 FTIR spectra of MSNs and surface modified MSNs samples. **.....38**

Figure 3.4 Zeta potential analysis of MSNs. **.....39**

Figure 3.5 Size distribution of MSNs. **.....40**

Figure 3.6 SEM images of (a) bare Ti, (b) 30 V-3 min coated Ti (MSN:HA = 1:4), (c) 30 V-3 min coated Ti (MSN:HA = 1:0.5) and (d) 30 V- 5-min coated Ti (MSN:HA = 1:0.5), where arrows indicates block like structures formed due to nanoparticle agglomeration. **.....42**

Figure 3.7 Cross sectional SEM images of (a) 3-min-coated and (b) 5-min-coated Ti surfaces. **.....43**

Figure 3.8 Contact angle analysis of Ti plates. **.....44**

Figure 3.9 Contact angle analysis of (a) Ti-Bare, (b) Ti-MSN, and (c) Ti-MSN-HA surfaces. **.....45**

Figure 3.10 Three-dimensional optical profilometry images of (a) uncoated Ti and (b) coated Ti surfaces used for comparison of surface topography. **.....45**

Figure 3.11 Calibration curve of ciprofloxacin.HCl. **.....47**

Figure 3.12 Drug loading efficiency (%). **.....48**

Figure 3.13 Drug release profiles of free MSNs prepared with different MSN:HA ratios. The sample labels MSN-4XHA, MSN-0.5XHA, and MSN-0.25XHA correspond to MSN:HA ratios of 1:4, 1:0.5, and 1:0.25, respectively. The arrows in the drug release profiles indicate the time points of HAse addition. **.....49**

Figure 3.14 Comparison of enzyme responsive drug release from HA coated and uncoated free MSN nanoparticles. The arrows in the drug release profiles indicate the time points of HAse addition. **.....50**

Figure 3.15 Enzyme responsive drug release from 30 V 5 min coated Ti surfaces. The arrows in the drug release profiles indicate the time points of HAse addition. **.....52**

Figure 3.16 Antibacterial activity of various Ti surfaces: (a) Colonization of *E. coli* on various Ti surfaces; (b) Colonization of *S. aureus* on various Ti surfaces. **.....53**

Figure 3.17 Quantitative assessment of bacterial colony forming units (CFUs) for *E. coli* on various Ti surfaces (***$p < 0.005$). **.....54**

Figure 3.18 Quantitative assessment of bacterial colony forming units (CFUs) for *S. aureus* on various Ti surfaces (***$p < 0.005$). **.....55**

LIST OF TABLES

Table 1.1 Classification of biomaterials.....**3**
Table 3.1 Main BET parameters of MSN and MSN-HA.....**41**

ABSTRACT

Hyaluronidase-Responsive MSN–HA Coatings for Infection-Triggered Antibiotic Delivery on Titanium Surfaces

Merve YOLUM

Department of Biomedical Engineering

Master of Science Thesis

Supervisor: Assoc. Prof. Dr. Sakip ÖNDER

Infections related to implants continue to pose an important clinical challenge, primarily because biofilm development is difficult to control and conventional coating strategies may lead to poorly regulated antibiotic release. In the study, enzyme-responsive nanoparticle-based coating was developed to achieve localized and on demand antibiotic delivery from titanium implant surfaces Hyaluronidase-responsive ciprofloxacin-loaded mesoporous silica nanoparticles coated with hyaluronic acid (MSN–CIP–HA) were prepared and subsequently deposited onto titanium substrates by electrophoretic deposition. The morphology and surface characteristics of prepared nanoparticles and coated surfaces were systematically analyzed. Drug release profiles were assessed at physiological pH (7.4) and infection-relevant acidic pH (5.0), in media containing or lacking hyaluronidase. After 72 h, ciprofloxacin release from the coated titanium surface was 0.51 µg at pH 7.4 in the absence of the enzyme, whereas it increased to 2.63 µg in the presence of hyaluronidase. Likewise, under acidic conditions (pH 5), drug release increased from 0.93 µg to 3.31 µg following enzyme exposure, confirming the effective enzyme-triggered degradation of the HA coating layer. Assays conducted with *Escherichia coli* and *Staphylococcus aureus* showed that bacterial colonization was lower on the modified titanium surfaces, whereas antibacterial efficacy increased

following hyaluronidase-mediated ciprofloxacin release. Collectively, these findings indicate that the developed coating combines anti-adhesive surface characteristics with controlled, infection triggered antibiotic release, thereby minimizing unnecessary drug exposure while improving localized antibacterial efficacy. Thus, HA coated MSN coatings represent a promising smart surface modification strategy to prevent implant associated infections and biofilm formation.

Keywords: Orthopedic implant infection, titanium (Ti), mesoporous silica nanoparticle (MSN), hyaluronic acid (HA), hyaluronidase (HAse)

ÖZET

Titanyum Yüzeylerde Enfeksiyonla Tetiklenen Antibiyotik Salımı İçin Hiyalüronidaza Duyarlı MSN–HA Kaplamaları

Merve YOLUM

Biyomedikal Mühendisliği Anabilim Dalı

Yüksek Lisans Tezi

Danışman: Doç. Dr. Sakip ÖNDER

İmplant ilişkili enfeksiyonlar, biyofilm oluşumu ve geleneksel kaplama sistemlerinde gözlenen kontrolsüz antibiyotik salımı nedeniyle önemli bir klinik problem olmaya devam etmektedir. Bu çalışmada, titanyum implant yüzeylerinde lokalize ve enfeksiyona yanıt veren antibiyotik salımı sağlamak amacıyla enzim duyarlı nanopartikül temelli bir kaplama sistemi geliştirilmiştir. Bu kapsamda, hiyalüronik asit ile kaplanmış, hiyalüronidaza duyarlı siprofloksasin yüklü mezogözenekli silika nanopartikülleri (MSN–CIP–HA) başarıyla sentezlenmiş ve elektroforetik biriktirme yöntemiyle titanyum yüzeylerine uygulanmıştır. Elde edilen nanopartiküller ile kaplanmış yüzeyler morfolojik özellikleri, yüzey karakteristikleri ve ıslanabilirlik davranışları açısından ayrıntılı olarak karakterize edilmiştir. İlaç salım profili, fizyolojik koşulları temsil eden pH 7.4 ortamında ve enfeksiyon bölgesini taklit eden asidik pH 5 koşullarında, hiyalüronidaz varlığında ve yokluğunda incelenmiştir. 72 saatin sonunda, kaplanmış titanyum yüzeylerden salınan siprofloksasin miktarı pH 7.4'te enzim yokluğunda 0.51 µg olarak belirlenirken, hiyalüronidaz varlığında bu değer 2.63 µg'a yükselmiştir. Benzer şekilde, pH 5 koşullarında 0.93 µg olarak ölçülen salım miktarı, enzim ilavesi sonrasında 3.31 µg'a ulaşmıştır. Bu artış, HA kaplama tabakasının enzim etkisiyle

bozunarak ilaç salımını tetiklediğini açıkça ortaya koymuştur. *Escherichia coli* ve *Staphylococcus aureus* üzerinde gerçekleştirilen antibakteriyel değerlendirmeler, kaplanmış yüzeylerde bakteri tutunmasının azaldığını ve enzim varlığında antibakteriyel etkinliğin belirgin biçimde arttığını göstermiştir. Elde edilen bulgular, geliştirilen kaplama sisteminin bakteri tutunmasını sınırlandıran yüzey özelliklerini, kontrollü ve enfeksiyonla tetiklenen antibiyotik salımı ile bir araya getirdiğini göstermektedir. Bu sayede gereksiz antibiyotik maruziyetinin önüne geçilirken, enfeksiyon bölgesinde lokal antibakteriyel etkinliğin artırılması mümkün olmuştur. Sonuç olarak, HA ile kaplanmış MSN esaslı bu kaplama sistemi, implant ilişkili enfeksiyonların ve biyofilm oluşumunun önlenmesine yönelik akıllı yüzey modifikasyonları arasında umut vadeden bir yaklaşım sunmaktadır.

Anahtar Kelimeler: Ortopedik implant enfeksiyonu, titanyum (Ti), mezogözenekli silika nanopartikül (MSN), hiyalüronik asit (HA), hiyalüronidaz (HAse)

1
INTRODUCTION

Titanium (Ti) based materials are commonly preferred in orthopedic implant design due to their compatibility with living tissues, stability against corrosion, and bone-like mechanical performance. However, these advantages do not eliminate the risk of microbial colonization, since bacteria can readily attach to titanium surfaces and develop biofilm structures. Thus, achieving reliable clinical outcomes is still challenged by microbial problems that arise around implant sites [1], [2]. To address this issue, smart coating systems capable of localized and controlled drug release from implant surfaces have been developed. Recently, smart delivery systems designed to respond to changes in their surroundings, including acidity, enzymatic activity, or temperature variations, have become an important research focus [3], [4], [5]. Previous studies have explored polymer-based coatings on Ti, including chitosan, poly(lactic acid), and poly-L-lysine, as reservoirs for the regulated delivery of antibacterial compounds. These approaches generally improve the antibacterial response without causing a marked loss in cellular compatibility [6], [7], [8], [9]. Nevertheless, many existing coatings still suffer from critical limitations, including burst release, non-specific drug release, subtherapeutic antibiotic concentrations, and the associated risk of resistance development. In particular, systems capable of on-demand antibiotic release triggered by the actual presence of infection remain relatively limited [10], [11], [12]. Accordingly, mesoporous silica nanoparticles (MSNs) represent a useful nanocarrier system for antibiotic delivery, since their adjustable pore network and large surface area support efficient drug loading. In addition, surface modification with hyaluronic acid (HA) provides an effective strategy for enzyme-responsive drug release, as HA can be selectively degraded by hyaluronidase (HAse) present

in the infection microenvironment [13], [14], [15]. Furthermore, electrophoretic deposition (EPD) provides an effective route for producing these functional surface layers, since the composition and thickness of the coating can be regulated by adjusting deposition parameters [16].

Considering the limitations of existing studies and the remaining research needs, this thesis focuses on the development of a nanoparticle based, enzyme responsive Ti coating system for managing implant associated infections. In this system, ciprofloxacin was incorporated into MSNs, taking advantage of their porous framework and large surface area for efficient drug loading. The MSNs were then coated with HA to provide sensitivity to HAse in the infection microenvironment. The resulting functional nanoparticles were then deposited onto Ti surfaces using the EPD method. The main hypothesis of this study is that the proposed smart coating system can effectively suppress implant-associated infections through targeted drug delivery. Specifically, the HA layer is expected to act as a protective barrier that prevents premature antibiotic release under normal conditions. At the early stage of infection, HAse induced breakdown of the HA coating is expected to activate localized ciprofloxacin release. This responsive release behavior is designed to restrict antibiotic delivery to the infection site, reducing unnecessary high dose exposure and lowering the likelihood of systemic toxicity and resistance development. Consequently, this coating is expected to exhibit strong antibacterial activity around the implant and significantly reduce infection-related complications in orthopedic applications.

1.1 Biomaterials

Biomaterials include natural and synthetic materials developed for use in contact with living systems. Their functions may involve supporting diagnosis, promoting tissue repair, improving biological performance, or replacing damaged tissues and organs [17], [18]. Biomaterials contribute to healthcare by enabling diagnostic, therapeutic, and regenerative applications. Their medical use extends to devices placed in the body, structures developed to replace lost function, materials used in dental repair, and porous matrices designed to support new tissue formation [19], [20]. Over the years, biomaterials research has undergone substantial development,

from the use of relatively inert materials for simple replacement purposes to the development of more advanced systems designed to actively interact with biological environments [21]. Today, biomaterials are used not only for tissue replacement and restoration of function, but also across regenerative approaches and drug delivery systems with controlled release capability [22], [23]. Owing to the broad range of clinical needs they are intended to address biomaterials encompass a range of material types with diverse structural attributes and functional behaviors [23], [24]. Differences in crystallinity, composition, macroscopic structure, and bonding behavior allow biomaterials to be commonly categorized into four principal groups: metallic, polymeric, ceramic, and composite materials [23], [25]. Such classification provides a useful basis for understanding the general characteristics and biomedical applications of different biomaterial classes. Within this classification, Table 1.1 provides an overview of major biomaterial groups, representative materials, and commonly associated biomedical uses.

Table 1.1 Classification of biomaterials

Biomaterial Class	**Typical Biomedical Applications**	**References**
Metals (Stainless steel, cobalt chromium alloys, and Ti based alloys)	Orthopedic implants, dental implants, fracture plates, vascular stents	[22], [24]
Ceramics (hydroxyapatite, calcium phosphate, bioactive glass, alumina, zirconia)	Bone grafts, implant coatings, dental restorations, joint prostheses	[22], [24]

Table 1.2 Classification of biomaterials (continued)

Biomaterial Class	Typical Biomedical Applications	References
Polymers (Natural polymers: collagen, gelatin, chitosan, alginate, hyaluronic acid; Synthetic polymers: polyethylene, polypropylene, PMMA, PET, polyurethane, PLA/PLGA)	Sutures, catheters, vascular grafts, bone cement, wound dressings, tissue engineering scaffolds, contact lenses, drug delivery systems, and resorbable implants	[22], [26]
Composites (hydroxyapatite/alumina, alumina/zirconia, zirconia-based composites)	Dental and orthopedic implant applications, bone regeneration, and tissue engineering	[23], [24]

Biomaterials selected or designed for medical applications must be evaluated to determine whether they possess the appropriate properties for their intended use. For this reason, the biological performance of a material, such as its biocompatibility, degradation behavior, and toxicity profile, should be considered alongside its chemical structure, physical features, and mechanical behavior; in long term use, it must be ensured that the material can maintain its function without causing an immune response, while eliciting an appropriate host response [18], [27]. Figure 1.1 summarizes a classification scheme that can address both traditional and emerging biomaterial functions and helps guide the selection and

design of suitable biomaterial candidates in line with the required functional performance.

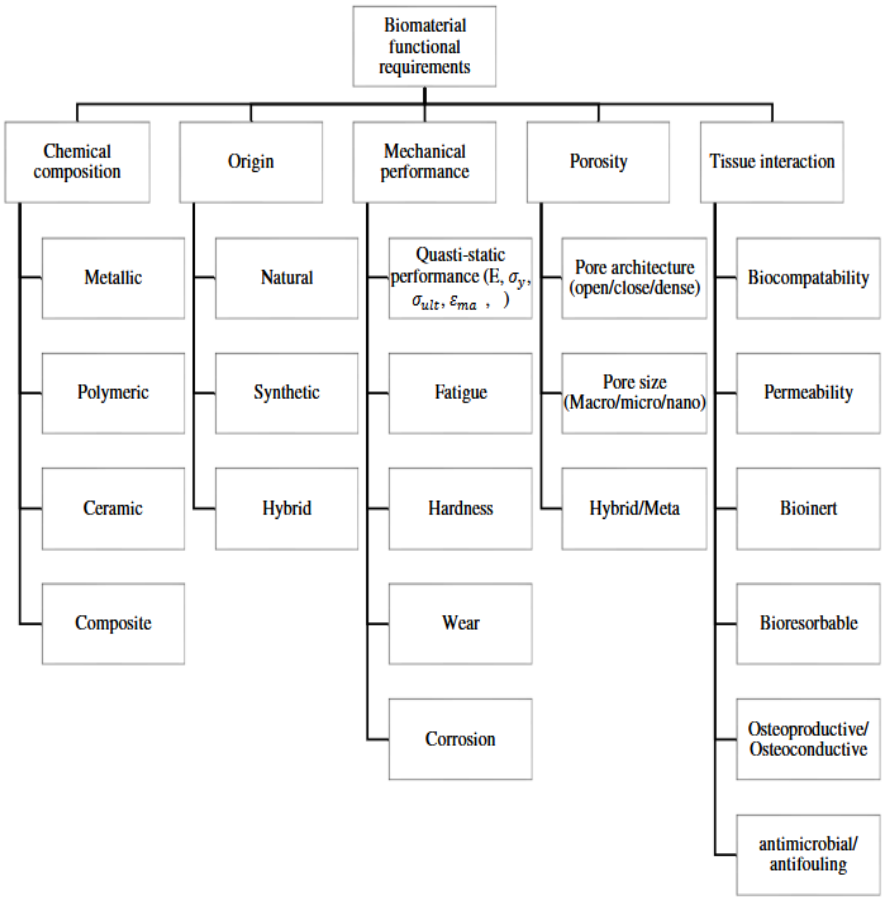


Figure 1.1 A classification scheme for the functional requirements of biomaterials [28].

1.2 Metallic Biomaterials

Metals are, by definition, materials are maintained by metallic bonds. Owing to the abundance of free electrons within these bonds, they exhibit high thermal and electrical conductivity [25]. Metallic biomaterials are valued for their superior strength, hardness, and toughness, which have supported their use over a long historical period. In biomedical applications, they are commonly grouped according to the dominant alloying element as stainless steels, Ti based alloys, cobalt based alloys, and magnesium alloys [25]. In implant manufacturing, these alloy groups are typically formulated with elements such as titanium, chromium, iron, cobalt, molybdenum, nickel, niobium, tantalum, and tungsten [29]. In biomedical

applications, metals and their alloys serve as load bearing biomaterials that support the structural integrity of biological tissues and therefore play a particularly important role in orthopedics [30], [31]. Their most common applications include prostheses, implants, orthopedic fixation devices, and stents [30].

1.3 Ti and Ti Alloys

Ti is notable for its biocompatibility, bioinertness, low density, high strength, excellent corrosion resistance, and favorable mechanical properties [19]. Pure Ti and Ti 6Al 4V are frequently selected for biomedical use due to their suitability as metallic biomaterials [32]. The broader biomedical use of Ti alloys compared with stainless steels and cobalt based alloys is mainly associated with their excellent biocompatibility, lower elastic modulus, and enhanced corrosion behavior, while alloying is also believed that the alloying process helps to increase the mechanical strength of Ti [30], [31]. Furthermore, their elastic modulus shows greater compatibility with bone tissue than the considerably higher modulus values of stainless steels and cobalt based alloys. which makes them widely preferred for dental and orthopedic implant applications [33]. Ti ensures both outstanding biocompatibility and protection against corrosion by forming a highly stable passive layer of Ti dioxide on its surface [34]. Furthermore, through the high dielectric constant of the Ti dioxide layer, as a result, cells can integrate more effectively with the implant surface, leading to a stronger tissue implant interface for Ti based materials than for stainless steel [30]. Despite these favorable characteristics, Ti based materials still exhibit relatively low wear resistance and shear strength [35].

1.4 Factors Affecting the Success of Metallic Biomaterials

The essential necessities that ought to be found in metallic biomaterials are biocompatibility, osseointegration capacity, mechanical compatibility with the target tissue and sufficient stability against corrosion and wear [31]. These fundamental properties are vital for ensuring that implants provide safe, stable, and long-term performance in a physiological environment. Metallic biomaterials in the human body are constantly exposed to mechanical stress, chemical interactions with bodily fluids, and complex biological responses. Therefore, they must maintain

their structural integrity while preventing adverse tissue reactions. Consequently, optimizing these fundamental properties plays a critical role in enhancing implant reliability, minimizing complications, and ultimately improving clinical outcomes.

1.4.1 Biocompatibility

An ideal biomaterial is expected to interact with living systems in a safe and controlled manner, without harming adjacent tissues. Accordingly, material is considered biocompatible when it can carry out its intended purpose in the body without provoking inflammatory or undesirable immune responses [19], [36]. The biocompatibility of a material is largely determined by how the surrounding biological environment reacts to it and how the material changes or breaks down after implantation [37].

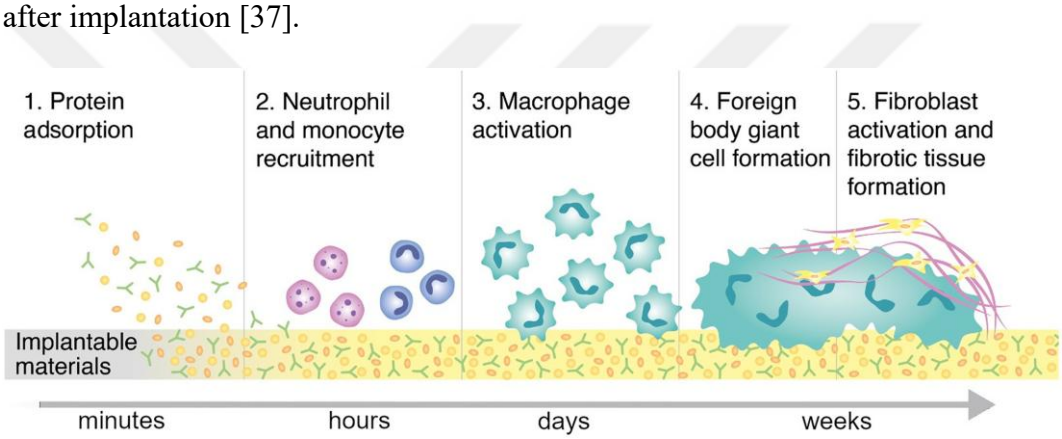


Figure 1.2 The foreign body reaction to an implanted material [38].

Upon exposure to human tissues and body fluids, metallic implants interact with the host environment, and the outcome of these interactions determines whether the material is accepted as biocompatible or induces an adverse biological response including foreign body reaction (Figure 1.2) [38], [39]. In metallic biomaterials, biological tolerance is associated with the ability of the surface oxide film to remain intact during exposure to physiological media, which serves to restrict metal ion release and minimize direct interactions with the surrounding biological environment thereby improves the chemical and mechanical properties of the substrate [40] . Furthermore, alloy composition and surface characteristics can also affect the biological response by modulating the overall compatibility of the implant with the host tissue [39].

1.4.2 Mechanical Properties

In biomedical applications, material selection depends on the specific intended use. For instance, surface properties particularly, chemical composition is critical for minimizing thrombogenicity in vascular implants, whereas in bone-related applications, biomaterials with adequate mechanical properties are of main concern [41]. In metallic implants intended for load-bearing orthopedic and dental applications, mechanical properties are a critical issue in material selection. These implants must provide mechanical reliability while minimizing stress concentration and should help maintain healthy bone adaptation at the implant interface. In addition, it should tolerate mechanical loading through sufficient strength, fracture resistance, fatigue endurance, and bone matched elastic behavior [42], [43], [44].

1.4.3 Corrosion Resistance and Wear Resistance

Although metals can tolerate substantial loading without easily deforming or fracturing, they may deteriorate through chemical reactions and electrochemical processes [45]. Implant materials can be subject to corrosion and wear. Corrosion is the destruction of metal through electrochemical reactions, whereas wear develops as repeated surface contact and sliding gradually cause small portions of the material to separate from the surface [45], [46]. Wear damages the oxide layer on implants, once this protective barrier is impaired, corrosion processes may progress more easily on the exposed metal surface. Furthermore, the resulting wear debris can trigger immune responses, leading to implant loosening and ultimately failure [47], [48], [49]. Accordingly, long lasting implant performance in the body requires surface designs that can reduce material degradation caused by corrosion and repeated mechanical contact.

1.4.4 Osseointegration

In osseointegration, the implant becomes firmly anchored as bone tissue forms in direct contact with its surface, rather than being separated from the surrounding bone by fibrous tissue [50]. However, bone attachment to an implant does not occur through a single step; rather, it results from a sequence of biological responses that may vary depending on the surface architecture, as illustrated in Figure 1.3 [51].

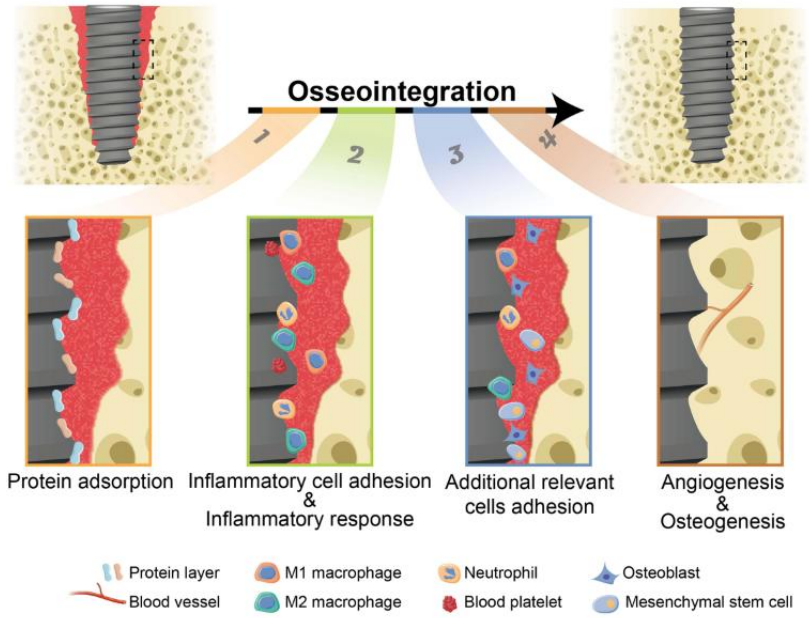


Figure 1.3 Schematic illustration of the implant bone osseointegration process [51].

Accordingly, successful osseointegration is closely associated with the chemical nature of the implant surface, its level of roughness, and the geometric features present on that surface [39]. In contrast, a weak bone implant connection can allow minor interfacial movements. If these small movements continue, soft fibrous tissue can form at the implant region, gradually weakening the prosthesis anchorage [52]. Therefore, appropriate surface properties are essential for achieving successful osseointegration with the surrounding bone.

1.5 Implant Associated Infection

The colonization of medical implants by bacteria can lead to infections in nearby tissues, potentially causing severe complications for patients [53]. These infections stand out from traditional surgical site infections because they can develop with a low bacterial load, stem from a wide variety of pathogens, exhibit resistance to antimicrobial therapy, and create an immunosuppressive environment due to foreign body reactions against the implant [54]. The increasing use of biomaterials and the extension of life expectancy are making this issue even more critical. The two main challenges, particularly regarding permanent implants, are the risk of infection and the inability to achieve sufficient integration with natural tissue.

Gristina (1987) defined this phenomenon as a "surface race," suggesting that tissue cells and bacteria compete for initial attachment and dominance on the implant surface. This competition is expected to result in favor of tissue cells due to the implant's successful integration with the host tissue and a robust host defense [55]. Nevertheless, infections often develop when microorganisms reach the implant site during surgery or before the wound has closed. These microorganisms may attach to the implant surface and develop into organized biofilm communities. Alternatively, they can avoid immune clearance and persist in a low activity state for long periods [53].

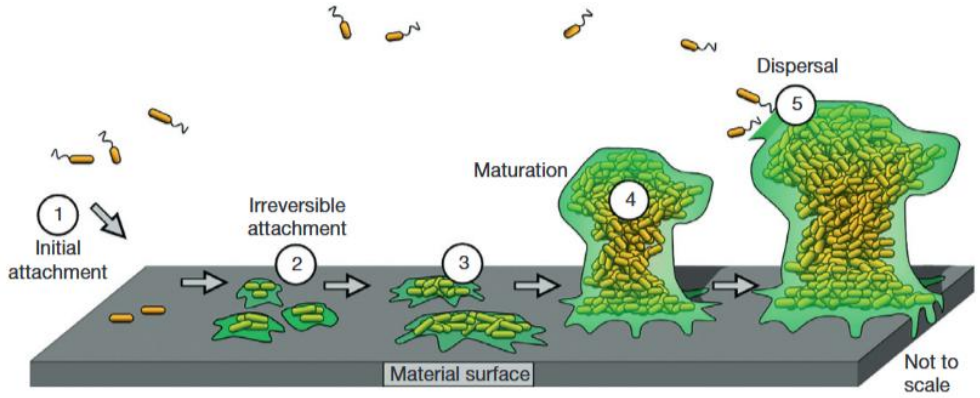


Figure 1.4 Biofilm formation [56].

A biofilm enables bacteria to survive by sheltering within an extracellular polymeric matrix they produce, which leads to the progression of infection and damage to surrounding tissues (Figure 1.4) [57]. In addition, the biofilm matrix can shield bacterial cells, making antibiotic therapy less successful, antibiotic treatment is often insufficient, and surgical removal of the implant may be necessary. It prolongs the healing process, negatively impacts patient health, and increases treatment costs [56].

1.5.1 Strategies to Prevent Implant Associated Infections

Considering the potential consequences of implant-related infections, preventing infection is the most sensible approach rather than treating it after it has developed [58]. Prevention methods usually include systemic antibiotic administration and the use of local antimicrobial agents during the perioperative period [59]. To reduce infection related complications after implantation, systemic antibiotics are

frequently administered, particularly in the early phase. Nevertheless, clear and consistent guidelines for their application have not been established. Furthermore, side effects and increasing antibiotic resistance pose significant challenges [60]. Alternatively, local protection can be achieved by designing the implant surface in a way that makes bacterial attachment less favorable [58]. Antibacterial coating of implants reduces systemic antibiotic accumulation by providing local and controlled drug release, offers long-term antimicrobial effects, and helps prevent implant associated infections by inhibiting bacterial colonization. Additionally, when properly designed, they can also reduce the risk of antibiotic resistance developing [59], [61].

1.6 Drug Delivery Systems

Through controlled administration and distribution of therapeutic agents, these systems support safer drug transport in the body and help achieve the intended clinical response [62]. As illustrated in Figure 1.5, therapeutic agents may reach the target site either through localized administration or by distribution through systemic pathways [63].

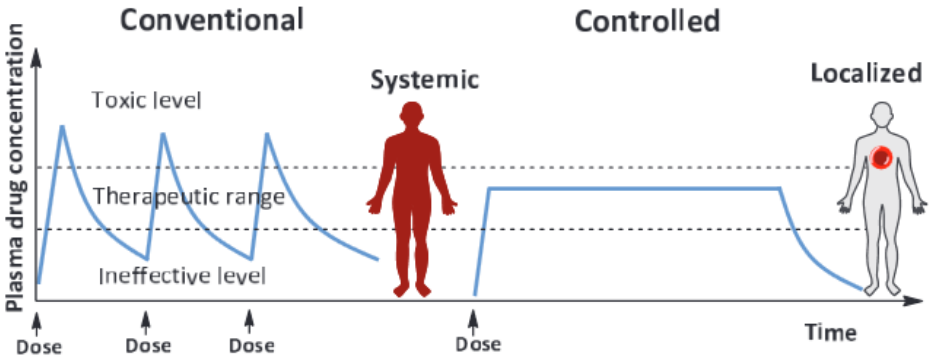


Figure 1.5 Conventional and controlled drug delivery systems [64].

With traditional dosing approaches, plasma drug concentration rises after each dose and gradually decreases until the next dose; therefore, maintaining effective and safe drug levels within the therapeutic range depends largely on the patient's adherence to treatment [64]. Alternatively, in controlled release strategies, drug liberation is not random; instead, it follows a predefined pattern that can be adjusted in terms of release speed, timing, or overall delivery profile [65]. In this approach, the administered dose is not made available immediately; instead, it is delivered in

small amounts over time to help keep plasma concentrations within the desired therapeutic window [64]. Beyond regulating release, these systems may improve therapy by keeping the drug effect concentrated where it is needed, slowing the loss of agents that are quickly cleared, limiting the number of additional clinical visits, and making treatment easier for the patient to follow [66].

1.7 Biomaterials for Drug Delivery Systems

Over the last six decades, progress in advanced drug delivery has been shaped by multiple research fields, with biomaterials becoming one of the main building blocks of these systems [67]. The requirement for controlled-release systems for drugs with varying molecular sizes, activities, stabilities, and hydrophobicity has encouraged the development of new biomaterials [68]. These materials enhance treatment efficacy by regulating the pharmacokinetic properties of drugs and enable long-term drug release in specific regions, thereby contributing to the minimization of the required dose and the decrease of toxicity risk [69], [70]. Different biomaterial platforms, such as polymer based and lipid-based structures, can be used to build drug carriers that hold therapeutic agents and control how they are released [71].

Biomaterial	Description	Applications
Poly(lactic-co-glycolic acid) (PLGA)	Biodegradable copolymer used for sustained drug release	Microspheres, nanoparticles, implants
Liposomes	Spherical lipid vesicles that can encapsulate hydrophobic and hydrophilic drugs	Targeted drug delivery, gene therapy
Alginate	Natural polysaccharide derived from algae, forms hydrogels	Controlled drug release, wound healing
Chitosan	Biopolymer derived from chitin, forms hydrogels	Oral drug delivery, wound dressings
Hyaluronic Acid (HA)	Natural component of the extracellular matrix	Ophthalmic, joint injections, skin creams
Polyethylene Glycol (PEG)	Synthetic polymer used to improve drug solubility	Nanoparticles, conjugates
Cyclodextrins	Cyclic oligosaccharides used for drug encapsulation	Increasing drug solubility
Dendrimers	Highly branched macromolecules with precise structures	Targeted drug delivery, gene therapy
Polylactic Acid (PLA)	Biodegradable polymer	Nanoparticles, implants
Polymeric Micelles	Self-assembling structures formed by amphiphilic block copolymers	Solubilization and delivery of hydrophobic drugs

Figure 1.6 List of representative biomaterials used in drug delivery systems [71].

Selected biomaterials applied in drug delivery systems are organized in tabular form in Figure 1.6. The selection of these materials should consider the formulation type, application site, and route of drug administration. Additionally, for such applications, material selection requires safe tissue interaction, controlled degradability, absence of toxicity, and mechanical reliability appropriate for the

intended use [69]. For drug delivery applications, the amount of accessible surface, the nature of the surface, and available functional groups help determine how much drug can be retained, how release proceeds, and how the system communicates with the biological environment [71]. However, the need for next-generation biomaterials for drug delivery systems continues. Responsive biomaterials are being studied because their behavior can be altered by signals present in the body or applied from outside. In drug delivery, this concept allows the release process to be adjusted by cues such as heat, local acidity, ultrasound, electrical input, or magnetic stimulation, so that the therapeutic agent can be supplied more precisely in terms of location and timing [69], [70].

1.7.1 Nanocarriers

In conventional drug delivery, patients receive medications at specific doses throughout treatment; however, this approach may result in toxic effects when drug levels become too high or insufficient therapeutic efficacy when drug concentrations fall below the desired range due to rapid metabolism, leakage from delivery systems, or drug degradation. Therefore, drug carriers should be engineered to achieve controlled release (Figure 1.7), maintaining therapeutic efficacy while minimizing unnecessary drug burden [72].

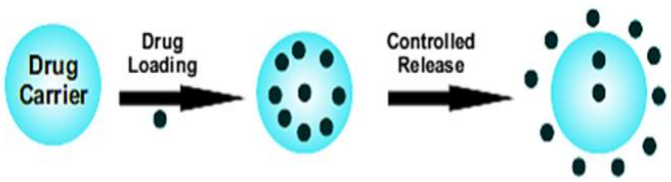


Figure 1.7 Mechanism of controlled drug release via drug carrier [73].

For topical therapy, carrier systems at the nanoscale provide a useful way to hold drugs within a confined structure and support their transfer to the treated area [74], [75]. Their nanoscale dimensions create a broad accessible surface, allowing more drug to be retained within the carrier while slowing clearance from the bloodstream compared with the free form of the drug, thereby enhancing drug bioavailability at the required site and time [69]. Nanocarriers can be engineered by placing drug molecules or recognition units on their outer surface, which helps determine where the drug goes and how gradually it becomes available. With this design, problems

often seen with free drugs, such as poor body distribution, rapid loss of activity, instability, low water compatibility, and unwanted side effects, may be reduced [69], [76]. Different nanoscale systems have been explored for regulating drug release, ranging from liposomes, polymeric and micellar carriers to dendrimers, gold particles, iron oxide structures, carbon-based materials, and silica-based formulations [75].

1.7.2 Silica Nanoparticles

With advances in nanoscale research, silica-based particles have been integrated into different biomedical systems, including sensor technologies, imaging applications, MRI contrast enhancement, and platforms developed to store or transport therapeutic agents [77]. Silicon nanoparticles can be either non-porous (i.e., solid) or mesoporous [78]. These particles fit well with biomedical systems because their size can be tuned during preparation, their structure remains durable under different conditions, and their broad surface allows effective interaction with surrounding molecules, hydrophilic surfaces, biocompatibility, and low toxicity [78], [79]. Silica nanoparticles allow design at both structural and surface levels. Changes in particle dimensions, pore arrangement, crystalline state, external geometry, and surface chemistry can direct their use in biomedical systems, including therapeutic transport, targeted treatment, imaging support, and biological monitoring [79].

1.8 Mesoporous Silica Nanoparticles (MSNs)

After the early 2000s, MSNs gradually became an important option for transporting therapeutic agents in drug delivery research [80]. Structurally, MSNs usually have nanoscale dimensions of about 50 to 200 nm, a porous network with 2 to 6 nm openings, pore volumes near 0.6 to 1, and a broad internal and external surface available for interaction [81]. MSNs are commonly classified into five main categories, and this classification is mainly based on their pore structure, particle size, surface area, and synthesis method, as shown in Figures 1.8 and 1.9.

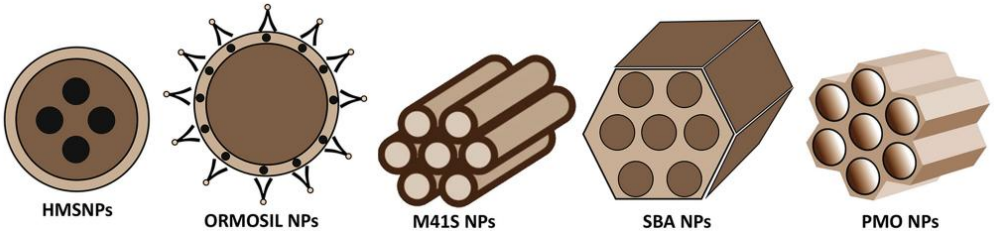


Figure 1.8 Different classes of MSNs: hollow-type MSNPs (HMSNPs), organically modified silica (ORMOSIL), molecular sieves (M41S), Santa Barbara Amorphous (SBA), and periodic mesoporous organosilica (PMO) [82].

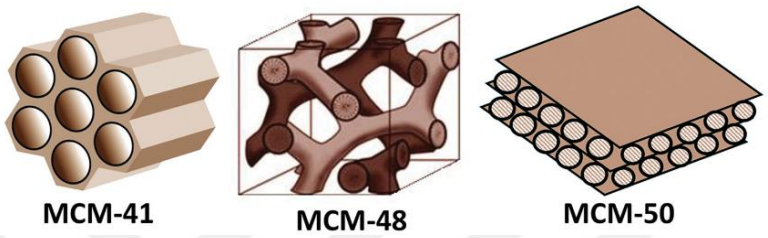


Figure 1.9 Representative M41S mesoporous silica materials, including Mobil Composition of Matter-41 (MCM-41), Mobil Composition of Matter-48 (MCM-48), and Mobil Composition of Matter-50 (MCM-50) [82].

MSNs differ from nonporous hard or soft carriers such as gold nanoparticles, iron oxide nanoparticles, polymer-based systems, and liposomes by offering an internal pore network. This structure provides more space for loading drugs and biomolecules, while the pore dimensions and framework stability can be adjusted for delivery purposes [81], [83]. Because MSNs can carry substantial amounts of drug while showing limited toxic effects, they are well suited for delivery systems where release behavior and target localization need to be regulated [84]. In addition, the silanol groups (Si–O–H) on MSN surfaces provide reactive sites for surface modification. Through these sites, MSNs can be adapted to retain drugs with different solubility profiles, incorporate selected functional features, and adjust both drug loading and release behavior [85]. Moreover, the strong Si–O bonds present in MSNs enhance their greater structural durability against breakdown and mechanical forces than liposome and niosome based carriers [84]. Overall, the combination of these characteristics supports the use of MSNs in delivery strategies

designed to control where, when, and under which conditions therapeutic agents are released [81].

1.8.1 Synthesis Methods for MSNs

MSN preparation can be directed by changing synthesis conditions such as medium acidity, the selected surfactant or copolymer, and both the amount and precursor type of silica. To obtain MSNs suitable for drug delivery, the particles should remain well dispersed, show a narrow size distribution, contain adjustable pores, and provide sufficient internal pore space [86].

MSN preparation is frequently carried out through sol gel chemistry. This route is preferred because it does not require complex processing, is relatively economical, and allows the pore architecture and surface characteristics of the particles to be adjusted during synthesis. In addition, because it is not a multistep process, it is relatively timesaving and requires fewer excipients [84]. In this method, silicon alkoxide precursors are mixed with water or acid to form a gel through a series of chemical reactions. The resulting pore architecture is shaped mainly by parameters such as surfactant type, surfactant concentration, and temperature [82], [87].

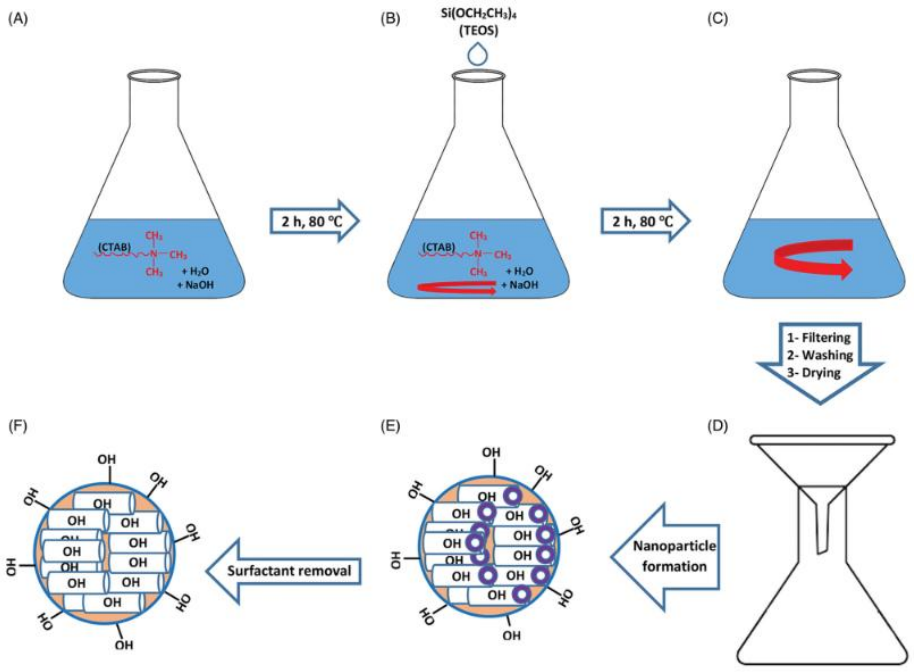


Figure 1.10 MSN synthesis using sol-gel method [82].

As presented in Figure 1.10, sol gel synthesis is initiated by producing a colloidal sol that serves as the base medium for inorganic framework formation. The process then proceeds to gelation, where the sol gradually converts into a gel like three-dimensional structure dispersed within the remaining liquid medium. After exposure to water or a weak acidic medium, the precursor turns into oxide species that remain distributed throughout the solution, giving rise to the sol phase. As solvent is gradually removed, the system evolves into a gel-like structure, and the final particle form is shaped during this transformation. In the final step, thermal treatment of the dried gel converts it into the oxide product [88].

In the preparation of ordered mesoporous structures, template-based synthesis is frequently preferred because it allows pore arrangement to be directed without requiring a high-cost process. In this method, a template directs the formation of the mesoporous structure, and the technique is generally classified into two main types: endotemplating and exotemplating [88]. Endotemplating relies on surfactant organized domains to guide pore formation, without using a hard solid template. This feature places the method under the category of soft templating, also known as soft matter templating [89]. Soft templating includes techniques such as single micelle templating, vesicle templating, and microemulsion templating [90]. In contrast, exotemplating, also referred to as nanocasting, employs porous solid materials rather than surfactants as templates. Here, the empty channels within the solid template are filled with the inorganic precursor, which subsequently solidifies under appropriate conditions. After removal of the template, a negative replica is obtained while preserving the porous structure; therefore, this approach is also called hard material templating [89]. Hard templating methods include polymer latex templating and the addition of nanoscale metal and oxide-based particles [90].

The microwave-assisted hydrothermal method has been employed to obtain oxide-based ceramics, porous solids, and powdered metals within a shorter synthesis period. Compared with conventional methods, it offers several advantages, including shorter crystallization time, faster heating, and rapid supersaturation [91]. The synthesis is initiated by adding the structure directing agent to water, followed by mixing until the medium becomes homogeneous. After HCl and the silica precursor are added, the reaction mixture is placed in Teflon containers and

subjected to heating in a microwave oven under specific temperature and time conditions. After synthesis, the product is filtered, washed, and dried [92]. Microwave-assisted synthesis enables the rapid preparation of mesoporous materials such as MCM-41 [93]. In addition, during microwave processing, heat may develop unevenly within the reaction mixture and reach local values above the temperature measured for the vessel. This feature makes microwave treatment advantageous for producing mesoporous structures [88].

Chemical etching creates mesoporosity without using a sacrificial template. In this process, acidic or alkaline treatment removes selected regions of the silica core/MS structure, and the different etching responses of the core and shell support the formation of hollow particles with adjustable pores. Compared with this route, template-based synthesis may offer less precise control over particle geometry and pore dimensions [94]. Alternatively, porous core shell particles can be obtained by removing material unevenly from different regions of the particle. When the etchant reacts more strongly with the inner region than with the external layer, the center is gradually emptied while the shell is retained [88].

1.8.2 Surface Modification of MSNs

MSNs have an ordered structure and a surface rich in silanol groups, which allows easy functionalization with various organic moieties. In biomedical fields, the surface charge behavior of the particles can be altered through these modifications, promote interactions with molecules located within or around the pores, and adjust the pore openings to improve the retention of cargo inside the nanoporous structure [85]. Surface functionalization can be performed either during or following nanoparticle preparation by forming covalent bonds with selected functional moieties such as carboxyl (-COOH), thiol (-SH), amino ($-NH_2$), and hydroxyl (-OH) groups [95]. These modifications enhance the physicochemical characteristics of nanoparticles, allowing the particles to act in a stimulus dependent manner when exposed to cues such as pH variation, temperature change, light, enzymes, glucose, redox shifts, or magnetic and electric inputs. As a result, by altering the particle surface, it becomes possible to increase drug retention, direct interactions toward selected cells, and regulate the release process more effectively, while also improving the biodegradability and biocompatibility of nanoparticles [96].

Additionally, the high density of surface groups and the variety of silanol functionalities provide suitable sites for linking MSNs with materials including aliphatic hyperbranched polymers, chitosan, PEG, and poly(N isopropyl acrylamide) thus transforming them into smart nanocarriers [97]. To achieve drug release under specific conditions, surface modification with stimuli responsive functional groups is required, whereas conjugation with targeting molecules enables MSNs to deliver their cargo selectively to the desired site [98].

1.9 Hyaluronic Acid (HA)

HA is a naturally derived polysaccharide whose repeating disaccharide structure, illustrated in Figure 1.11, contains D glucuronic acid and N acetyl D glucosamine [99]. HA can break down in biological environments, shows good compatibility with tissues, and usually does not trigger toxic or immune related effects. Because of these features, it is applied in several clinical areas, including arthritis management, ophthalmic procedures, tissue regeneration, and wound repair [100]. Within the extracellular matrix (ECM), HA functions as a structural molecule that can influence how cells move, divide, and progress toward specialized phenotypes [101]. In addition, the hydroxyl, carboxyl, and N acetyl groups in HA provide reactive points for chemical tailoring, allowing this polymer to be adapted for drug delivery systems [102]. Due to its high reactivity, HA can efficiently encapsulate different therapeutic compounds and can be converted into network-like structures through cross linking or conjugated with various biomacromolecules [103].

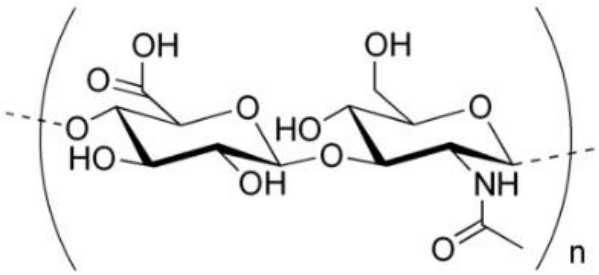


Figure 1.11 Chemical structure of HA [103].

Beyond its general advantages as a drug carrier, HA has also attracted attention in smart drug delivery systems because it can act both as a targeting moiety and as a capping material [104]. In such systems, HA is particularly useful because it can be

degraded by hyaluronidase (HAse), an enzyme present in mammalian tissues, through enzymatic hydrolysis [105]. Moreover, HA is more susceptible to degradation under acidic conditions, while remaining relatively stable in normal tissues at neutral pH, thereby allowing HA based systems to adjust drug release in response to selected environmental cues [104].

1.10 Drug Eluting Implant

Failure of orthopedic implants is often linked to the development of infection at the implantation site and may result in prolonged hospitalization, revision procedures, and secondary surgery; therefore, the use of antibacterial agents has encouraged the development of metallic implants coated with antibacterial drugs [106]. As shown in Figure 1.12, Ti implants capable of releasing drugs can be produced by altering the surface through coating or adsorption.

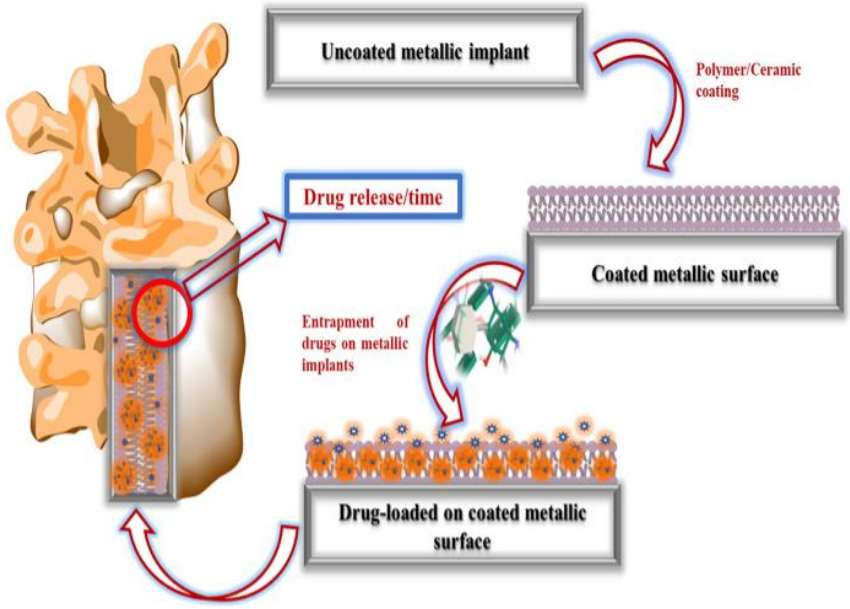


Figure 1.12 Illustration of a metallic implant-based drug delivery platform [106].

Two main design routes are used for this purpose. One route place a therapeutic agent loaded carrier on the implant surface or within the pore network, while the second relies on incorporating the drug directly into the implant material without a carrier [107]. Among these strategies, coating implant surfaces with biocompatible and bioactive materials is considered one of the most effective local approaches for overcoming such complications and extending implant longevity. By using this

coating design, bioactive compounds can be supplied in a localized manner to the region requiring tissue regeneration and thus provide a more localized and precise effect than conventional systemic pharmacological treatment [108]. Moreover, drug containing polymer ceramic layers on permanent metallic implants can alter the response of cells participating in bone healing. This local cellular effect may contribute to new bone formation around the implant [109].

1.10.1 Surface Coating Techniques

Coating materials can be deposited by various mechanisms, each of which should be carefully evaluated in terms of its advantages and limitations for the intended application. Among the available coating techniques are electrodeposition, thermal spraying, sol gel processing, physical vapor deposition (PVD), and chemical vapor deposition (CVD) [110].

PVD forms coatings by converting the source material into a vapor phase, guiding this vapor through a vacuum or reduced pressure environment, and collecting it as a thin layer on the target surface [111]. It encompasses several deposition techniques, including evaporation, laser ablation, vacuum arc deposition, and sputtering [112]. PVD has attracted considerable attention because it enables the formation of dense and compact coatings and thereby enhancing the substrate's resistance to chemical degradation and mechanical stress. In addition, this technique offers several advantages, including relatively low cost, procedural simplicity, chemical resistance, good biocompatibility, high hardness, strong adhesion, and high wear resistance [113], [114]. Owing to these properties, PVD coatings provide effective protection and have been increasingly used to support better operation and reliability of medical devices [114].

During CVD, gaseous reactants are activated by heat and converted into a solid layer as the reaction takes place at or close to the substrate surface [115]. In this technique, precursor gases are introduced into a chamber containing the heated substrate. Once they reach the substrate region, they react to form a thin coating layer. Any remaining gases and gaseous products are then removed from the system [116]. For biomedical use, CVD can deposit protective layers on different substrate

materials. These layers may improve tissue compatibility, restrict bacterial colonization, and reduce surface damage caused by wear or corrosion [117].

Thermal spraying has long been used to create protective surface layers, particularly suitable for producing coatings thicker than approximately 50 μm [118]. During this process, the material to be applied as a coating is first heated until the feedstock becomes fully or partly melted, after which it is accelerated toward the target surface. When the particles strike the surface, they spread out, rapidly solidify into splats, and gradually accumulate to generate the coating layer [119], [120]. The main methods within the thermal spray family are plasma spray, high velocity oxy fuel (HVOF) spray, flame spray, electric arc spray, and detonation gun spray [119]. For biomedical surface engineering, thermal spraying provides a way to cover implant surfaces with different material systems and modify their interaction with the biological environment. Such coatings may reduce bacterial attachment and help protect the implant against corrosion and wear related damage [121]. Therefore, this technique is frequently chosen for coated medical devices, especially in orthopedic and dental implant applications [122].

Thin films can be prepared on many substrate types using the sol gel route, which remains an actively developed coating approach due to its processing flexibility [123]. During sol gel dip coating, a substrate is lifted from the sol, leaving behind a wet layer on the surface. Drainage, solvent loss, and continuing condensation reactions then transform this layer into a solid film [124]. Because this process usually avoids severe heat or pressure, it can be used to prepare different material systems under relatively gentle conditions [125]. In addition, the process can be carried out without complex equipment or demanding steps, which lowers fabrication costs and broadens its use for different material systems, offering considerable flexibility in coating composition and sample geometry [126]. Therefore, sol–gel technology has shown promising applications in optics, electronics, mechanics, energy, environmental science, biology, and medicine, including sensors and functional smart coatings [125].

Electrodeposition, or electrochemical deposition, generally refers to an electrolysis-based process in which solids or condensed substances are deposited in various forms and shapes [127]. In this process, after voltage is applied to the cell, charged

species begin to migrate through the electrolyte. At the surface of the submerged substrate, reduction reactions convert these species into a solid deposit, and the coating layer develops gradually [110]. This technique is typically carried out in aqueous solution under atmospheric pressure and at moderate temperatures (20–60 °C), making it a relatively low-cost coating method [128]. Electrodeposition processes are mainly classified into electrolytic deposition (ELD), electrophoretic deposition (EPD), and electrostatic deposition (ESD) [129]. In addition, Ti can be coated through electrodeposition to create surfaces with more than one function. Depending on the deposited layer, the implant surface may suppress bacterial colonization, manage drug release, encourage osteoblast attachment, and react to selected environmental signals [130].

1.10.2 Electrophoretic Deposition (EPD)

In EPD, the starting suspension contains particles dispersed in a liquid phase, either as colloidal entities or as powder particles smaller than 30 μm. After the electric field is applied, the charged particles go through the suspension and collect on the electrode carrying the opposite charge [131], [132]. As a coating method, EPD offers several advantages, including short processing times, simple equipment requirements, and the absence of a need for crosslinking agents [133]. It also enables the tuning of coating properties through variations in process parameters and allows the deposition of sensitive biomaterials at room temperature. In addition, EPD can produce high purity and homogeneous coatings on substrates with complex geometries, while also allowing the formation of porous coatings that support tissue ingrowth. Its ability to facilitate thin film formation, precise control of coating thickness, and high production efficiency further highlights its potential for industrial applications [16].

The main elements of an EPD system are presented in Figure 1.13 and consist of the power source, the electrode pair, and a particle suspension suitable for deposition [134]. In EPD, coating formation can be described as a two-stage process. First, the electric field drives suspended particles through the liquid medium toward an electrode. Then, the arriving particles settle on the electrode surface and gradually develop into a compact deposit [132].

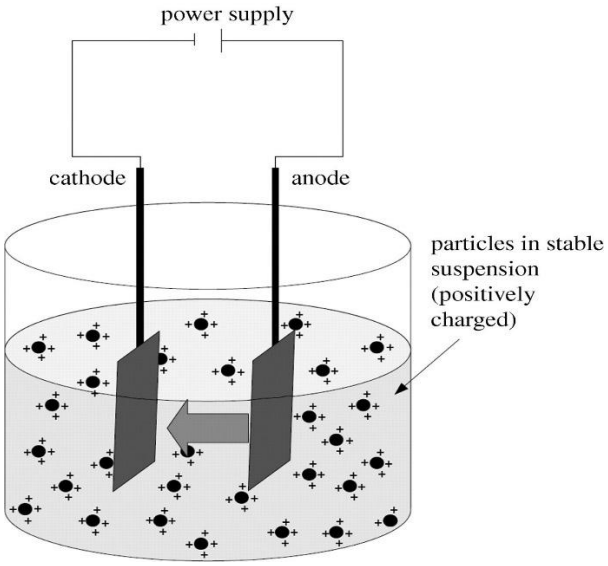


Figure 1.13 EPD process [134].

EPD is classified based on the electrode surface where the coating develops. In cathodic deposition, particles carrying positive charge move toward the cathode and accumulate on its surface. In anodic deposition, negatively charged particles are collected on the anode [135]. Both deposition routes are schematically presented in Figure 1.14.

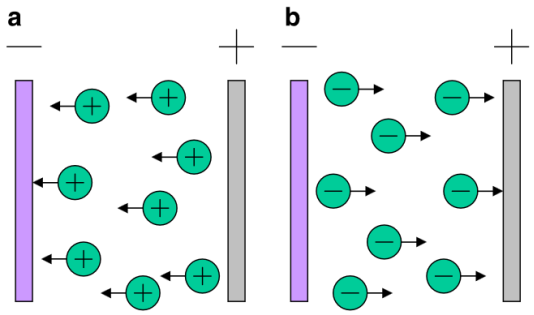


Figure 1.14 (a) Cathodic EPD and (b) anodic EPD [135].

The final EPD coating is shaped by both the properties of the suspension and the selected deposition conditions. Factors such as zeta potential, particle size, dielectric constant, conductivity, and viscosity determine whether the particle dispersion remains stable and suitable for coating formation. At the same time, applied voltage, deposition duration, and substrate conductivity directly affect how the coating develops on the surface [136].

The homogeneity of the deposited layer is largely governed by the stability and distribution of particles within the suspension. In particular, larger particles are more prone to sedimentation because of the competition between gravitational settling and electrophoretic motion, which may lead to deposition gradients. In addition, changes in surface charge after EPD may broaden the electrical double layer surrounding the particles [136]. A high zeta potential generally improves suspension stability by strengthening electrostatic repulsion between particles, thereby reducing agglomeration and precipitation. In electrophoretic systems, this is especially important because higher zeta potential also promotes particle movement under an electric field [137]. Overall, an ideal suspension should have low conductivity, high dielectric constant, and low viscosity [136].

The choice of solvent is another critical factor in EPD. The solvent must be chemically inert toward the powder, and organic liquids are often preferred over water [138]. Since water undergoes electrolysis even at relatively low voltages, its use in EPD suspension preparation is limited. Therefore, non-aqueous solvents, such as alcohols, are frequently used [139]. However, organic media with low dielectric constants may reduce both zeta potential and electrophoretic mobility, thereby lowering suspension stability and adversely affecting coating quality. For this reason, mixed solvent systems, particularly water–ethanol mixtures, are often preferred [140]. Coating characteristics are also shaped by the conditions selected during the deposition process. Under otherwise identical bath conditions, increasing the applied voltage increases the deposition weight and thus the coating thickness [141]. Similarly, under a constant applied voltage, increasing the deposition time results in greater current, a higher deposition rate, and the formation of thicker coatings [142]. Finally, substrate conductivity is a key factor in film quality, since poor conductivity can result in slower and less uniform deposition [141].

Because of these capabilities, EPD is used in different biomedical studies involving surface engineering, material structuring, and device related applications. This technique can be employed to prepare functional or composite coatings, nanoscale surface layers, graded biomaterial structures, thin films, porous materials, scaffolds for tissue engineering, drug release platforms, and biosensor components. In addition, EPD can be used for the deposition of biopolymer-based coatings,

including chitosan and gelatin containing systems, proteins, enzymes, and bioactive ceramic components such as bioactive glass and hydroxyapatite can be incorporated onto engineered nanostructured biomaterials and biomedical device surfaces [134], [143], [144], [145], [146].

2
MATERIALS AND METHODS

2.1 Materials

3-aminopropyltriethoxysilane (APTES, 98%, product No.: A3648), hyaluronic acid sodium salt from *Streptococcus equi* (HA, product No.: 53747), hyaluronidase from bovine testes (HAse, product No.: H3506), MES hydrate (MES, ≥ 99.5%, product No.: M8250), N-(3-dimethylaminopropyl)-N′-ethylcarbodiimide hydrochloride (EDC, product No.: 03499), N-hydroxysuccinimide (NHS, product No.: 56480), nitric acid (HNO_3, product No.: 438073), potassium chloride (KCl, product No.: P9541), potassium phosphate monobasic (KH_2PO_4, product No.: P5379), sodium chloride (NaCl, product No.: 134239), sodium phosphate dibasic (Na_2HPO_4, product No.: 04276), and tetraethyl orthosilicate (TEOS, product No.: 131903) were purchased from Sigma-Aldrich; cetyltrimethylammonium bromide (CTAB, product No.: 301256) was purchased from AFG Bioscience; ciprofloxacin.HCl (CIP, product No.: PHR1044) and ethylene glycol (EG, product No.: 1.09621) were purchased from Merck; hydrofluoric acid (HF, product No.: 932.116), sodium hydroxide (NaOH, product No.: 969.113), and toluene (product No.: 973.015) were obtained from Isolab Chemicals. Yeast extract (product No.: 4122202), tryptone (product No.: 4122902), and agar bios special LL/agar bacteriological (product No.: 4110302) were purchased from BioLife. Grade 2 titanium plates were supplied by Bag-San. Distilled water was used for the preparation of all aqueous solutions.

2.2 Methods

2.2.1 Synthesis of MSNs

The synthesis of MSNs was carried out by a sol gel procedure adapted from the literature [147]. Distilled water (100 mL) and ethylene glycol (EG, 20 mL) were combined, after which CTAB (0.25 g) and NaOH (0.175 g) were introduced into the medium. The mixture was kept at 80 °C under vigorous stirring for 1 h. Then, TEOS (1340 µL) was added rapidly, and stirring was continued for another 2 h. The obtained suspension was centrifuged at 12,000 rpm for 20 min, washed with water, and oven dried. To remove the template, the dried powder was calcined at 550 °C for 5 h, resulting in MSNs (Figure 2.1).

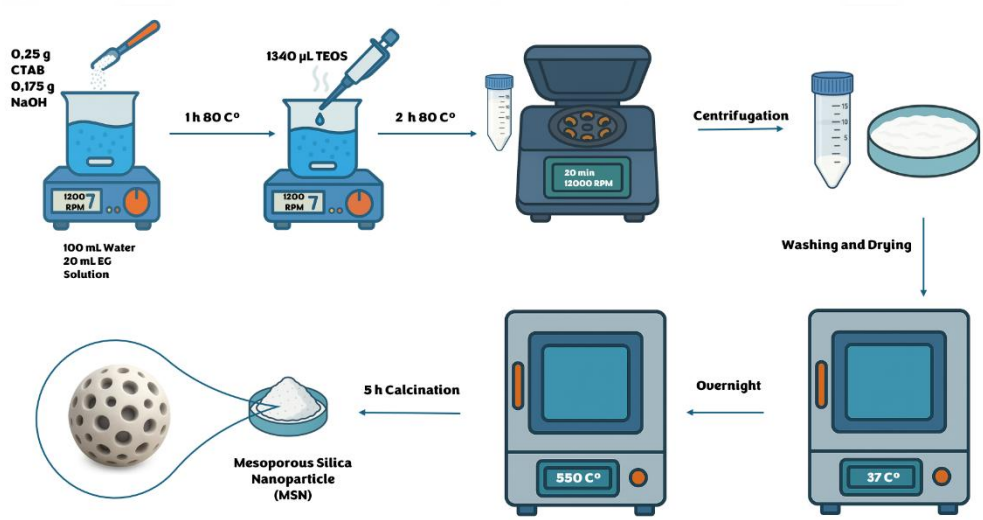


Figure 2.1 Schematic illustration of MSN synthesis.

2.2.2 Synthesis of Amino-Modified MSNs (MSNs-NH_2)

For amine modification, calcined MSN (1.5 g) was added to toluene (60 mL) and the dispersion was magnetically stirred at 600 rpm for 6 h. APTES (1 mL) was then introduced into the reaction medium, which was maintained at room temperature under stirring for 24 h. After completion of the reaction, the transparent dispersion was centrifuged at 5000 rpm for 5 min. The separated solid was rinsed with toluene, dried in an oven, and labeled as MSN–NH_2 (Figure 2.2) [148].

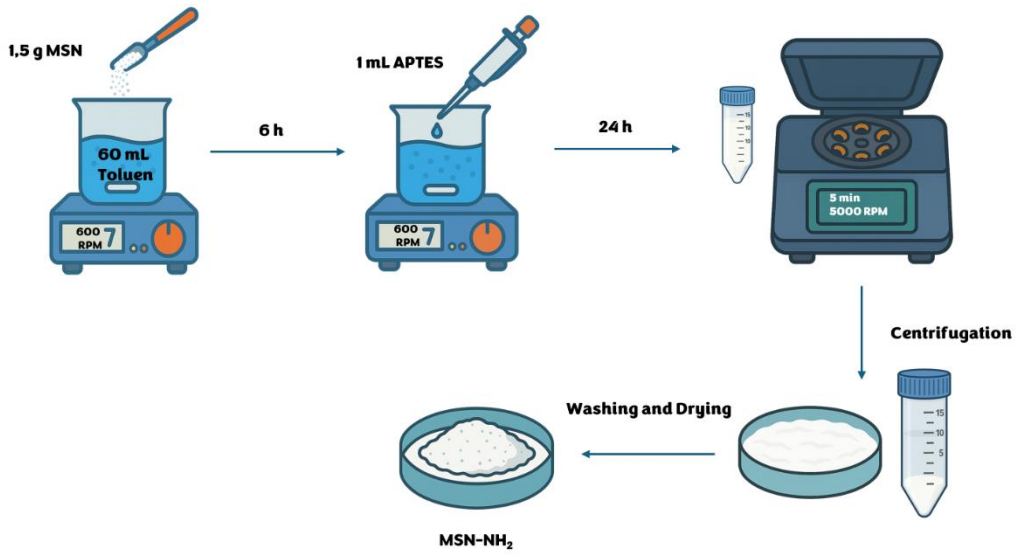


Figure 2.2 Schematic illustration of amino modified MSNs (MSNs-NH_2) synthesis.

2.2.3 Drug Loading and HA Coating

$MSN–NH_2$ (40 mg) was transferred into MES buffer (12 mL, pH 5 or pH 9), and the dispersion was combined with ciprofloxacin (4 mg) for the loading step. The suspension was kept under stirring at 300 rpm for 24 h. The solid phase was then isolated by centrifugation at 10,000 rpm for 15 min, washed with water, and oven dried.

Ciprofloxacin loading was evaluated using an indirect method by analyzing the amount of unloaded drug remaining in the supernatant after centrifugation. Ciprofloxacin in the samples was measured at 270 nm using a UV Vis spectrophotometer (SOIF UV 5100H). The concentration was obtained from the ciprofloxacin calibration curve, and drug loading efficiency (DLE%) was determined using the following equation.

$$DLE\ (\%) = \frac{W_{initially\ added\ drug} - W_{free\ drug\ in\ supernatant}}{W_{initially\ added\ drug}} \times 100 \qquad (2.1)$$

For surface coating with HA, MSN–CIP particles (20 mg) were placed in MES buffer (4 mL, 0.01 M, pH 5.5). HA was introduced at three different amounts, 80, 10, or 5 mg (these formulations corresponded to MSN:HA mass ratios of 1:4, 1:0.5, and 1:0.25) and the mixture was allowed to homogenize for 5 min. Afterward, EDC

(10 mg) and NHS (10 mg) were added to activate the coupling reaction, which was continued at 600 rpm for 4 h. The particles were separated by centrifugation at 10,000 rpm for 15 min, rinsed with water, and dried to give MSN–CIP–HA (Figure 2.3).

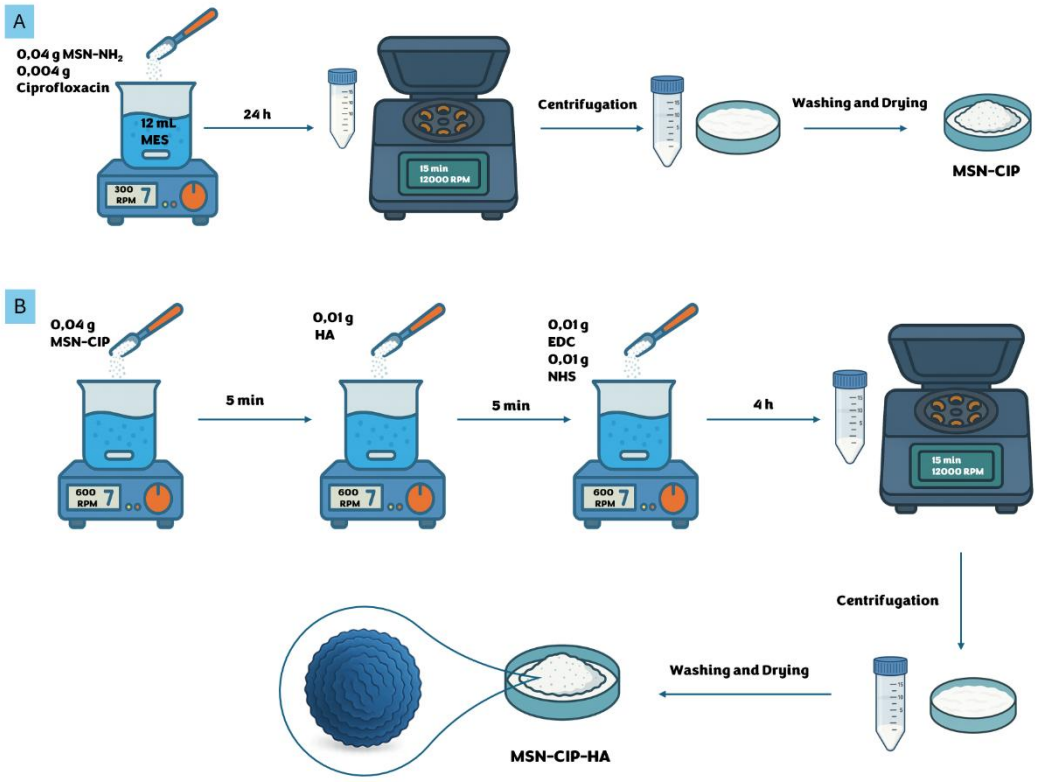


Figure 2.3 Schematic illustration of (a) drug loading and (b) HA Coating.

2.2.4 Characterization of MSNs

The prepared nanoparticles were examined using several characterization methods: Fourier Transform Infrared Spectroscopy (FT-IR), Scanning Electron Microscopy (SEM), Transmission Electron Microscopy (TEM), zeta potential analysis, and Brunauer Emmett Teller (BET) measurements. FT-IR spectra were collected with a Nicolet iS10 Thermo Scientific instrument to obtain information on the chemical structure and surface functional groups of the nanoparticles. Surface morphology and topographical characteristics were investigated by SEM using a Zeiss EVO LS 10. TEM images were recorded with a JEOL JEM 2100Plus to observe particle dimensions, morphology, size distribution, and pore structure. The surface charge behavior and colloidal stability of the particles were evaluated through zeta

potential measurements using an Anton Paar Litesizer 500. Zeta potential analyses were performed in triplicate, and the results were reported as mean ± standard deviation. Specific surface area and porosity related properties were determined by BET analysis with a Micromeritics ASAP 2020 system.

2.2.5 Coating of Ti Surfaces

Ti plates (grade 2, 10 × 20 × 0.145 mm) were prepared for coating through sequential mechanical and chemical pretreatments. Initially, silicon carbide papers were used to polish the plate surfaces and remove the native oxide film. The polished samples were rinsed with water and then immersed for 3 min in an etching mixture containing HF (10 mL), HNO_3 (40 mL), and distilled water (50 mL). After etching, the samples were washed once more with water and dried, resulting in cleaned Ti substrates (Figure 2.4).

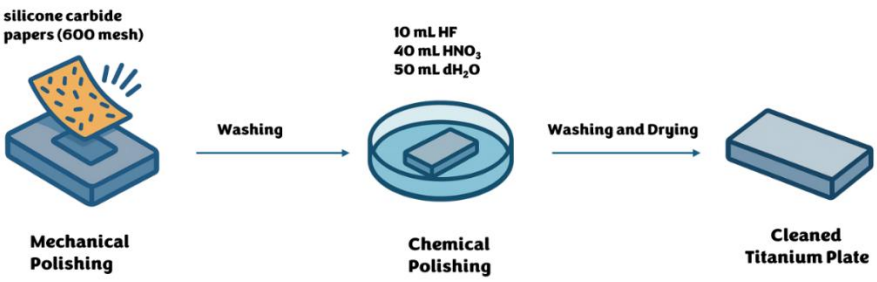


Figure 2.4 Schematic illustration of preparation of Ti plates.

The EPD suspension was prepared by adding MSN–CIP–HA to 70% ethanol at 0.65 g/L. After stirring for 30 min, the dispersion was probe sonicated for 15 min using a JY88 IIN Ultrasonic Homogenizer, allowing the particles to become more uniformly distributed before coating (Figure 2.5).

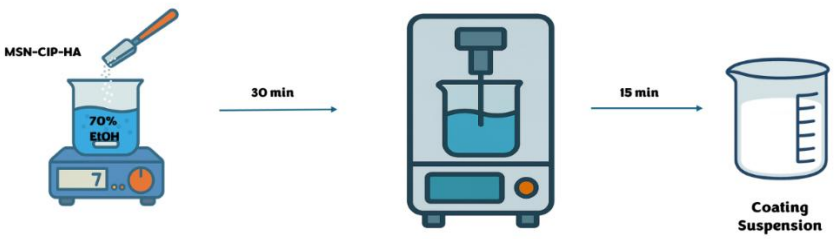


Figure 2.5 Schematic illustration of preparation of coating suspension.

As illustrated in Figure 2.6, EPD was applied to deposit MSN based coatings onto Ti surfaces. In the deposition cell, the pretreated Ti plate acted as the anode, whereas the platinum plate functioned as the cathode. Both electrodes were immersed in the MSN suspension and kept 10 mm apart. Deposition was conducted at 30 V using three different coating times, 1, 3, and 5 min, resulting in coated Ti substrates.

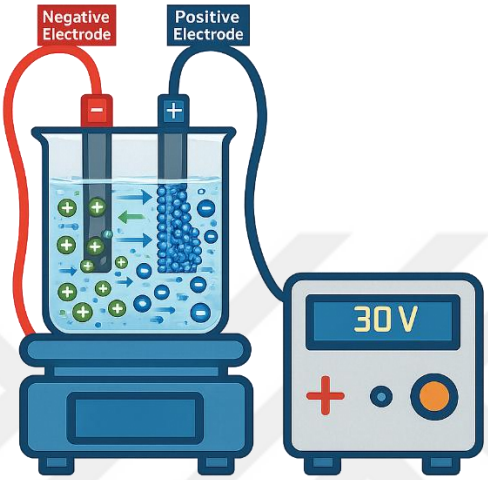


Figure 2.6 EPD Process.

2.2.6 Characterization of Coated Ti Plates

The coated Ti plates were examined by SEM, optical profilometry, and contact angle analysis. SEM images were recorded with a Zeiss EVO LS 10 to observe coating morphology, surface uniformity, and possible defects such as cracks or particle agglomeration. Surface topography was analyzed with an AEP Nanomap 1000WLI optical profilometer, which also provided quantitative information on roughness and height variation across the coated Ti surfaces. Wettability was evaluated by contact angle measurements using a Biolin Scientific Attension Theta Lite system, allowing the hydrophilic or hydrophobic behavior of the coatings to be determined. Contact angle measurements were performed in triplicate for each sample, and the results were presented as mean ± standard deviation.

2.2.7 Drug Release Studies

Drug release was investigated using two sample formats: dispersed nanoparticles and coated Ti plates (Figure 2.7). For nanoparticle-based release experiments, drug loaded particles, MSN–CIP or MSN–CIP–HA (3 mg), were placed in PBS (1 mL, 0.01 M) adjusted to pH 5 or pH 7.4. In the coated surface experiments, coated Ti plates were incubated in PBS (2 mL, 0.01 M) at the same pH values. All release tests were conducted at 37 °C and 100 rpm using an orbital shaker (PSU 10i, Biosan) placed in an oven (GEMO TT104). Release samples were collected at predetermined time points during the release study. At each sampling point, the entire release medium was withdrawn for analysis and replaced with an equal volume of fresh PBS at the corresponding pH. For enzyme-responsive release studies, HAse was added to the fresh release medium after sampling to obtain final enzyme concentrations of 150 U mL^{-1} at 2, 4, and 6 h, 300 U mL^{-1} at 24 h, 600 U mL^{-1} at 48 h, and 1200 U mL^{-1} at 72 h.

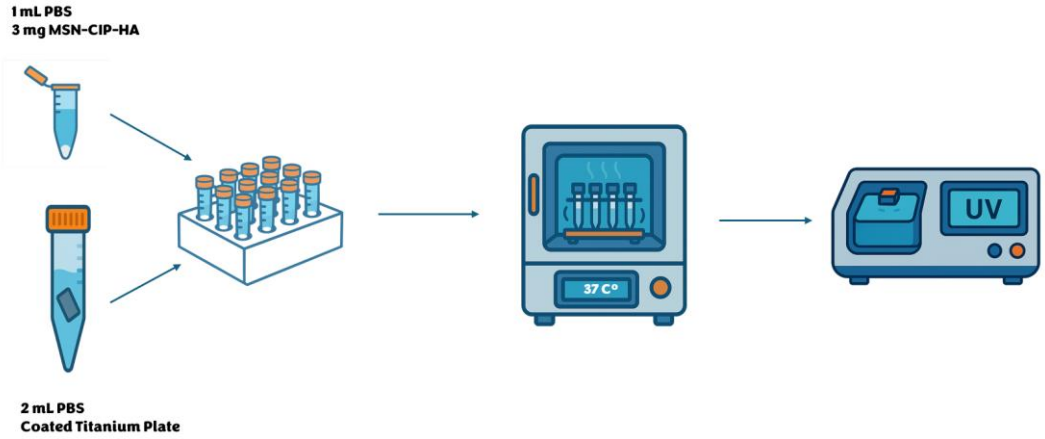


Figure 2.7 Schematic illustration of drug release studies.

The collected release media were analyzed at 270 nm using a UV Vis spectrophotometer to determine the released CIP amount. For UV Vis measurements, drug-free samples with the same composition as the corresponding release groups were used as blank controls under identical release conditions. Accordingly, MSN suspensions were used as blanks for MSN–CIP samples, MSN–HA suspensions were used as blanks for MSN–CIP–HA samples, and Ti–MSN–HA-coated titanium substrates were used as blanks for Ti–MSN–CIP–HA-coated samples. For enzyme-containing groups, the corresponding drug-free enzyme-

containing blanks were used, including MSN–HA + HAse for MSN–CIP–HA + HAse samples and Ti–MSN–HA + HAse for Ti–MSN–CIP–HA + HAse samples. This blank correction was performed to eliminate background absorbance from the nanoparticles, HA coating, HAse, or coated titanium substrate before calculating the CIP concentration. All experiments were carried out in triplicate, and the results were expressed as mean ± standard deviation.

2.2.8 Antibacterial Activity Test

Antibacterial performance was evaluated by adapting the spread plate assay reported in the literature (Figure 2.8) [149]. Overnight cultures of Escherichia coli (BL21) and Staphylococcus aureus (ATCC 29213) were prepared in Luria–Bertani (LB) medium at 37 °C with shaking at 180 rpm. Bacterial suspensions were obtained from separate colonies and adjusted to 1×10^6 colony-forming units (CFU) mL^{-1}.

Before testing, Ti plates were sterilized for 15 min in a UV ozone system (PSD Pro Series Digital UV Ozone System). The sterile Ti samples (1 × 1 cm) were placed into 24 well plates, and each sample received bacterial suspension (1×10^6 CFU mL^{-1},). In selected groups, the bacterial concentration was set to 2×10^6 CFU mL^{-1}, and HAse (300 U mL^{-1}) was included in the suspension to examine enzyme triggered antibacterial response. The samples were incubated for 24 h at 37 °C under shaking at 180 rpm.

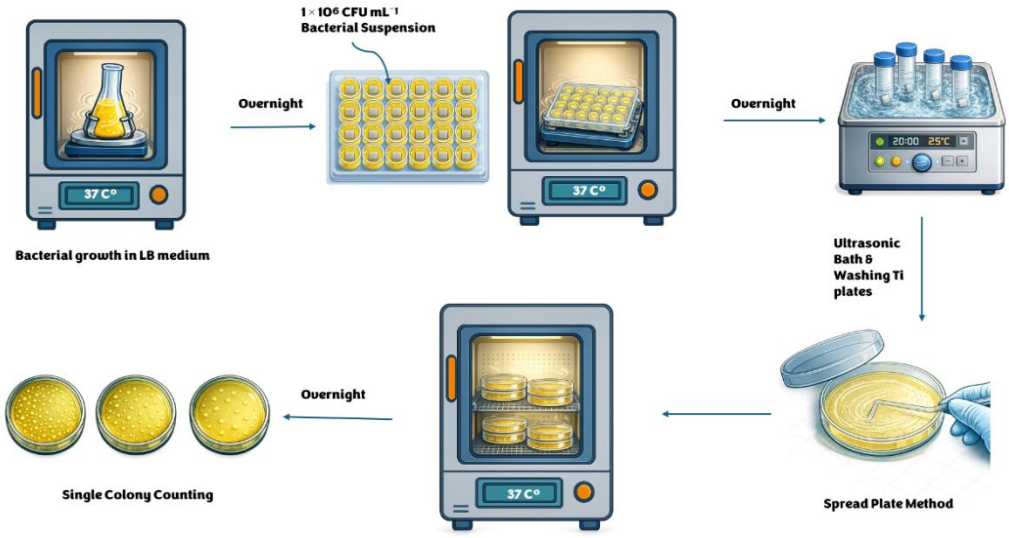


Figure 2.8 Schematic illustration of antibacterial activity test procedure.

After incubation, the Ti plates were washed gently with PBS and moved into sterile tubes containing PBS (3 mL) for recovery of surface attached bacteria. Bacterial detachment was performed by sonication for 20 min. The obtained suspensions were serially diluted, spread onto LB agar plates, and incubated overnight at 37 °C. Viable bacteria were quantified by counting colonies, and the results were reported as CFU. All antibacterial activity tests were performed in triplicate, and the results were reported as mean ± standard deviation.

2.2.9 Statistical Analysis

All experiments were performed in triplicate, and the data were expressed as mean ± standard deviation (SD). Statistical evaluation was conducted by one-way ANOVA followed by Tukey's post hoc test, and differences were considered statistically significant at $p < 0.05$. Data analysis, statistical calculations, and graph generation were performed using Origin 2026 software.

3
RESULTS AND DISCUSSIONS

3.1 Characterization of MSNs

MSN formation and the stepwise changes introduced on the particle surface were validated by comprehensive structural and surface characterization analyses. TEM analysis revealed that the synthesized MSNs possessed a spherical morphology with a clearly defined mesoporous structure, and the mean particle diameter was determined to be 250 ± 30 nm (Figure 3.1a). Following HA coating at an MSN:HA ratio of 1:4, the average particle size increased to 450 ± 50 nm, accompanied by a reduction in the clarity of the porous structure (Figure 3.1b). This observation indicates that the HA layer was successfully deposited onto the particle surface, leading to partial masking of the mesoporous structure.

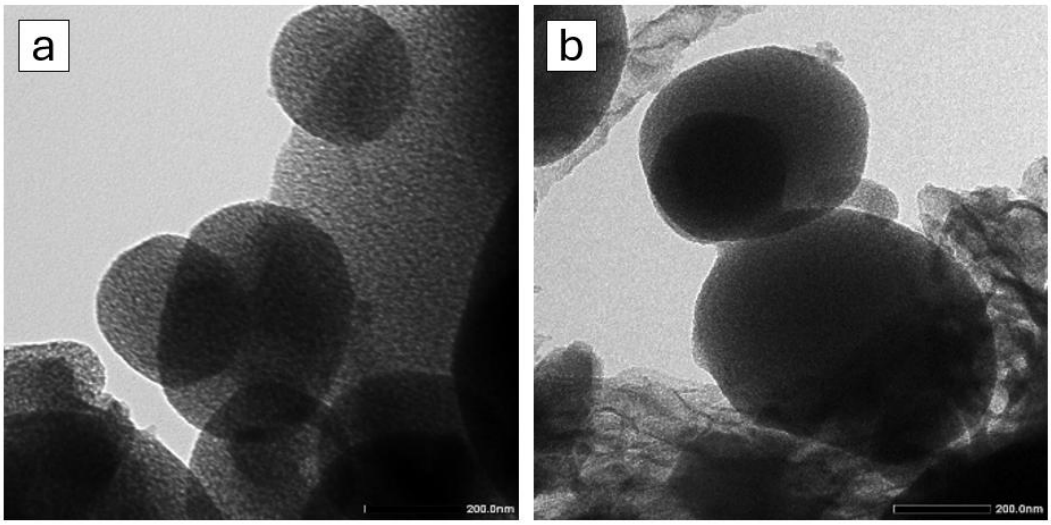


Figure 3.1 TEM images of a) MSN and b) MSN–CIP–HA.

SEM analysis presented in Figure 3.2 demonstrated distinct morphological differences between bare MSN and CIP containing HA coated MSN (MSN–CIP–HA) particles. Compared with the relatively uniform surface of MSN, the MSN–CIP–HA sample exhibited a denser and more compact surface morphology, with partially blocked regions, indicating that HA was present on the outer particle surface. In addition, the agglomerated areas observed in Figure 3.2b are highlighted with arrows, and these features were particularly evident in the sample prepared at an MSN:HA ratio of 1:0.5.

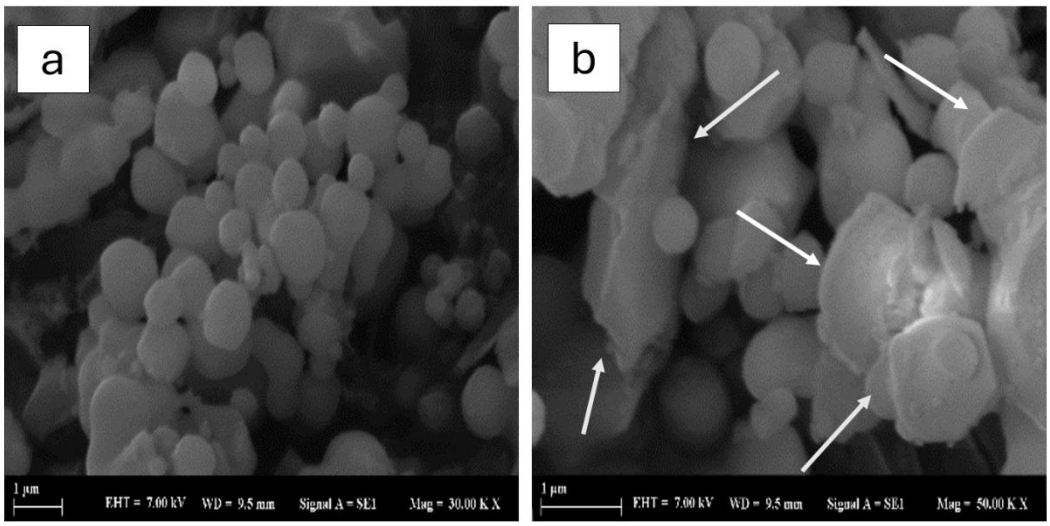


Figure 3.2 SEM images of a) MSN and b) MSN–CIP–HA, where arrows indicate block like structures formed due to nanoparticle agglomeration.

Throughout the HA coating optimization process, different MSN: HA ratios (1:4, 1:0.5, and 1:0.25) were systematically examined. TEM analysis of the composition prepared at a 1:4 MSN: HA ratio revealed significant agglomeration as well as a marked increase in particle size; this showed that excessive HA content may promote interparticle interactions rather than forming a homogeneous coating layer. Therefore, the HA content was reduced to a 1:0.5 ratio; however, agglomerated regions were still observed in the SEM images, as indicated by the arrows in Figure 3.2b. These findings indicate that excessive HA content may increase the particle size and promote aggregation, potentially due to polymer mediated bridging effects between particles. This interpretation is supported by previous studies reporting that an increase in HA content can lead to larger nanoparticle sizes and the formation of

aggregates or precipitates under conditions of reduced colloidal stability [150], [151]. Furthermore, changes in HA amount were associated with differences in the dispersion behavior of the particles such as nanoparticle size and zeta potential; this emphasizes the importance of optimizing HA content in nanoparticle-based systems [152], [153].

Chemical changes in the MSN based particles were examined using the FTIR spectra given in Figure 3.3. The characteristic silica network was identified from the bands located at 1050 cm^{-1} and 791 cm^{-1}, which correspond to asymmetric and symmetric Si–O–Si stretching vibrations. In addition, the signals observed at 3385 cm^{-1} and 1640 cm^{-1} indicate the presence of surface –OH groups and physically retained water molecules [154], [155]. After treatment with APTES, the appearance of bands at 696 cm^{-1} and 1560 cm^{-1}, related to N–H and NH_2 bending modes, showed that amine containing groups had been incorporated onto the MSN surface [156].

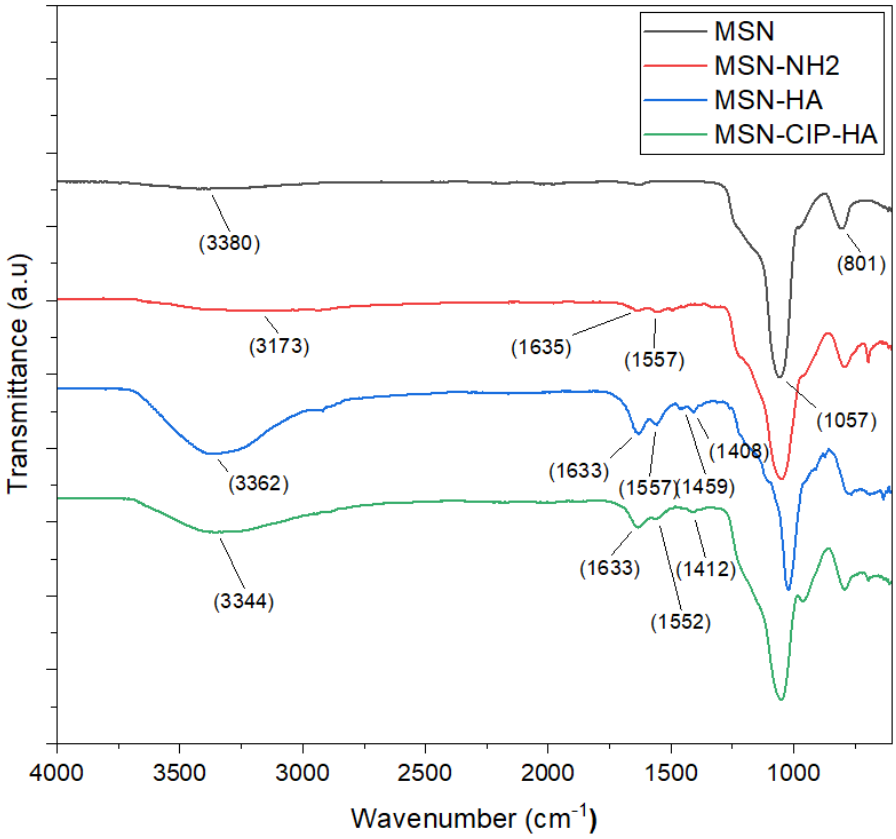


Figure 3.3 FTIR spectra of MSNs and surface modified MSNs samples.

In the MSN–HA spectrum, the signals near 1633 cm^{-1} and within 1410–1459 cm^{-1} indicate the asymmetric and symmetric stretching modes of HA related carboxylate groups ($–COO^-$), showing that HA was introduced onto the MSN surface [157], [158]. For MSN–CIP–HA, these characteristic signals remained visible; however, small shifts and intensity variations appeared in the 1633–1552 cm^{-1} region. The broad absorption in the ~3300–3400 cm^{-1} range, assigned to O–H and N–H stretching, became weaker after CIP incorporation. This change may result from interactions between CIP and the –OH/–NH groups present in the system [159]. Although ciprofloxacin typically exhibits a characteristic carbonyl (C=O) band around ~1700 cm^{-1}, this band may not be clearly observed here, possibly due to overlapping and masking effects caused by the HA coating [160].

Zeta potential and particle size measurements were then used to assess the electrostatic and dispersion behavior of the nanoparticles. The data in Figure 3.4 indicate that surface modification changed the charge characteristics of the particles. Bare MSNs had a negative zeta potential value of −33 mV, mainly arising from deprotonated surface silanol groups [161].

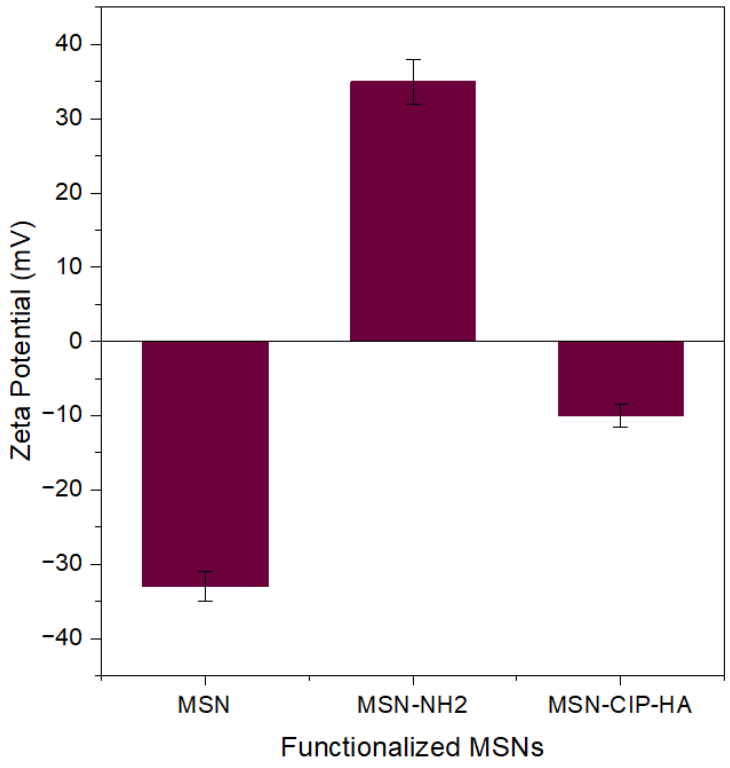


Figure 3.4 Zeta potential analysis of MSNs.

Following amine functionalization, the surface charge shifted to the positive direction due to the amine ($–NH_2$ / $–NH_3^+$ under physiological conditions) groups introduced to the surface, and the zeta potential increased to +35 mV [162]. In ciprofloxacin loaded and HA coated MSNs, the surface charge has become negative again due to the carboxyl ($–COOH$ / $–COO^-$) groups of the HA present on the surface, and the zeta potential has been determined as −10 mV [161], [162], [163], [164].

Regarding particle size distribution analysis, MSNs exhibited a distribution peak at approximately 248 nm, as shown in Figure 3.5. This finding shows that the sizes of the synthetic MSNs are between 200 and 300 nm, which is in line with what other studies have shown about MSN sizes [162]. MSN size is also consistent with the sizes of MSNs observed in TEM and SEM results.

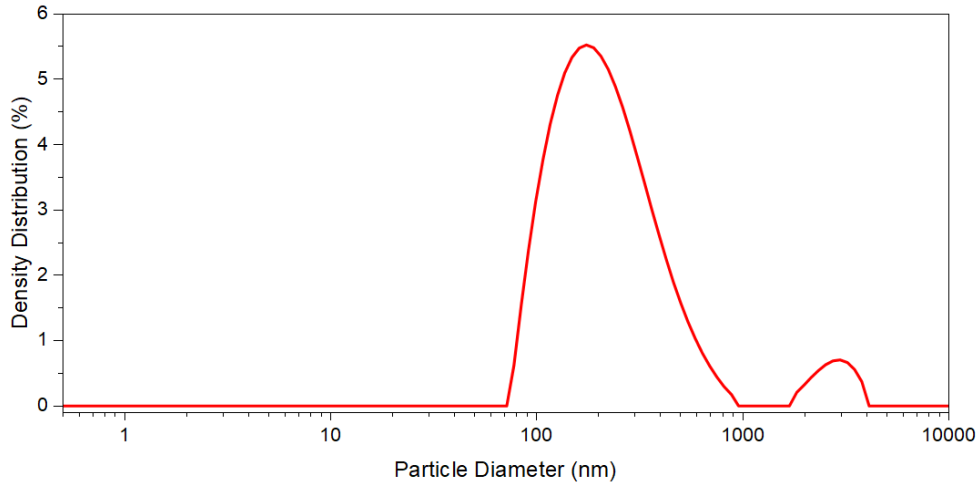


Figure 3.5 Size distribution of MSNs.

The pore related properties of the prepared MSNs were investigated by BET analysis, as presented in Table 3.1. The results indicate the formation of an open mesoporous network with large accessible surface area and pore volume, supporting the suitability of the particles for drug incorporation [163], [164]. Following HA coating, a decrease of approximately 65.5% in BET surface area, approximately 57.6% in total pore volume, and approximately 60.8% in total pore volume calculated using Density Functional Theory (DFT) was observed.

Table 3.1 Main BET parameters of MSN and MSN-HA

Parameter	MSN	MSN-HA
BET surface area	730.03 m^2/g	251.53 m^2/g
Total pore volume	0.643 cm^3/g	0.273 cm^3/g
Average pore width	3.52 nm	4.34 nm
DFT total pore volume	0.5915 cm^3/g	0.2317 cm^3/g

These significant decreases indicate that the HA layer covers the MSN surface and partially restricts the pore entrances or internal surface area accessible via nitrogen adsorption. In contrast, a limited increase in the average pore width was observed. This increase can be explained not by the physical expansion of the pores, but rather by the partial closure of small or narrow pores following the HA coating and a shift in the measurable pore population toward larger pores. Therefore, the BET results support the conclusion that the HA coating reduces the accessible pore volume without eliminating the mesoporous structure of MSN and creates a barrier effect that could contribute to controlled drug release.

Overall, the results obtained from the structural, morphological, and surface characterization analyses collectively confirmed the successful synthesis of MSNs, the introduction of amino groups onto their surfaces, and the subsequent deposition of the HA layer. These findings demonstrate that the developed particles possess the required surface properties and structural features for further application as coating materials on Ti surfaces in drug incorporation and release studies

3.2 Characterization of Coated Ti Plates

The surface morphology of Ti samples prepared under different EPD parameters was examined by SEM, and the corresponding images are given in Figure 3.6. The surface coated at 30 V for 3 min using MSN–CIP–HA particles prepared with an MSN:HA ratio of 1:4 is presented in Figure 3.6b. At this high HA content, distinct

spherical MSN structures could not be clearly identified on the surface. This morphology suggests that excess HA promoted bridging and agglomeration between the particles rather than forming a discrete layer around individual MSNs, causing the particles to remain embedded within the coating matrix and resulting in a more uniform and continuous surface appearance.

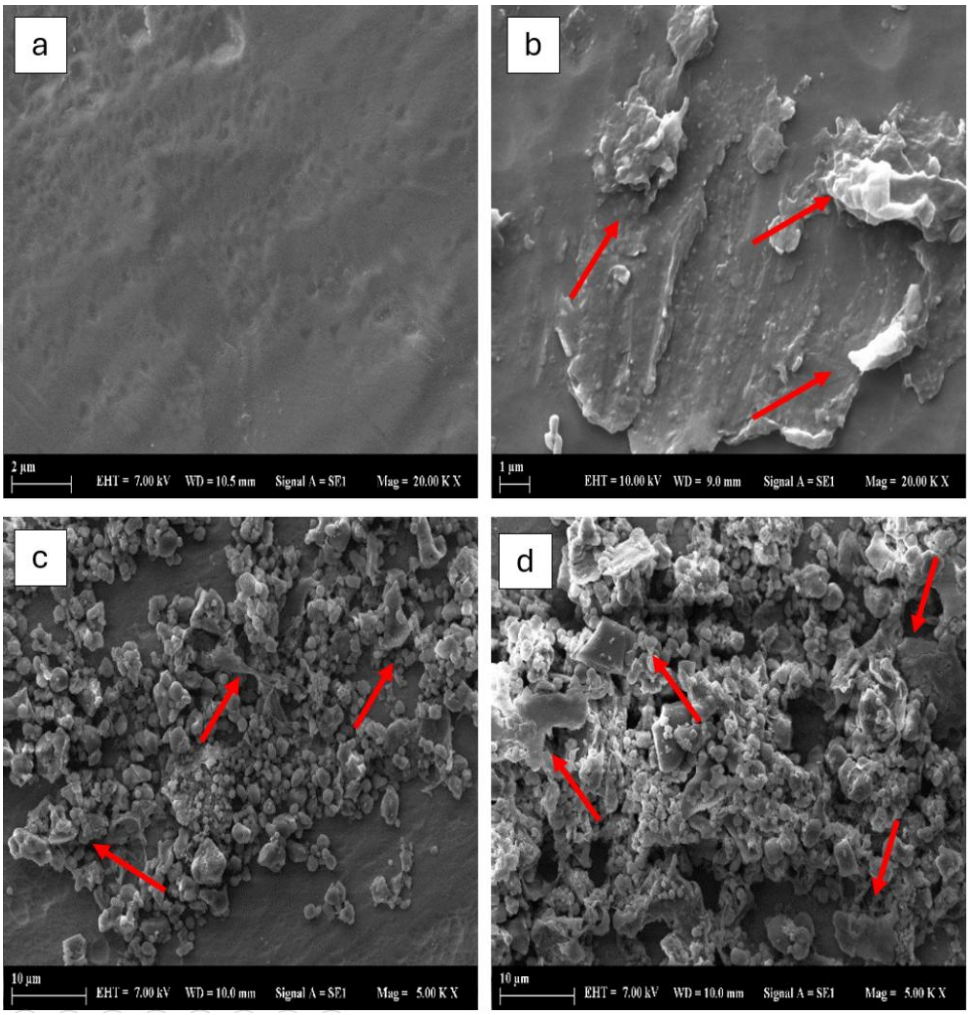


Figure 3.6 SEM images of (a) bare Ti, (b) 30 V-3 min coated Ti (MSN:HA = 1:4), (c) 30 V-3 min coated Ti (MSN:HA = 1:0.5) and (d) 30 V- 5-min coated Ti (MSN:HA = 1:0.5), where arrows indicates block like structures formed due to nanoparticle agglomeration.

Figures 3.6c and 3.6d represent the samples deposited for 3 and 5 min, respectively, under an applied voltage of 30 V, using MSN–CIP–HA particles prepared with an MSN:HA ratio of 1:0.5. Under these conditions, the particulate nature of the coating became more apparent, and spherical structures could be distinguished more

clearly. A comparison of Figures 3.6c and 3.6d further indicates that increasing the coating time enhanced surface coverage, resulting in a thick and more homogeneously coated area after 5 min compared to 3 min. Moreover, comparison of Figures 3.6b and 3.6c, obtained under the same deposition conditions but with different MSN:HA ratios, highlights the significant effect of HA content on coating morphology. While the 1:4 ratio led to a coating in which the particles were largely embedded within the matrix, reducing the HA amount to a ratio of 1:0.5 produced a more distinct particulate morphology. Nevertheless, some agglomerated and fused regions were still observed at this ratio, although less prominently than in the 1:4 sample. Based on these findings, an MSN:HA ratio of 1:0.25 was also evaluated, and coatings with lower HA content were preferred in subsequent drug release studies.

The cross-sectional SEM images given in Figure 3.7 also show that the Ti substrate was covered by an uninterrupted coating layer. Thickness measurements obtained from these cross-sectional images revealed that the coating prepared at 30 V for 3 min (Figure 3.7a) had a thickness of approximately 2.34 µm, whereas the thickness increased to approximately 5.4 µm for the sample obtained after 5 min of deposition under 30 V (Figure 3.7b). These findings indicate that prolonging the coating time promoted the deposition of a thicker layer, which follows the trend described in previous studies [165].

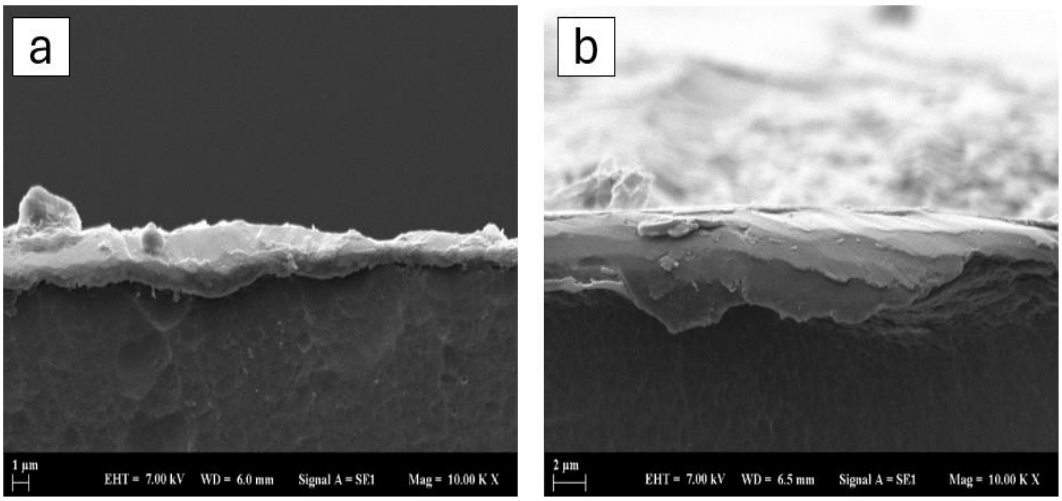


Figure 3.7 Cross sectional SEM images of (a) 3-min-coated and (b) 5-min-coated Ti surfaces.

Changes in surface wettability after modification were evaluated by measuring the contact angle of bare Ti, Ti–MSN, and Ti–MSN–HA surfaces (Figure 3.8). The measured contact angle values were 38.29° for bare Ti, 28.84° for Ti–MSN, and 23.41° for Ti–MSN–HA.

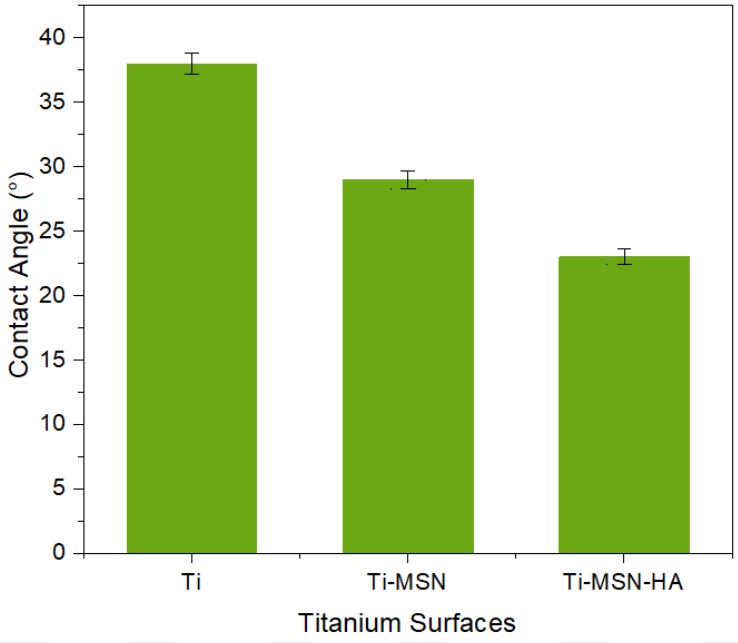


Figure 3.8 Contact angle analysis of Ti plates.

When the contact angle becomes smaller, the droplet covers a larger area on the surface, reflecting improved wettability and therefore reflects enhanced wettability or hydrophilicity (Figure 3.9) [166]. In this respect, the bare Ti surface exhibited lower wettability than the coated samples, whereas the reduced contact angle observed for the Ti–MSN surface suggests that MSN coating imparted a more hydrophilic character to the surface. Previous studies have described a similar trend, suggesting that water interaction with silica-based surfaces is strongly influenced by chemical properties such as the density of surface hydroxyl/silanol groups and their protonation–deprotonation state [167]. The lowest contact angle was recorded for the Ti–MSN–HA surface, indicating the highest hydrophilicity among the tested groups. HA contains carboxyl and hydroxyl functionalities that may increase the tendency of the coated surface to interact with water and confer a distinctly hydrophilic character to the surface [168].

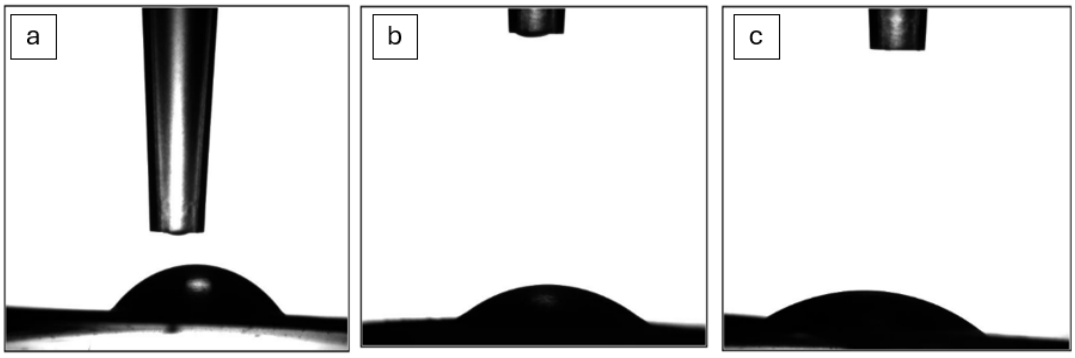


Figure 3.9 Contact angle analysis of (a) Ti-Bare, (b) Ti-MSN, and (c) Ti-MSN-HA surfaces.

To assess coating induced changes in the surface profile, optical profilometry measurements were included. The uncoated Ti surface was used as the reference and compared with the sample produced by EPD for 5 min at 30 V. Qualitative comparison of the three-dimensional surface maps showed that the directional features of the Ti substrate remained visible after coating; however, the coated surface exhibited a more uniform height distribution and less pronounced asperities (Figure 3.10).

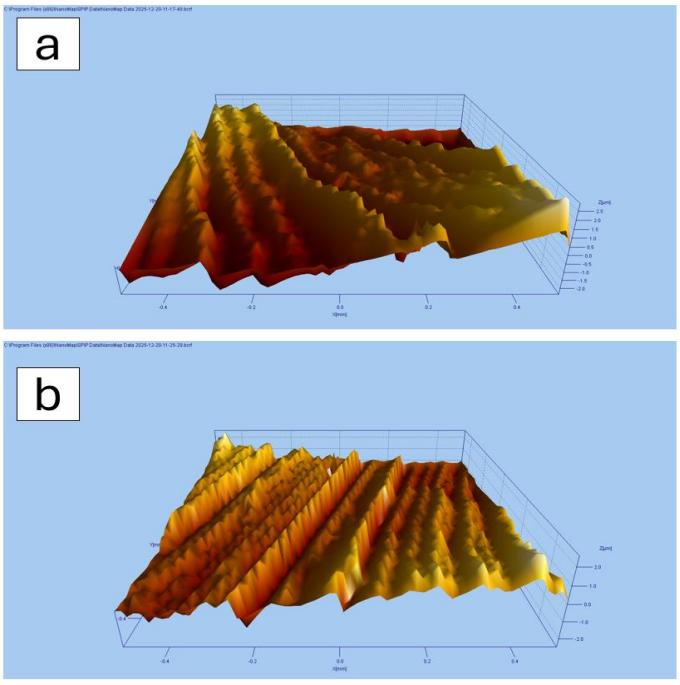


Figure 3.10 Three-dimensional optical profilometry images of (a) uncoated Ti and (b) coated Ti surfaces used for comparison of surface topography.

The three-dimensional areal surface parameters were interpreted in line with observations from prior studies [169], [170], [171]. In agreement with these observations, the decreases in Sa (arithmetic mean height) and Sq (root mean square height) by approximately 26% and 27%, respectively, indicate a clear reduction in overall surface roughness, suggesting that the coating partially filled the surface asperities. This smoothing effect is further supported by the decrease in Sz (maximum height), reflecting the suppression of extreme peak and valley features. Moreover, the marked decrease in Sku (kurtosis) from about 28 to nearly 3 indicates a more homogeneous height distribution with reduced sharp topographical irregularities. In contrast, the increase in Sdr (developed interfacial area ratio) suggests that the coating introduced additional micro/nanoscale features, thereby increasing the effective surface area despite the overall reduction in roughness. These findings show that the coating smooths the Ti surface while also increasing micro/nanoscale surface complexity.

Collectively, the results obtained from the morphological, wettability, and surface topography analyses confirmed the successful deposition of the MSN–CIP–HA coating onto the Ti surface. The observed changes in surface morphology, coating thickness, contact angle, and data obtained from optical profilometry revealed that Ti surface features were markedly reshaped after coating. This suggests that the coated Ti surfaces possess suitable structural and surface features for subsequent drug loading/release and biological performance studies.

3.3 Drug Loading and Drug Release Studies

Evaluation of ciprofloxacin loading and release required a calibration plot prepared from known ciprofloxacin concentrations, as presented in Figure 3.11. The concentration absorbance relationship obtained from this plot was used as the basis for later calculations. Thus, ciprofloxacin amounts in the loaded particles and release media were determined from the absorbance values measured at 270 nm.

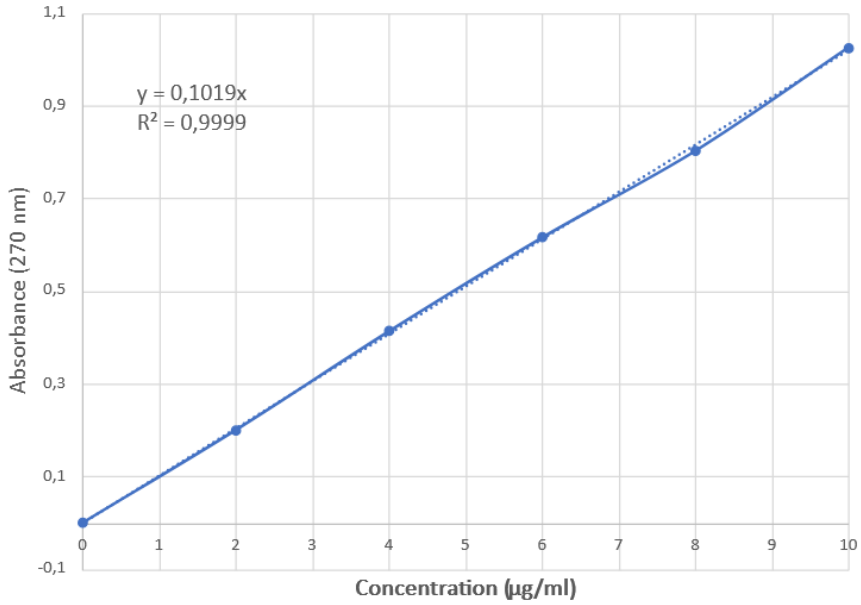


Figure 3.11 Calibration curve of ciprofloxacin.HCl.

The drug loading efficiencies obtained at pH 5 and pH 9 are shown in Figure 3.12. When the loading process was carried out at pH 5, the drug loading efficiency was calculated as 15%, whereas a markedly higher loading efficiency of 73% was obtained at pH 9. This pronounced difference can be attributed to the pH dependent change in the ionic form of ciprofloxacin, which exhibits a zwitterionic structure [172], [173]. During the drug loading stage, amine functionalized MSN (MSN–NH_2) was used, and as indicated by the zeta potential analysis, these particles possess a positively charged surface. At pH 5, ciprofloxacin predominantly exists in its cationic form, creating charge based repulsive interactions among the positively charged drug molecules and the MSN–NH_2 surface. As a result, drug loading remained limited, with an efficiency of approximately 15%. In contrast, at pH 9, the anionic form of ciprofloxacin becomes dominant, promoting electrostatic attraction between ciprofloxacin and the positively charged MSN–NH_2 surface. This interaction led to a substantial increase in drug loading, with the loading efficiency reaching 73%. Based on this result, subsequent drug loading studies were carried out at pH 9.

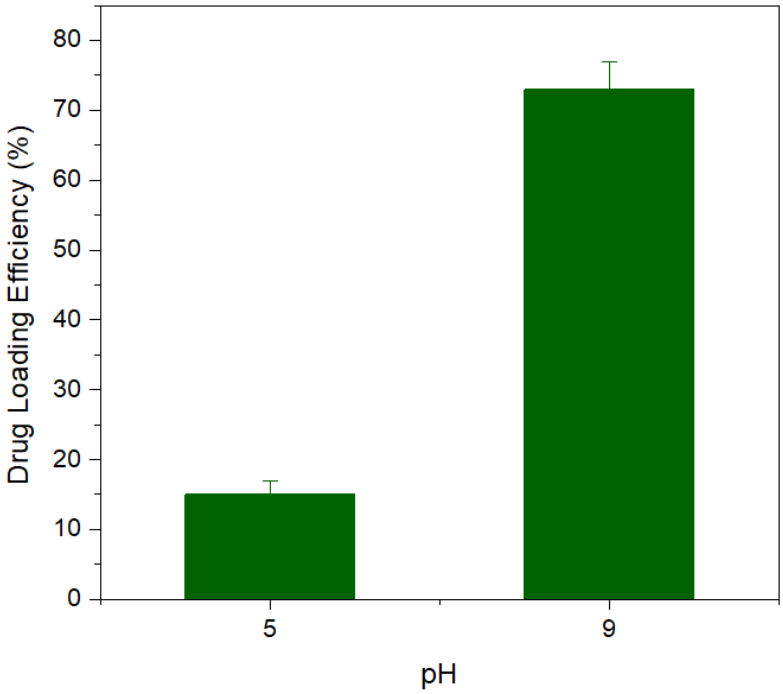


Figure 3.12 Drug loading efficiency (%).

Following the loading step, the release behavior of free MSN particles was examined in vitro. The cumulative profiles obtained during HA optimization are given in Figure 3.13, where the pH 5 release data are shown for MSN:HA ratios of 1:4, 1:0.5, and 1:0.25. In the absence of HAse, the cumulative drug release at 72 h was 5.31%, 8.86%, and 16.82% for MSN-4xHA, MSN-0.5xHA, and MSN-0.25xHA, respectively. These results indicate that drug release increased as the HA amount decreased, likely due to weakening of the diffusion barrier. In the HAse containing groups, the enzyme was added at the time points indicated by arrows in the graph: 150 U/mL at 0, 2, and 4 h; 300 U/mL at 24 h; and 600 U/mL at 48 and 72 h. In addition, for enzyme additions after 24 h, measurements were repeated 2 h later to assess the short-term enzyme effect. This design explains the stepwise increases observed in the release curves. Although fresh PBS was added after each enzyme treatment, the continued increase in cumulative release suggests that HAse degraded the HA coating and thereby facilitated drug diffusion, as also noted in prior studies [15], [174].

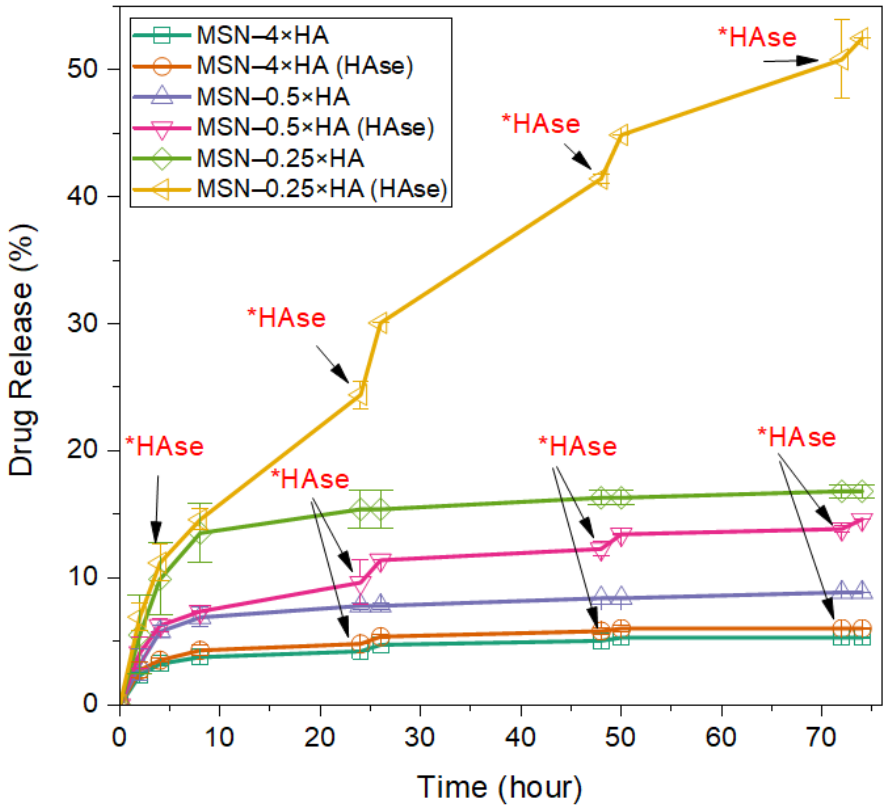


Figure 3.13 Drug release profiles of free MSNs prepared with different MSN:HA ratios. The sample labels MSN-4XHA, MSN-0.5XHA, and MSN-0.25XHA correspond to MSN:HA ratios of 1:4, 1:0.5, and 1:0.25, respectively. The arrows in the drug release profiles indicate the time points of HAse addition.

At 72 h, the cumulative release values in the enzyme containing groups were 6.00%, 14.61%, and 52.45% for MSN-4xHA, MSN-0.5xHA, and MSN-0.25xHA, respectively. For each formulation, the higher release observed in the presence of HAse indicates that the enzyme accelerated drug release by degrading the HA layer. Moreover, as the HA amount decreased, the thinner barrier likely allowed more effective enzyme penetration, resulting in greater degradation and a more pronounced release increase. Among all groups, the MSN:HA ratio of 1:0.25 showed the highest release under both enzymatic and non-enzymatic conditions. Considering its more favorable release profile together with the aim of obtaining a more homogeneous coating without excessive thickening or agglomeration, this ratio was selected for the subsequent stages of the study.

After HA optimization, drug release studies were conducted on drug loaded free MSNs (MSN–CIP) and HA-coated MSNs (MSN–CIP–HA) under conditions with and without HAse, and the cumulative drug release results are presented in Figure 3.14. The release tests were designed to compare two biologically relevant media. A pH value of 7.4 was selected to reflect normal physiological surroundings, while pH 5 was used to model the acidic environment that can occur around infected or biofilm covered sites [175]. These pH values were selected to evaluate release behavior under both normal and infection related conditions, while the enzyme effect was assessed at both pH levels because HAse activity may be enhanced under acidic conditions [176].

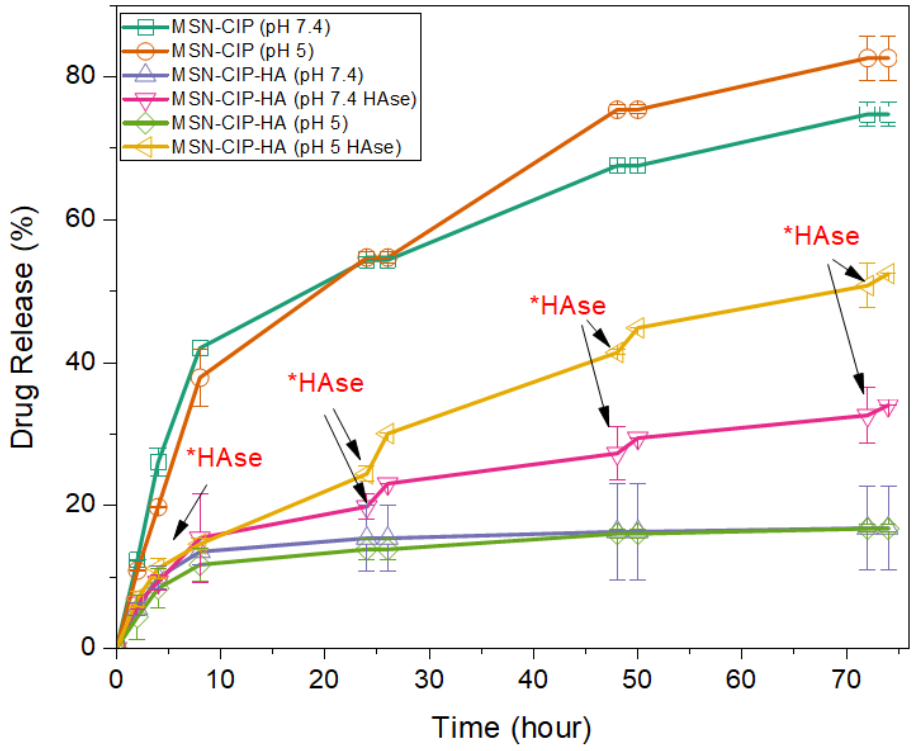


Figure 3.14 Comparison of enzyme responsive drug release from HA coated and uncoated free MSN nanoparticles. The arrows in the drug release profiles indicate the time points of HAse addition.

In the uncoated MSN–CIP group, the cumulative drug release at 72 h reached 74.78% at pH 7.4 and 82.63% at pH 5, which can be attributed to the open pore structure allowing diffusion with minimal barrier. In contrast, the MSN–CIP–HA groups showed substantially lower release, with cumulative values after 72 h, the

released amount reached 16.76% under pH 7.4 and 16.82% under pH 5 conditions, indicating that the HA coating partially blocked the pore outlets, limited diffusion, and suppressed burst release, thereby providing a more controlled release profile. When HAse was added, at the 72 h time point, cumulative release reached 34.04% under pH 7.4 conditions and increased further to 52.45% in the pH 5 medium. This marked increase compared with the corresponding enzyme free HA coated groups indicates that HAse degraded the HA layer and thereby facilitated drug diffusion. The more pronounced increase observed at pH 5 further suggests that enzymatic degradation of HA was more effective under acidic conditions. In addition to enzyme activity, the pH dependent release behavior may also be influenced by changes in ciprofloxacin ionization and solubility, the swelling and diffusion properties of the HA layer, and adsorption–desorption interactions on the MSN surface [173], [177], [178], [179]. Overall, these findings demonstrate that HA coating enabled controlled release under baseline conditions, whereas HAse triggered degradation of the HA layer promoted increased drug release when needed.

As described in the previous sections, HA optimization was performed on free MSNs by investigating different MSN:HA ratios. Based on these findings, the most suitable HA coating condition was identified, and drug release studies were subsequently conducted on both HA coated and uncoated free MSNs. Subsequently, drug loaded and HA coated free MSN particles were deposited onto Ti surfaces via EPD, followed by the evaluation of drug release behavior from the coated Ti substrates. A constant voltage of 30 V was applied during EPD, and the deposition time was varied as 1, 3, and 5 min. However, when the SEM images and release data were evaluated together, the 30 V–5 min condition was found to provide a more homogeneous coating and a more suitable release profile than the other groups. Therefore, this coating condition was selected for the subsequent stages of the study. In the release studies performed with free particles in suspension, cumulative drug release could be expressed as a percentage because the amount of loaded drug was known. In contrast, for the Ti coated samples, the mass of the MSN–CIP–HA coating adhered to the surface could not be directly quantified. For coated Ti samples, the release data were evaluated using the

absolute amount of ciprofloxacin released (µg), rather than percentage based cumulative release. Figure 3.15 compares the release behavior of the coated surfaces in pH 7.4 and pH 5 media under HAse free and HAse containing conditions.

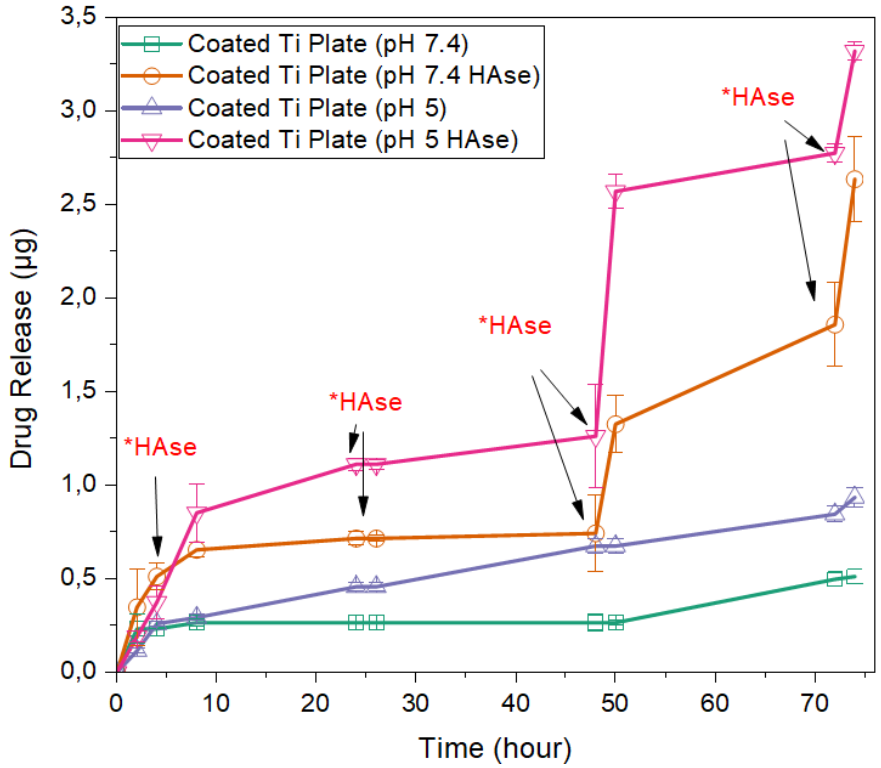


Figure 3.15 Enzyme responsive drug release from 30 V 5 min coated Ti surfaces. The arrows in the drug release profiles indicate the time points of HAse addition.

Since Ti surfaces were coated only with MSN–CIP–HA particles, the graph does not include a separate MSN–CIP coated Ti group. The results indicated that enzyme addition markedly increased drug release under both pH conditions. After 72 h, the ciprofloxacin amount measured in the pH 7.4 medium increased from 0.51 µg in the enzyme free group to 2.63 µg in the presence of HAse. Similarly, at pH 5, the release amount increased from 0.93 µg without enzyme to 3.31 µg with enzyme. These findings indicate that HAse degraded the HA coating, reduced its barrier effect, and thereby facilitated drug diffusion. Moreover, the greater increase observed at pH 5 suggests that enzymatic degradation and/or matrix–drug interactions were more strongly affected under acidic conditions.

3.4 Antibacterial Activity Test

The antibacterial results revealed distinct adhesion and colonization behaviors on the tested Ti surfaces against *Escherichia coli* and *Staphylococcus aureus*. In particular, the higher CFU values observed for *S. aureus* are consistent with previous reports showing that this bacterium adheres more readily to implant surfaces because of its strong adhesins and pronounced biofilm forming capacity (Figure 3.16) [180], [181].

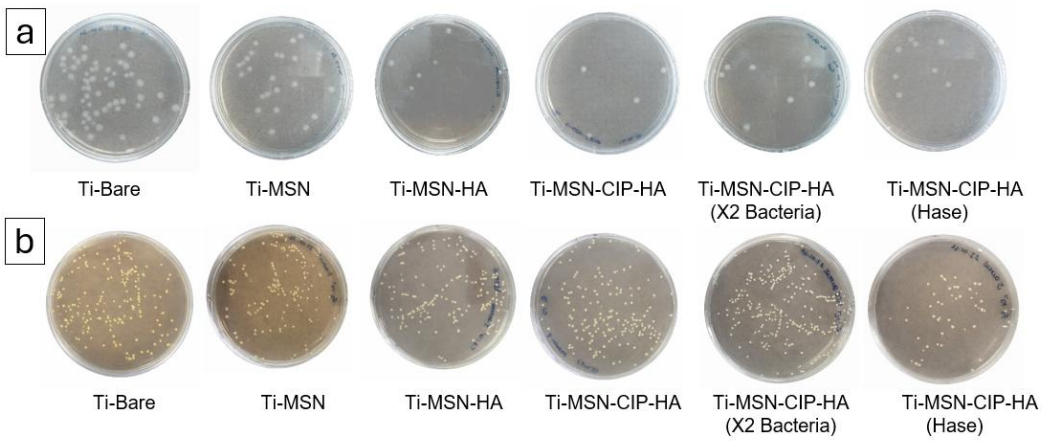


Figure 3.16 Antibacterial activity of various Ti surfaces: (a) Colonization of *E. coli* on various Ti surfaces; (b) Colonization of *S. aureus* on various Ti surfaces.

Although MSNs are primarily described in the literature as carrier systems rather than intrinsically potent antibacterial agents, they may still contribute to reduced initial bacterial adhesion by modifying surface wettability and nano topography [182], [183]. Similarly, HA coating does not exert a direct bactericidal effect; instead, it creates a water rich surface layer that acts against fouling by limiting protein accumulation, bacterial settlement, and the later development of biofilm [184], [185], [186]. As reflected in Figures 3.16–3.18, the response to the HA layer varied between *E. coli* and *S. aureus,* which may be related to species dependent differences in how they adhere to the surface. Adhesion of *E. coli,* a representative Gram-negative bacterium, has been reported to decrease on hydrophilic and negatively charged surfaces, whereas *S. aureus* can more effectively overcome passive anti adhesive barriers through MSCRAMM mediated interactions and its strong biofilm forming ability [186], [187], [188].

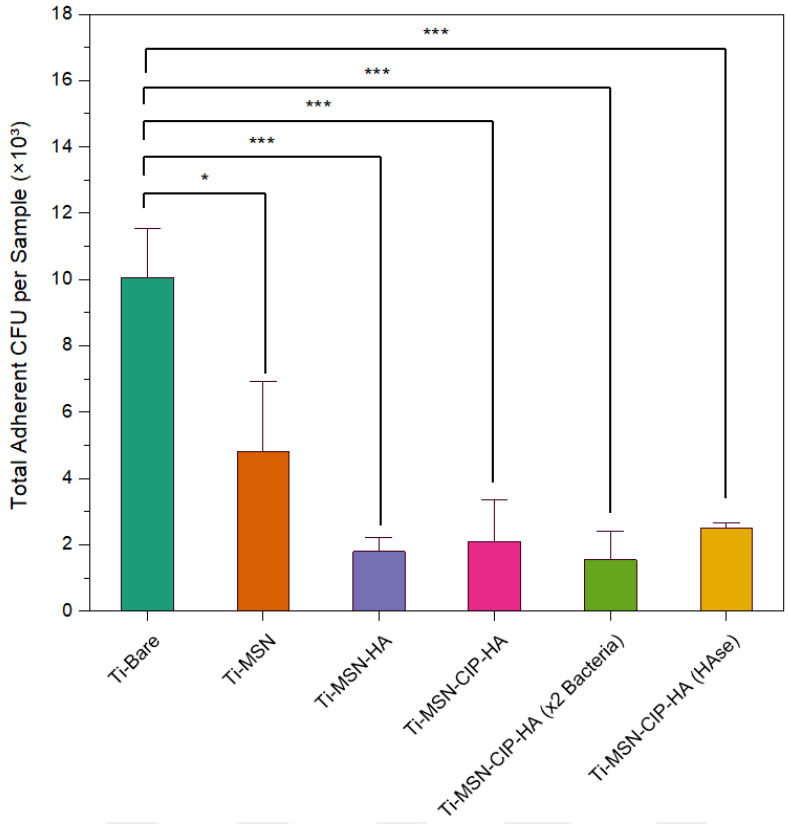


Figure 3.17 Quantitative assessment of bacterial colony forming units (CFUs) for *E. coli* on various Ti surfaces (***p < 0.005).

Moreover, the similar antibacterial performance of the MSN–HA and MSN–CIP–HA groups suggests that the effect observed in the MSN–CIP–HA group cannot be attributed solely to ciprofloxacin release. The limited change observed in the MSN–CIP–HA (×2 bacteria) group may also be related to species specific enzyme production, since *E. coli* produces little or no HAse and therefore would not be expected to markedly enhance HA degradation or enzyme triggered drug release even at higher inoculum levels [189]. However, this does not mean that the enzyme-responsive concept is only valid for all bacterial species equally, since not all bacteria are required to produce hyaluronidase or to produce it at comparable levels. Instead, the degree of system activation depends on the enzyme profile of the target microorganism and the local infection microenvironment. In contrast, *S. aureus* is capable of producing HAse, which may promote HA degradation and thereby accelerate drug release; however, this advantage may be partially counterbalanced by the higher initial bacterial burden and faster biofilm formation associated with

the inoculum effect [190], [191], [192], [193]. Therefore, the HAase-responsive behavior observed in this study should be considered a model enzyme-triggered release strategy rather than a universal response expected from every bacterial strain.

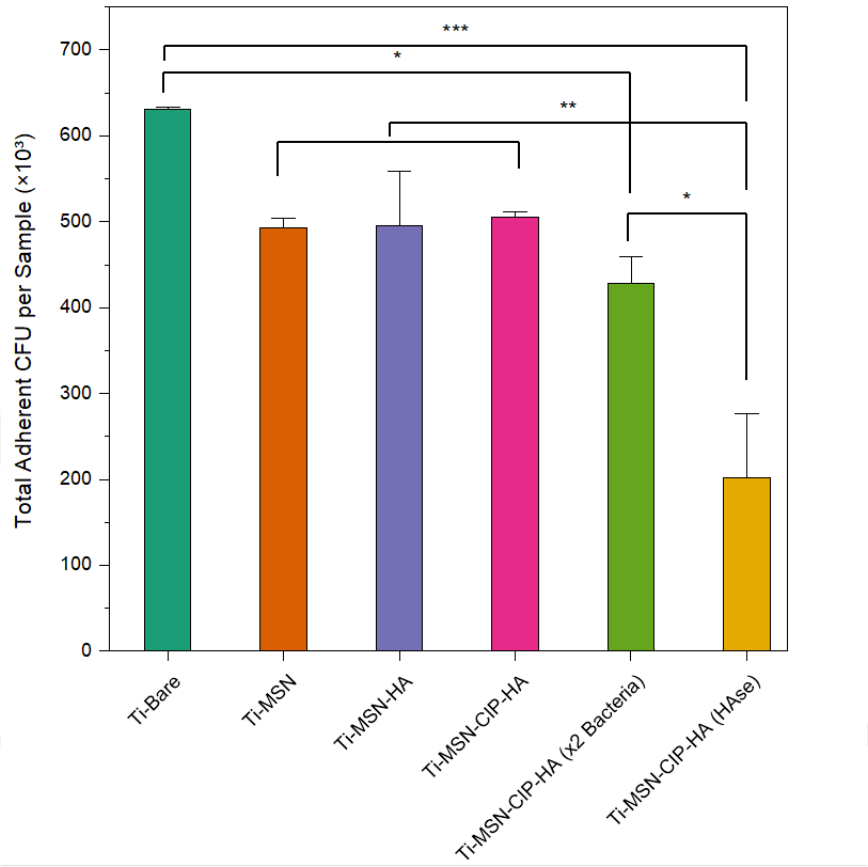


Figure 3.18 Quantitative assessment of bacterial colony forming units (CFUs) for *S. aureus* on various Ti surfaces (***$p < 0.005$).

Notably, the MSN–CIP–HA (HAse) group showed the most pronounced reduction in viable *S. aureus* cells, indicating that controlled external HAse addition effectively degraded the HA layer and promoted enzyme triggered ciprofloxacin release. By contrast, a comparable enhancement was not observed for *E. coli*, which may be explained by the permeability barrier of its lipopolysaccharide containing outer membrane that restricts antibiotic entry and reduces ciprofloxacin efficacy in Gram negative bacteria [194]. This also suggests that similar enzyme-responsive coating platforms could be further adapted by selecting other enzyme-degradable

gatekeepers or coatings, as well as different antibacterial agents, according to the dominant bacterial species and infection-related triggers.

Based on these findings, the MSN–CIP–HA coating can be considered a functional coating system capable of providing controlled drug release on implant surfaces, particularly under enzymatic conditions where its antibacterial efficacy is enhanced.

4
CONCLUSION

Infections developing around implants remain a serious challenge in clinical practice owing to bacterial adhesion, biofilm development, and the limited performance of conventional antibiotic releasing coatings. In many currently available systems, uncontrolled drug release under noninfectious conditions may result in unnecessary antibiotic exposure and diminished therapeutic benefit. In the present study, HAse responsive ciprofloxacin loaded MSNs were successfully fabricated and deposited onto Ti surfaces as a functional coating using the electrophoretic deposition method. At physiological pH, HA modified MSNs prevented ciprofloxacin from being released rapidly during the initial stage, while allowing markedly increased antibiotic release in enzyme rich environments simulating infection. Surface analyses verified the formation of a uniform and hydrophilic coating, which not only improved surface wettability but also helped reduce bacterial adhesion. In addition, when HAse triggered release was activated, the coated surfaces showed stronger antibacterial behavior, most noticeably against *S. aureus.* However, the strain dependent differences in bacterial response suggest that the effectiveness of the coating is also shaped by the intrinsic properties of the microorganism. Taken together, these results suggest that the developed coating offers a dual function approach by integrating passive anti adhesive surface characteristics with active infection responsive antibiotic delivery. This performance underscores the promise of HA coated MSN based coatings as smart implant surface modifications that can reduce unnecessary drug exposure while enhancing localized antibacterial effectiveness.

Consequently, although the coating system developed in this study exhibits promising properties, it also has certain limitations. Since the findings are largely based on in vitro conditions, the system's long-term stability, efficacy, and reliability in biological environments must be validated through advanced in vivo studies. In addition, the exact amount of particles deposited on the titanium surface could not be directly quantified. Therefore, the precise amount of ciprofloxacin incorporated into the coating could not be determined, and the drug release results from coated samples were evaluated based on the cumulative amount of released drug rather than percentage release. This represents an important limitation for accurately comparing coating efficiency and release performance. Moreover, the antibacterial performance of the coating was strain-dependent, indicating that its efficacy may vary depending on the bacterial species or strain tested. Therefore, future studies should evaluate the system against a broader range of clinically relevant microorganisms. Additionally, critical application-related properties include how the coating responds to mechanical stress, how it withstands wear, and whether it can preserve strong adhesion to the implant surface during long-term use. Furthermore, more accurate control over the rate and extent of drug release, as well as improved adaptability to different physiological conditions, is a key requirement for future studies. In future research, the system's performance may be further enhanced by incorporating different therapeutic agents and optimizing the coating architecture. Finally, a comprehensive examination of parameters such as biocompatibility, toxicity, and immune response is of critical importance during the transition to clinical application.

REFERENCES

[1] J. Quinn, R. McFadden, C.-W. Chan, and L. Carson, "Titanium for Orthopedic Applications: An Overview of Surface Modification to Improve Biocompatibility and Prevent Bacterial Biofilm Formation," *iScience*, vol. 23, no. 11, p. 101745, Nov. 2020, doi: 10.1016/j.isci.2020.101745.

[2] H. Chouirfa, H. Bouloussa, V. Migonney, and C. Falentin-Daudré, "Review of titanium surface modification techniques and coatings for antibacterial applications," *Acta Biomater.*, vol. 83, pp. 37–54, Jan. 2019, doi: 10.1016/j.actbio.2018.10.036.

[3] K. Yang *et al.*, "Unlocking the potential of stimuli-responsive biomaterials for bone regeneration," *Front. Pharmacol.*, vol. 15, Jul. 2024, doi: 10.3389/fphar.2024.1437457.

[4] S. Talebian *et al.*, "Biopolymeric Coatings for Local Release of Therapeutics from Biomedical Implants," *Advanced Science*, vol. 10, no. 12, Apr. 2023, doi: 10.1002/advs.202207603.

[5] M. U. Joshi, S. P. Kulkarni, M. Choppadandi, M. Keerthana, and G. Kapusetti, "Current state of art smart coatings for orthopedic implants: A comprehensive review," *Smart Mater. Med.*, vol. 4, pp. 661–679, 2023, doi: 10.1016/j.smaim.2023.06.005.

[6] S. Asadi *et al.*, "Ciprofloxacin-Loaded Titanium Nanotubes Coated with Chitosan: A Promising Formulation with Sustained Release and Enhanced Antibacterial Properties," *Pharmaceutics*, vol. 14, no. 7, p. 1359, Jun. 2022, doi: 10.3390/pharmaceutics14071359.

[7] Y. He *et al.*, "A Novel Antibacterial Titanium Modification with a Sustained Release of Pac-525," *Nanomaterials*, vol. 11, no. 12, p. 3306, Dec. 2021, doi: 10.3390/nano11123306.

[8] C. Guo *et al.*, "Poly-lysine/Sodium Alginate Coating Loading Nanosilver for Improving the Antibacterial Effect and Inducing Mineralization of Dental Implants," *ACS Omega*, vol. 5, no. 18, pp. 10562–10571, May 2020, doi: 10.1021/acsomega.0c00986.

[9] F. Ghilini *et al.*, "Highly Stabilized Nanoparticles on Poly-Lysine-Coated Oxidized Metals: A Versatile Platform with Enhanced Antimicrobial Activity," *ACS Appl. Mater. Interfaces*, vol. 10, no. 28, pp. 23657–23666, Jul. 2018, doi: 10.1021/acsami.8b07529.

[10] W. Ahmed, Z. Zhai, and C. Gao, “Adaptive antibacterial biomaterial surfaces and their applications,” *Mater. Today Bio*, vol. 2, p. 100017, Mar. 2019, doi: 10.1016/j.mtbio.2019.100017.

[11] T. Wang *et al.*, “Nanovalves-Based Bacteria-Triggered, Self-Defensive Antibacterial Coating: Using Combination Therapy, Dual Stimuli-Responsiveness, and Multiple Release Modes for Treatment of Implant-Associated Infections,” *Chemistry of Materials*, vol. 29, no. 19, pp. 8325–8337, Oct. 2017, doi: 10.1021/acs.chemmater.7b02678.

[12] Y. Yang, X. Jiang, H. Lai, and X. Zhang, “Smart Bacteria-Responsive Drug Delivery Systems in Medical Implants,” *J. Funct. Biomater.*, vol. 13, no. 4, p. 173, Oct. 2022, doi: 10.3390/jfb13040173.

[13] M. Colilla and M. Vallet-Regí, “Targeted Stimuli-Responsive Mesoporous Silica Nanoparticles for Bacterial Infection Treatment,” *Int. J. Mol. Sci.*, vol. 21, no. 22, p. 8605, Nov. 2020, doi: 10.3390/ijms21228605.

[14] Y. Wu *et al.*, “Layer-by-Layer (LBL) Self-Assembled Biohybrid Nanomaterials for Efficient Antibacterial Applications,” *ACS Appl. Mater. Interfaces*, vol. 7, no. 31, pp. 17255–17263, Aug. 2015, doi: 10.1021/acsami.5b04216.

[15] M. Zhang *et al.*, “A Hyaluronidase-Responsive Nanoparticle-Based Drug Delivery System for Targeting Colon Cancer Cells,” *Cancer Res.*, vol. 76, no. 24, pp. 7208–7218, Dec. 2016, doi: 10.1158/0008-5472.CAN-16-1681.

[16] E. Avcu, F. E. Baştan, H. Z. Abdullah, M. A. U. Rehman, Y. Y. Avcu, and A. R. Boccaccini, “Electrophoretic deposition of chitosan-based composite coatings for biomedical applications: A review,” *Prog. Mater. Sci.*, vol. 103, pp. 69–108, Jun. 2019, doi: 10.1016/j.pmatsci.2019.01.001.

[17] R. Song, M. Murphy, C. Li, K. Ting, C. Soo, and Z. Zheng, “Current development of biodegradable polymeric materials for biomedical applications,” *Drug Des. Devel. Ther.*, vol. Volume 12, pp. 3117–3145, Sep. 2018, doi: 10.2147/DDDT.S165440.

[18] M. S. Birajdar, H. Joo, W.-G. Koh, and H. Park, “Natural bio-based monomers for biomedical applications: a review,” *Biomater. Res.*, vol. 25, no. 1, Feb. 2021, doi: 10.1186/s40824-021-00208-8.

[19] K. M. Agarwal, P. Singh, U. Mohan, S. Mandal, and D. Bhatia, “Comprehensive study related to advancement in biomaterials for medical applications,” *Sensors International*, vol. 1, p. 100055, 2020, doi: 10.1016/j.sintl.2020.100055.

[20] A. Bharadwaj, “An Overview on Biomaterials and Its Applications in Medical Science,” *IOP Conf. Ser. Mater. Sci. Eng.*, vol. 1116, no. 1, p. 012178, Apr. 2021, doi: 10.1088/1757-899X/1116/1/012178.

[21] S. Iqbal *et al.*, “Biomaterials evolution: from inert to instructive,” *Biomater. Sci.*, vol. 11, no. 18, pp. 6109–6115, 2023, doi: 10.1039/D3BM00322A.

[22] E. T. J. Chong, J. W. Ng, and P.-C. Lee, “Classification and Medical Applications of Biomaterials–A Mini Review,” *BIO Integration*, vol. 4, no. 2, 2023, doi: 10.15212/bioi-2022-0009.

[23] P. Baskaran, B. Muthiah, and V. Uthirapathy, “A systematic review on biomaterials and their recent progress in biomedical applications: bone tissue engineering,” *Reviews in Inorganic Chemistry*, vol. 45, no. 4, pp. 747–781, Nov. 2025, doi: 10.1515/revic-2024-0062.

[24] L. Vaiani *et al.*, “Ceramic Materials for Biomedical Applications: An Overview on Properties and Fabrication Processes,” *J. Funct. Biomater.*, vol. 14, no. 3, p. 146, Mar. 2023, doi: 10.3390/jfb14030146.

[25] G. Radenković and D. Petković, “Metallic Biomaterials,” in *Biomaterials in Clinical Practice*, Cham: Springer International Publishing, 2018, pp. 183–224. doi: 10.1007/978-3-319-68025-5_8.

[26] T. Hu *et al.*, “Advances of naturally derived biomedical polymers in tissue engineering,” *Front. Chem.*, vol. 12, Nov. 2024, doi: 10.3389/fchem.2024.1469183.

[27] D. F. Williams, “On the mechanisms of biocompatibility,” *Biomaterials*, vol. 29, no. 20, pp. 2941–2953, Jul. 2008, doi: 10.1016/j.biomaterials.2008.04.023.

[28] A. Arjunan, A. Baroutaji, A. S. Praveen, J. Robinson, and C. Wang, “Classification of Biomaterial Functionality,” in *Encyclopedia of Smart Materials*, Elsevier, 2022, pp. 86–102. doi: 10.1016/B978-0-12-815732-9.00027-9.

[29] P. Parida, A. Behera, and S. C. Mishra, “Classification of Biomaterials used in Medicine,” *International Journal of Advances in Applied Sciences (IJAAS)*, vol. 1, no. 3, pp. 31–35, 2012.

[30] K. Prasad *et al.*, “Metallic Biomaterials: Current Challenges and Opportunities,” *Materials*, vol. 10, no. 8, p. 884, Jul. 2017, doi: 10.3390/ma10080884.

[31] Q. Chen and G. A. Thouas, “Metallic implant biomaterials,” *Materials Science and Engineering: R: Reports*, vol. 87, pp. 1–57, Jan. 2015, doi: 10.1016/j.mser.2014.10.001.

[32] M. Niinomi, “Metallic biomaterials,” *Journal of Artificial Organs*, vol. 11, no. 3, pp. 105–110, Sep. 2008, doi: 10.1007/s10047-008-0422-7.

[33] G. Manivasagam, D. Dhinasekaran, and A. Rajamanickam, “Biomedical Implants: Corrosion and its Prevention-A Review,” 2010.

[34] L. Mohan and C. Anandan, “Wear and corrosion behavior of oxygen implanted biomedical titanium alloy Ti–13Nb–13Zr,” *Appl. Surf. Sci.*, vol. 282, pp. 281–290, Oct. 2013, doi: 10.1016/j.apsusc.2013.05.120.

[35] M. Long and H. J. Rack, “Titanium alloys in total joint replacement—a materials science perspective,” *Biomaterials*, vol. 19, no. 18, pp. 1621–1639, Sep. 1998, doi: 10.1016/S0142-9612(97)00146-4.

[36] M. Hussein, A. Mohammed, and N. Al-Aqeeli, “Wear Characteristics of Metallic Biomaterials: A Review,” *Materials*, vol. 8, no. 5, pp. 2749–2768, May 2015, doi: 10.3390/ma8052749.

[37] V. S. de Viteri and E. Fuentes, “Titanium and Titanium Alloys as Biomaterials,” in *Tribology - Fundamentals and Advancements*, InTech, 2013. doi: 10.5772/55860.

[38] S. Capuani, G. Malgir, C. Y. X. Chua, and A. Grattoni, “Advanced strategies to thwart foreign body response to implantable devices,” *Bioeng. Transl. Med.*, vol. 7, no. 3, Sep. 2022, doi: 10.1002/btm2.10300.

[39] M. Geetha, A. K. Singh, R. Asokamani, and A. K. Gogia, “Ti based biomaterials, the ultimate choice for orthopaedic implants – A review,” *Prog. Mater. Sci.*, vol. 54, no. 3, pp. 397–425, May 2009, doi: 10.1016/j.pmatsci.2008.06.004.

[40] T. Hanawa, “Metal ion release from metal implants,” *Materials Science and Engineering: C*, vol. 24, no. 6–8, pp. 745–752, Dec. 2004, doi: 10.1016/j.msec.2004.08.018.

[41] S. Bauer, P. Schmuki, K. von der Mark, and J. Park, “Engineering biocompatible implant surfaces,” *Prog. Mater. Sci.*, vol. 58, no. 3, pp. 261–326, Apr. 2013, doi: 10.1016/j.pmatsci.2012.09.001.

[42] R. Davis *et al.*, “A comprehensive review on metallic implant biomaterials and their subtractive manufacturing,” *The International Journal of Advanced Manufacturing Technology*, vol. 120, no. 3–4, pp. 1473–1530, May 2022, doi: 10.1007/s00170-022-08770-8.

[43] A. Bandyopadhyay, I. Mitra, S. B. Goodman, M. Kumar, and S. Bose, “Improving biocompatibility for next generation of metallic implants,” *Prog. Mater. Sci.*, vol. 133, p. 101053, Mar. 2023, doi: 10.1016/j.pmatsci.2022.101053.

[44] M. Niinomi, Y. Liu, M. Nakai, H. Liu, and H. Li, “Biomedical titanium alloys with Young’s moduli close to that of cortical bone,” *Regen. Biomater.*, vol. 3, no. 3, pp. 173–185, Jun. 2016, doi: 10.1093/rb/rbw016.

[45] U. Kamachimudali, T. M. Sridhar, and B. Raj, “Corrosion of bio implants,” *Sadhana*, vol. 28, no. 3–4, pp. 601–637, Jun. 2003, doi: 10.1007/BF02706450.

[46] J. Alvarado, R. Maldonado, J. Marxuach, and R. Otero, “BIOMECHANICS OF HIP AND KNEE PROSTHESES 1,” 2003. [Online]. Available: http://www.ece.uprm.edu/~m_goyal/home.htm

[47] N. Eliaz, “Corrosion of Metallic Biomaterials: A Review,” *Materials*, vol. 12, no. 3, p. 407, Jan. 2019, doi: 10.3390/ma12030407.

[48] M. Kaur and K. Singh, “Review on titanium and titanium based alloys as biomaterials for orthopaedic applications,” *Materials Science and Engineering: C*, vol. 102, pp. 844–862, Sep. 2019, doi: 10.1016/j.msec.2019.04.064.

[49] D. R. Unune, G. R. Brown, and G. C. Reilly, “Thermal based surface modification techniques for enhancing the corrosion and wear resistance of metallic implants: A review,” *Vacuum*, vol. 203, p. 111298, Sep. 2022, doi: 10.1016/j.vacuum.2022.111298.

[50] T. , Albrektsson and C. , Johansson, “Osteoinduction, osteoconduction and osseointegration,” *European Spine Journal*, vol. 10, no. 0, pp. S96–S101, Oct. 2001, doi: 10.1007/s005860100282.

[51] B. Wu, Y. Tang, K. Wang, X. Zhou, and L. Xiang, “Nanostructured Titanium Implant Surface Facilitating Osseointegration from Protein Adsorption to Osteogenesis: The Example of TiO2 NTAs,” *Int. J. Nanomedicine*, vol. Volume 17, pp. 1865–1879, Apr. 2022, doi: 10.2147/IJN.S362720.

[52] M. Viceconti, R. Muccini, M. Bernakiewicz, M. Baleani, and L. Cristofolini, “Large-sliding contact elements accurately predict levels of bone–implant micromotion relevant to osseointegration,” *J. Biomech.*, vol. 33, no. 12, pp. 1611–1618, Dec. 2000, doi: 10.1016/S0021-9290(00)00140-8.

[53] H. J. Busscher *et al.*, “Biomaterial-Associated Infection: Locating the Finish Line in the Race for the Surface,” *Sci. Transl. Med.*, vol. 4, no. 153, Sep. 2012, doi: 10.1126/scitranslmed.3004528.

[54] T. F. Moriarty, A. H. C. Poulsson, E. T. J. Rochford, and R. G. Richards, “4.8 Bacterial Adhesion and Biomaterial Surfaces,” in *Comprehensive Biomaterials II*, Elsevier, 2017, pp. 101–129. doi: 10.1016/B978-0-08-100691-7.00106-3.

[55] A. G. Gristina, “Biomaterial-Centered Infection: Microbial Adhesion Versus Tissue Integration,” *Science (1979).*, vol. 237, no. 4822, pp. 1588–1595, Sep. 1987, doi: 10.1126/science.3629258.

[56] T. F. Moriarty, A. H. C. Poulsson, E. T. J. Rochford, and R. G. Richards, “Bacterial Adhesion and Biomaterial Surfaces,” in *Comprehensive Biomaterials*, Elsevier, 2011, pp. 75–100. doi: 10.1016/B978-0-08-055294-1.00007-6.

[57] R. M. Donlan and J. W. Costerton, “Biofilms: Survival Mechanisms of Clinically Relevant Microorganisms,” *Clin. Microbiol. Rev.*, vol. 15, no. 2, pp. 167–193, Apr. 2002, doi: 10.1128/CMR.15.2.167-193.2002.

[58] H. Y. Ahmadabadi, K. Yu, and J. N. Kizhakkedathu, “Surface modification approaches for prevention of implant associated infections,” *Colloids Surf. B Biointerfaces*, vol. 193, p. 111116, Sep. 2020, doi: 10.1016/j.colsurfb.2020.111116.

[59] R. O. Darouiche, “Antimicrobial Approaches for Preventing Infections Associated with Surgical Implants,” *Clinical Infectious Diseases*, vol. 36, no. 10, pp. 1284–1289, May 2003, doi: 10.1086/374842.

[60] E. Roca-Millan, A. Estrugo-Devesa, A. Merlos, E. Jané-Salas, T. Vinuesa, and J. López-López, “Systemic Antibiotic Prophylaxis to Reduce Early Implant Failure: A Systematic Review and Meta-Analysis,” *Antibiotics*, vol. 10, no. 6, p. 698, Jun. 2021, doi: 10.3390/antibiotics10060698.

[61] A. Montali, “Antibacterial coating systems,” *Injury*, vol. 37, no. 2, pp. S81–S86, May 2006, doi: 10.1016/j.injury.2006.04.013.

[62] C. Li *et al.*, “Recent progress in drug delivery,” *Acta Pharm. Sin. B*, vol. 9, no. 6, pp. 1145–1162, Nov. 2019, doi: 10.1016/j.apsb.2019.08.003.

[63] J. F. Coelho *et al.*, “Drug delivery systems: Advanced technologies potentially applicable in personalized treatments,” *EPMA Journal*, vol. 1, no. 1, pp. 164–209, Mar. 2010, doi: 10.1007/s13167-010-0001-x.

[64] R. Hakala, “Crosslinked poly(ester anhydrides) for controlled drug delivery,” 2013.

[65] N. Sharma, N. Purwar, and P. Chandra Gupta, “Microspheres as drug carriers for controlled drug delivery: a review,” *Sharma et al., IJPSR, 2015; Vol. 6(11): 4579-4587. E-ISSN: 0975-8232; P-ISSN: 2320-5148 International Journal of Pharmaceutical Sciences and Research*, vol. 6, no. 11, p. 11, 2015, doi: 10.13040/IJPSR.0975-8232.6(11).4579-87.

[66] R. Langer, “New Methods of Drug Delivery,” 1990.

[67] Y. H. Yun, B. K. Lee, and K. Park, “Controlled Drug Delivery: Historical perspective for the next generation,” *Journal of Controlled Release*, vol. 219, pp. 2–7, Dec. 2015, doi: 10.1016/j.jconrel.2015.10.005.

[68] G. D. Prestwich and Y. Luo, “Novel biomaterials for drug delivery,” *Expert Opin. Ther. Pat.*, vol. 11, no. 9, pp. 1395–1410, Sep. 2001, doi: 10.1517/13543776.11.9.1395.

[69] S. Adepu and S. Ramakrishna, “Controlled Drug Delivery Systems: Current Status and Future Directions,” *Molecules*, vol. 26, no. 19, p. 5905, Sep. 2021, doi: 10.3390/molecules26195905.

[70] O. S. Fenton, K. N. Olafson, P. S. Pillai, M. J. Mitchell, and R. Langer, “Advances in Biomaterials for Drug Delivery,” *Advanced Materials*, vol. 30, no. 29, Jul. 2018, doi: 10.1002/adma.201705328.

[71] P. Trucillo, “Biomaterials for Drug Delivery and Human Applications,” *Materials*, vol. 17, no. 2, p. 456, Jan. 2024, doi: 10.3390/ma17020456.

[72] S. O. Adeosun, M. O. Ilomuanya, O. P. Gbenebor, M. O. Dada, and C. C. Odili, “Biomaterials for Drug Delivery: Sources, Classification, Synthesis, Processing, and Applications,” in *Advanced Functional Materials*, IntechOpen, 2020. doi: 10.5772/intechopen.93368.

[73] A. Hardenia, N. Maheshwari, S. S. Hardenia, S. K. Dwivedi, R. Maheshwari, and R. K. Tekade, “Scientific Rationale for Designing Controlled Drug Delivery Systems,” in *Basic Fundamentals of Drug Delivery*, Elsevier, 2019, pp. 1–28. doi: 10.1016/B978-0-12-817909-3.00001-7.

[74] Z. Zhang, P. Tsai, T. Ramezanli, and B. B. Michniak-Kohn, “Polymeric nanoparticles-based topical delivery systems for the treatment of dermatological diseases,” *WIREs Nanomedicine and Nanobiotechnology*, vol. 5, no. 3, pp. 205–218, May 2013, doi: 10.1002/wnan.1211.

[75] S. Wang, Sun, Zhu, Du, Liu, and W.-Y. Qian, “pH-sensitive strontium carbonate nanoparticles as new anticancer vehicles for controlled etoposide release,” *Int. J. Nanomedicine*, p. 5781, Nov. 2012, doi: 10.2147/IJN.S34773.

[76] M. Chamundeeswari, J. Jeslin, and M. L. Verma, “Nanocarriers for drug delivery applications,” *Environ. Chem. Lett.*, vol. 17, no. 2, pp. 849–865, Jun. 2019, doi: 10.1007/s10311-018-00841-1.

[77] T. G. Kim, G. S. An, J. S. Han, J. U. Hur, B. G. Park, and S.-C. Choi, “Synthesis of Size Controlled Spherical Silica Nanoparticles via Sol-Gel Process within Hydrophilic Solvent,” *Journal of the Korean Ceramic Society*, vol. 54, no. 1, pp. 49–54, Jan. 2017, doi: 10.4191/kcers.2017.54.1.10.

[78] V. Biju, “Chemical modifications and bioconjugate reactions of nanomaterials for sensing, imaging, drug delivery and therapy,” *Chem. Soc. Rev.*, vol. 43, no. 3, pp. 744–764, 2014, doi: 10.1039/C3CS60273G.

[79] A. Liberman, N. Mendez, W. C. Trogler, and A. C. Kummel, “Synthesis and surface functionalization of silica nanoparticles for nanomedicine,” *Surf. Sci. Rep.*, vol. 69, no. 2–3, pp. 132–158, Sep. 2014, doi: 10.1016/j.surfrep.2014.07.001.

[80] A. Shah, S. Aftab, J. Nisar, M. N. Ashiq, and F. J. Iftikhar, “Nanocarriers for targeted drug delivery,” *J. Drug Deliv. Sci. Technol.*, vol. 62, p. 102426, Apr. 2021, doi: 10.1016/j.jddst.2021.102426.

[81] Y. Alyassin *et al.*, “Application of mesoporous silica nanoparticles as drug delivery carriers for chemotherapeutic agents,” *Drug Discov. Today*, vol. 25, no. 8, pp. 1513–1520, Aug. 2020, doi: 10.1016/j.drudis.2020.06.006.

[82] M. Ghaferi, M. Koohi Moftakhari Esfahani, A. Raza, S. Al Harthi, H. Ebrahimi Shahmabadi, and S. E. Alavi, “Mesoporous silica nanoparticles: synthesis methods and their therapeutic use-recent advances,” *J. Drug Target.*, vol. 29, no. 2, pp. 131–154, Feb. 2021, doi: 10.1080/1061186X.2020.1812614.

[83] Z. Li, Y. Zhang, and N. Feng, “Mesoporous silica nanoparticles: synthesis, classification, drug loading, pharmacokinetics, biocompatibility, and application in drug delivery,” *Expert Opin. Drug Deliv.*, vol. 16, no. 3, pp. 219–237, Mar. 2019, doi: 10.1080/17425247.2019.1575806.

[84] C. Bharti, N. Gulati, U. Nagaich, and A. Pal, “Mesoporous silica nanoparticles in target drug delivery system: A review,” *Int. J. Pharm. Investig.*, vol. 5, no. 3, p. 124, 2015, doi: 10.4103/2230-973X.160844.

[85] S. Kwon, R. K. Singh, R. A. Perez, E. A. Abou Neel, H.-W. Kim, and W. Chrzanowski, “Silica-based mesoporous nanoparticles for controlled drug delivery,” *J. Tissue Eng.*, vol. 4, Jan. 2013, doi: 10.1177/2041731413503357.

[86] S.-H. Wu, C.-Y. Mou, and H.-P. Lin, “Synthesis of mesoporous silica nanoparticles,” *Chem. Soc. Rev.*, vol. 42, no. 9, p. 3862, 2013, doi: 10.1039/c3cs35405a.

[87] C. J. Brinker and G. W. Scherer, *Sol-Gel Science: The Physics and Chemistry of Sol-Gel Processing*. 1990.

[88] S. Kumar, M. M. Malik, and R. Purohit, "Synthesis Methods of Mesoporous Silica Materials," *Mater. Today Proc.*, vol. 4, no. 2, pp. 350–357, 2017, doi: 10.1016/j.matpr.2017.01.032.

[89] F. Hoffmann, M. Cornelius, J. Morell, and M. Fröba, "Silica-Based Mesoporous Organic–Inorganic Hybrid Materials," *Angew. Chem. Int. Ed.*, vol. 45, no. 20, pp. 3216–3251, May 2006, doi: 10.1002/anie.200503075.

[90] A. Mehmood, H. Ghafar, S. Yaqoob, U. F. Gohar, and B. Ahmad, "Mesoporous Silica Nanoparticles: A Review," *J. Dev. Drugs*, vol. 06, no. 02, 2017, doi: 10.4172/2329-6631.1000174.

[91] B. L. Newalkar, S. Komarneni, and H. Katsuki, "Rapid synthesis of mesoporous SBA-15 molecular sieve by a microwave–hydrothermal process," *Chemical Communications*, no. 23, pp. 2389–2390, 2000, doi: 10.1039/b0074411.

[92] B. E. Grabicka and M. Jaroniec, "Microwave-assisted synthesis of periodic mesoporous organosilicas with ethane and disulfide groups," *Microporous and Mesoporous Materials*, vol. 119, no. 1–3, pp. 144–149, Mar. 2009, doi: 10.1016/j.micromeso.2008.10.006.

[93] Y. Yao, M. Zhang, J. Shi, M. Gong, H. Zhang, and Y. Yang, "Encapsulation of fluorescein into MCM-41 mesoporous molecular sieve by a sol–gel method," *Mater. Lett.*, vol. 48, no. 1, pp. 44–48, Mar. 2001, doi: 10.1016/S0167-577X(00)00278-0.

[94] Y. Chen *et al.*, "Hollow/Rattle-Type Mesoporous Nanostructures by a Structural Difference-Based Selective Etching Strategy," *ACS Nano*, vol. 4, no. 1, pp. 529–539, Jan. 2010, doi: 10.1021/nn901398j.

[95] M. H. Lim and A. Stein, "Comparative Studies of Grafting and Direct Syntheses of Inorganic−Organic Hybrid Mesoporous Materials," *Chemistry of Materials*, vol. 11, no. 11, pp. 3285–3295, Nov. 1999, doi: 10.1021/cm990369r.

[96] T. T. Hoang Thi, V. Du Cao, T. N. Q. Nguyen, D. T. Hoang, V. C. Ngo, and D. H. Nguyen, "Functionalized mesoporous silica nanoparticles and biomedical applications," *Materials Science and Engineering: C*, vol. 99, pp. 631–656, Jun. 2019, doi: 10.1016/j.msec.2019.01.129.

[97] R. Bafkary *et al.*, "Amphiphilic hyperbranched polyester coated rod mesoporous silica nanoparticles for pH-responsive doxorubicin delivery," *DARU Journal of Pharmaceutical Sciences*, vol. 28, no. 1, pp. 171–180, Jun. 2020, doi: 10.1007/s40199-020-00328-x.

[98] Y. Yang *et al.*, "An Efficient Cell-Targeting Drug Delivery System Based on Aptamer-Modified Mesoporous Silica Nanoparticles," *Nanoscale Res. Lett.*, vol. 14, no. 1, p. 390, Dec. 2019, doi: 10.1186/s11671-019-3208-3.

[99] A. K. Yadav, P. Mishra, and G. P. Agrawal, “An insight on hyaluronic acid in drug targeting and drug delivery,” *J. Drug Target.*, vol. 16, no. 2, pp. 91–107, Jan. 2008, doi: 10.1080/10611860701794296.

[100] Y.-J. Jin, T. Ubonvan, and D.-D. Kim, “Hyaluronic Acid in Drug Delivery Systems,” *J. Pharm. Investig.*, vol. 40, no. spc, pp. 33–43, May 2010, doi: 10.4333/KPS.2010.40.S.033.

[101] H. Knopf-Marques *et al.*, “Hyaluronic Acid and Its Derivatives in Coating and Delivery Systems: Applications in Tissue Engineering, Regenerative Medicine and Immunomodulation,” *Adv. Healthc. Mater.*, vol. 5, no. 22, pp. 2841–2855, Nov. 2016, doi: 10.1002/adhm.201600316.

[102] G. Huang and H. Huang, “Application of hyaluronic acid as carriers in drug delivery,” *Drug Deliv.*, vol. 25, no. 1, pp. 766–772, Jan. 2018, doi: 10.1080/10717544.2018.1450910.

[103] I. S. Bayer, “Hyaluronic Acid and Controlled Release: A Review,” *Molecules*, vol. 25, no. 11, p. 2649, Jun. 2020, doi: 10.3390/molecules25112649.

[104] S. Naz *et al.*, “Enzyme-responsive mesoporous silica nanoparticles for tumor cells and mitochondria multistage-targeted drug delivery,” *Int. J. Nanomedicine*, vol. Volume 14, pp. 2533–2542, Apr. 2019, doi: 10.2147/IJN.S202210.

[105] R. D. Price, M. G. Berry, and H. A. Navsaria, “Hyaluronic acid: the scientific and clinical evidence,” *Journal of Plastic, Reconstructive & Aesthetic Surgery*, vol. 60, no. 10, pp. 1110–1119, Oct. 2007, doi: 10.1016/j.bjps.2007.03.005.

[106] M. Rama and U. Vijayalakshmi, “Drug delivery system in bone biology: an evolving platform for bone regeneration and bone infection management,” *Polymer Bulletin*, vol. 80, no. 7, pp. 7341–7388, Jul. 2023, doi: 10.1007/s00289-022-04442-5.

[107] M. Singh, A. S. Gill, P. K. Deol, A. Agrawal, and S. S. Sidhu, “Drug eluting titanium implants for localised drug delivery,” *J. Mater. Res.*, vol. 37, no. 16, pp. 2491–2511, Aug. 2022, doi: 10.1557/s43578-022-00609-y.

[108] M. Kumar, R. Kumar, and S. Kumar, “Coatings on orthopedic implants to overcome present problems and challenges: A focused review,” *Mater. Today Proc.*, vol. 45, pp. 5269–5276, 2021, doi: 10.1016/j.matpr.2021.01.831.

[109] S. Bagherifard, “Mediating bone regeneration by means of drug eluting implants: From passive to smart strategies,” *Materials Science and Engineering: C*, vol. 71, pp. 1241–1252, Feb. 2017, doi: 10.1016/j.msec.2016.11.011.

[110] B. Fotovvati, N. Namdari, and A. Dehghanghadikolaei, “On Coating Techniques for Surface Protection: A Review,” *Journal of Manufacturing and Materials Processing*, vol. 3, no. 1, p. 28, Mar. 2019, doi: 10.3390/jmmp3010028.

[111] D. M. Mattox, “Physical vapor deposition (PVD) processes,” *Metal Finishing*, vol. 97, no. 1, pp. 417–430, Jan. 1999, doi: 10.1016/S0026-0576(99)80043-9.

[112] S. M. Rossnagel, “Thin film deposition with physical vapor deposition and related technologies,” *Journal of Vacuum Science & Technology A: Vacuum, Surfaces, and Films*, vol. 21, no. 5, pp. S74–S87, Sep. 2003, doi: 10.1116/1.1600450.

[113] J. de Damborenea, C. Navas, J. A. García, M. A. Arenas, and A. Conde, “Corrosion–erosion of TiN-PVD coatings in collagen and cellulose meat casing,” *Surf. Coat. Technol.*, vol. 201, no. 12, pp. 5751–5757, Mar. 2007, doi: 10.1016/j.surfcoat.2006.10.009.

[114] L. Geyao, D. Yang, C. Wanglin, and W. Chengyong, “Development and application of physical vapor deposited coatings for medical devices: A review,” *Procedia CIRP*, vol. 89, pp. 250–262, 2020, doi: 10.1016/j.procir.2020.05.149.

[115] J.-O. Carlsson and P. M. Martin, “Chemical Vapor Deposition,” in *Handbook of Deposition Technologies for Films and Coatings*, Elsevier, 2010, pp. 314–363. doi: 10.1016/B978-0-8155-2031-3.00007-7.

[116] J. R. Creighton and P. Ho, “Introduction to Chemical Vapor Deposition (CVD),” 2001. [Online]. Available: www.asminternational.org

[117] T. Saba, K. S. K. Saad, and A. Bin Rashid, “Precise surface engineering: Leveraging chemical vapor deposition for enhanced biocompatibility and durability in biomedical implants,” *Heliyon*, vol. 10, no. 18, p. e37976, Sep. 2024, doi: 10.1016/j.heliyon.2024.e37976.

[118] H. Herman and S. Sampath, “Thermal spray coatings,” in *Metallurgical and Ceramic Protective Coatings*, Dordrecht: Springer Netherlands, 1996, pp. 261–289. doi: 10.1007/978-94-009-1501-5_10.

[119] N. Ce and S. Paul, “Thermally Sprayed Aluminum Coatings for the Protection of Subsea Risers and Pipelines Carrying Hot Fluids,” *Coatings*, vol. 6, no. 4, p. 58, Nov. 2016, doi: 10.3390/coatings6040058.

[120] C.-J. Li, X.-T. Luo, X.-Y. Dong, L. Zhang, and C.-X. Li, “Recent Research Advances in Plasma Spraying of Bulk-Like Dense Metal Coatings with Metallurgically Bonded Lamellae,” *Journal of Thermal Spray Technology*, vol. 31, no. 1–2, pp. 5–27, Jan. 2022, doi: 10.1007/s11666-022-01327-x.

[121] J. S. Kumar, R. Kumar, and R. Verma, “Surface Modification Aspects for Improving Biomedical Properties in Implants: A Review,” *Acta Metallurgica Sinica (English Letters)*, vol. 37, no. 2, pp. 213–241, Feb. 2024, doi: 10.1007/s40195-023-01631-7.

[122] L. Sun, “Thermal Spray Coatings on Orthopedic Devices: When and How the FDA Reviews Your Coatings,” *Journal of Thermal Spray Technology*, vol. 27, no. 8, pp. 1280–1290, Dec. 2018, doi: 10.1007/s11666-018-0759-2.

[123] Y. S. Ubhale and A. P. More, “Antimicrobial sol–gel coating: a review,” *J. Coat. Technol. Res.*, vol. 22, no. 2, pp. 527–548, Mar. 2025, doi: 10.1007/s11998-024-01014-2.

[124] C. J. Brinker, G. C. Frye, A. J. Hurd, and C. S. Ashley, “Fundamentals of sol-gel dip coating,” *Thin Solid Films*, vol. 201, no. 1, pp. 97–108, Jun. 1991, doi: 10.1016/0040-6090(91)90158-T.

[125] S. Amiri and A. Rahimi, “Hybrid nanocomposite coating by sol–gel method: a review,” *Iranian Polymer Journal*, vol. 25, no. 6, pp. 559–577, Jun. 2016, doi: 10.1007/s13726-016-0440-x.

[126] A. Dehghanghadikolaei, J. Ansary, and R. Ghoreishi, “Sol-gel process applications: A mini-review,” *Proceedings of the Nature Research Society*, vol. 2, p. 02008, 2018, doi: 10.11605/j.pnrs.201802008.

[127] F. Nasirpouri, *Electrodeposition of Nanostructured Materials*, vol. 62. Cham: Springer International Publishing, 2017. doi: 10.1007/978-3-319-44920-3.

[128] A. Lelevic and F. C. Walsh, “Electrodeposition of Ni P alloy coatings: A review,” *Surf. Coat. Technol.*, vol. 369, pp. 198–220, Jul. 2019, doi: 10.1016/j.surfcoat.2019.03.055.

[129] A. K. Shukla, “Comparative Study of Electrodeposition Processes for Polymer Composites for Technological Applications-An Overview,” 2021, [Online]. Available: www.ijsrst.com

[130] J. Yi, M. Li, J. Zhu, Z. Wang, and X. Li, “Recent development and applications of electrodeposition biocoatings on medical titanium for bone repair,” *J. Mater. Chem. B*, vol. 12, no. 39, pp. 9863–9893, 2024, doi: 10.1039/D4TB01081G.

[131] T. Galvin, N. C. Hyatt, W. M. Rainforth, I. M. Reaney, and D. Shepherd, “Laser sintering of electrophoretically deposited (EPD) Ti3SiC2 MAX phase coatings on titanium,” *Surf. Coat. Technol.*, vol. 366, pp. 199–203, May 2019, doi: 10.1016/j.surfcoat.2019.03.031.

[132] O. O. Van der Biest and L. J. Vandeperre, “ELECTROPHORETIC DEPOSITION OF MATERIALS,” *Annual Review of Materials Science*, vol. 29, no. 1, pp. 327–352, Aug. 1999, doi: 10.1146/annurev.matsci.29.1.327.

[133] T. Jiang *et al.*, “Surface Functionalization of Titanium with Chitosan/Gelatin via Electrophoretic Deposition: Characterization and Cell Behavior,” *Biomacromolecules*, vol. 11, no. 5, pp. 1254–1260, May 2010, doi: 10.1021/bm100050d.

[134] A. R. Boccaccini, S. Keim, R. Ma, Y. Li, and I. Zhitomirsky, “Electrophoretic deposition of biomaterials,” *J. R. Soc. Interface*, vol. 7, no. suppl_5, Oct. 2010, doi: 10.1098/rsif.2010.0156.focus.

[135] L. Besra and M. Liu, “A review on fundamentals and applications of electrophoretic deposition (EPD),” *Prog. Mater. Sci.*, vol. 52, no. 1, pp. 1–61, Jan. 2007, doi: 10.1016/j.pmatsci.2006.07.001.

[136] P. Amrollahi, J. S. Krasinski, R. Vaidyanathan, L. Tayebi, and D. Vashaee, “Electrophoretic Deposition (EPD): Fundamentals and Applications from Nano- to Micro-Scale Structures,” in *Handbook of Nanoelectrochemistry*, Cham: Springer International Publishing, 2015, pp. 1–27. doi: 10.1007/978-3-319-15207-3_7-1.

[137] D. Hanaor, M. Michelazzi, C. Leonelli, and C. C. Sorrell, “The effects of carboxylic acids on the aqueous dispersion and electrophoretic deposition of ZrO2,” *J. Eur. Ceram. Soc.*, vol. 32, no. 1, pp. 235–244, Jan. 2012, doi: 10.1016/j.jeurceramsoc.2011.08.015.

[138] A. A. Abdeltawab, M. A. Shoeib, and S. G. Mohamed, “Electrophoretic deposition of hydroxyapatite coatings on titanium from dimethylformamide suspensions,” *Surf. Coat. Technol.*, vol. 206, no. 1, pp. 43–50, Oct. 2011, doi: 10.1016/j.surfcoat.2011.06.034.

[139] M. Farrokhi-Rad and T. Shahrabi, “Effect of triethanolamine on the electrophoretic deposition of hydroxyapatite nanoparticles in isopropanol,” *Ceram. Int.*, vol. 39, no. 6, pp. 7007–7013, Aug. 2013, doi: 10.1016/j.ceramint.2013.02.038.

[140] D. Jugowiec *et al.*, “Influence of the electrophoretic deposition route on the microstructure and properties of nano-hydroxyapatite/chitosan coatings on the Ti-13Nb-13Zr alloy,” *Surf. Coat. Technol.*, vol. 324, pp. 64–79, Sep. 2017, doi: 10.1016/j.surfcoat.2017.05.056.

[141] T. Ishihara, K. Shimose, T. Kudo, H. Nishiguchi, T. Akbay, and Y. Takita, “Preparation of Yttria-Stabilized Zirconia Thin Films on Strontium-Doped $LaMnO_3$ Cathode Substrates via Electrophoretic Deposition for Solid Oxide Fuel Cells,” *Journal of the American Ceramic Society*, vol. 83, no. 8, pp. 1921–1927, Aug. 2000, doi: 10.1111/j.1151-2916.2000.tb01491.x.

[142] P. Rodrigues, S. J. Ali, J. K. Abbas, T. Alawsi, H. Liu, and P. Gong, “Electrophoretic Deposition of Hydroxyapatite Coating on TiNi Shape Memory Alloy,” *Powder Metallurgy and Metal Ceramics*, vol. 63, no. 3–4, pp. 207–216, Jul. 2024, doi: 10.1007/s11106-025-00452-w.

[143] R. Sikkema, K. Baker, and I. Zhitomirsky, “Electrophoretic deposition of polymers and proteins for biomedical applications,” *Adv. Colloid Interface Sci.*, vol. 284, p. 102272, Oct. 2020, doi: 10.1016/j.cis.2020.102272.

[144] R. Drevet, J. Fauré, and H. Benhayoune, “Electrophoretic Deposition of Bioactive Glass Coatings for Bone Implant Applications: A Review,” *Coatings*, vol. 14, no. 9, p. 1084, Aug. 2024, doi: 10.3390/coatings14091084.

[145] K. Malisz *et al.*, “Research of chitosan coatings deposited by electrophoretic deposition method at various voltage and time parameters,” *Mater. Chem. Phys.*, vol. 315, p. 128984, Mar. 2024, doi: 10.1016/j.matchemphys.2024.128984.

[146] B. Minhas *et al.*, “The electrochemical and in-vitro study on electrophoretic deposition of chitosan/gelatin/hydroxyapatite coating on 316L stainless

steel," *Carbohydrate Polymer Technologies and Applications*, vol. 5, p. 100322, Jun. 2023, doi: 10.1016/j.carpta.2023.100322.

[147] C. Chen, W. Sun, X. Wang, Y. Wang, and P. Wang, "pH-responsive nanoreservoirs based on hyaluronic acid end-capped mesoporous silica nanoparticles for targeted drug delivery," *Int. J. Biol. Macromol.*, vol. 111, pp. 1106–1115, May 2018, doi: 10.1016/j.ijbiomac.2018.01.093.

[148] Y. Erşan, "Alteration of titanium surfaces using hyaluronic acid coated mesoporous silica nanoparticles for local drug release," İstanbul, 2021.

[149] E. A. Demirci, S. Önder, T. Acar, S. Z. Sunar, and G. Torun Köse, "KR12 peptide-modified ECM coating for enhanced osteogenic and antimicrobial activity of titanium surfaces," *Biomaterials Advances*, vol. 179, p. 214515, Feb. 2026, doi: 10.1016/j.bioadv.2025.214515.

[150] A. Motamedifar, H. Ghafouri, and N. Alizadeh, "Hyaluronic acid-coated magnetic solid lipid nanoparticles for cancer-targeted delivery of gemcitabine and imaging agent," *Carbohydrate Polymer Technologies and Applications*, vol. 11, p. 100946, Sep. 2025, doi: 10.1016/j.carpta.2025.100946.

[151] S. Sakulwech, N. Lourith, U. Ruktanonchai, and M. Kanlayavattanakul, "Preparation and characterization of nanoparticles from quaternized cyclodextrin-grafted chitosan associated with hyaluronic acid for cosmetics," *Asian J. Pharm. Sci.*, vol. 13, no. 5, pp. 498–504, Sep. 2018, doi: 10.1016/j.ajps.2018.05.006.

[152] J.-E. Kim and Y.-J. Park, "Hyaluronan self-agglomerating nanoparticles for non-small cell lung cancer targeting," *Cancer Nanotechnol.*, vol. 13, no. 1, p. 9, Dec. 2022, doi: 10.1186/s12645-022-00115-0.

[153] E. Taha, S. A. Nour, M. S. Khattab, A. M. Yassin, N. A. AbdElkader, and M. M. El Taweel, "Accelerated wound healing efficacy of hyaluronic acid-coated silver nanoparticles loaded with vancomycin: preparation, in vitro characterization, optimization, and in vivo assessments," *Futur. J. Pharm. Sci.*, vol. 11, no. 1, p. 100, Jul. 2025, doi: 10.1186/s43094-025-00851-1.

[154] V. Loryuenyong, T. Muanghom, T. Apinyanukul, and P. Rutthongjan, "Synthesis of templated mesoporous silica nanoparticles under base catalysis," *Advances in Applied Ceramics*, vol. 110, no. 6, pp. 335–339, Aug. 2011, doi: 10.1179/1743676111Y.0000000024.

[155] P. Zhao *et al.*, "A study of chitosan hydrogel with embedded mesoporous silica nanoparticles loaded by ibuprofen as a dual stimuli-responsive drug release system for surface coating of titanium implants," *Colloids Surf. B Biointerfaces*, vol. 123, pp. 657–663, Nov. 2014, doi: 10.1016/j.colsurfb.2014.10.013.

[156] J. Ma, Z. Wang, Y. Shi, and Q. Li, "Synthesis and characterization of lysine-modified SBA-15 and its selective adsorption of scandium from a solution of rare earth elements," *RSC Adv.*, vol. 4, no. 78, pp. 41597–41604, 2014, doi: 10.1039/C4RA07571D.

[157] A. Uemura, S. Ogawa, Y. Isono, and R. Tanaka, “Elucidation of the time-dependent degradation process in insoluble hyaluronic acid formulations with a controlled degradation rate,” *J. Tissue Eng.*, vol. 10, Jan. 2019, doi: 10.1177/2041731419885032.

[158] Z. Fang *et al.*, “Hyaluronic acid-modified mesoporous silica-coated superparamagnetic Fe3O4 nanoparticles for targeted drug delivery,” *Int. J. Nanomedicine*, vol. Volume 14, pp. 5785–5797, Jul. 2019, doi: 10.2147/IJN.S213974.

[159] D. Kowalczuk, A. Gładysz, M. Pitucha, D. M. Kamiński, A. Barańska, and B. Drop, “Spectroscopic Study of the Molecular Structure of the New Hybrid with a Potential Two-Way Antibacterial Effect,” *Molecules*, vol. 26, no. 5, p. 1442, Mar. 2021, doi: 10.3390/molecules26051442.

[160] S. Pandey, P. Pandey, G. Tiwari, R. Tiwari, and A. Rai, “FTIR spectroscopy: A tool for quantitative analysis of ciprofloxacin in tablets,” *Indian J. Pharm. Sci.*, vol. 74, no. 1, p. 86, 2012, doi: 10.4103/0250-474X.102551.

[161] A. Almatroudi, “Advances in Mesoporous Silica and Hybrid Nanoparticles for Drug Delivery: Synthesis, Functionalization, and Biomedical Applications,” *Pharmaceutics*, vol. 17, no. 12, p. 1602, Dec. 2025, doi: 10.3390/pharmaceutics17121602.

[162] M. Colilla, B. González, and M. Vallet-Regí, “Mesoporous silicananoparticles for the design of smart delivery nanodevices,” *Biomater. Sci.*, vol. 1, no. 2, pp. 114–134, 2013, doi: 10.1039/C2BM00085G.

[163] K. B. Seljak, P. Kocbek, and M. Gašperlin, “Mesoporous silica nanoparticles as delivery carriers: An overview of drug loading techniques,” *J. Drug Deliv. Sci. Technol.*, vol. 59, p. 101906, Oct. 2020, doi: 10.1016/j.jddst.2020.101906.

[164] M. Vallet-Regí, M. Colilla, I. Izquierdo-Barba, and M. Manzano, “Mesoporous Silica Nanoparticles for Drug Delivery: Current Insights,” *Molecules*, vol. 23, no. 1, p. 47, Dec. 2017, doi: 10.3390/molecules23010047.

[165] I. Corni, M. P. Ryan, and A. R. Boccaccini, “Electrophoretic deposition: From traditional ceramics to nanotechnology,” *J. Eur. Ceram. Soc.*, vol. 28, no. 7, pp. 1353–1367, Jan. 2008, doi: 10.1016/j.jeurceramsoc.2007.12.011.

[166] A. H. Bin, V. Reddy, P. Kumar, J. Raj, and S. S. Babu, “Evaluation of wetting ability of five new saliva substitutes on heat-polymerized acrylic resin for retention of complete dentures in dry mouth patients: a comparative study,” *Pan African Medical Journal*, vol. 27, 2017, doi: 10.11604/pamj.2017.27.185.9098.

[167] C. Chen, N. Zhang, W. Li, and Y. Song, “Water Contact Angle Dependence with Hydroxyl Functional Groups on Silica Surfaces under CO_2 Sequestration Conditions,” *Environ. Sci. Technol.*, vol. 49, no. 24, pp. 14680–14687, Dec. 2015, doi: 10.1021/acs.est.5b03646.

[168] K. Palenčárová, R. Köszagová, and J. Nahálka, “Hyaluronic Acid and Its Synthases—Current Knowledge,” *Int. J. Mol. Sci.*, vol. 26, no. 15, p. 7028, Jul. 2025, doi: 10.3390/ijms26157028.

[169] A. Heydari Astaraee, S. Bagherifard, S. Monti, and M. Guagliano, “Evaluating the Homogeneity of Surface Features Induced by Impact-Based Surface Treatments,” *Materials*, vol. 14, no. 13, p. 3476, Jun. 2021, doi: 10.3390/ma14133476.

[170] V. Alar, A. Razumić, B. Runje, I. Stojanović, M. Kurtela, and B. Štrbac, “Application of Areal Topography Parameters in Surface Characterization,” *Applied Sciences*, vol. 15, no. 12, p. 6573, Jun. 2025, doi: 10.3390/app15126573.

[171] P. Pawlus, R. Reizer, and W. Zelasko, “Prediction of Parameters of Equivalent Sum Rough Surfaces,” *Materials*, vol. 13, no. 21, p. 4898, Oct. 2020, doi: 10.3390/ma13214898.

[172] J. Ma, M. Yang, F. Yu, and J. Zheng, “Water-enhanced Removal of Ciprofloxacin from Water by Porous Graphene Hydrogel,” *Sci. Rep.*, vol. 5, no. 1, p. 13578, Sep. 2015, doi: 10.1038/srep13578.

[173] F. C. D. A. Lima *et al.*, “Ciprofloxacin (Zwitterion, Chloride, and Sodium Forms): Experimental and DFT Characterization by Vibrational and Solid-State NMR Spectroscopies,” *ACS Omega*, vol. 10, no. 41, pp. 48773–48786, Oct. 2025, doi: 10.1021/acsomega.5c06384.

[174] H. Jiang, X. Shi, X. Yu, X. He, Y. An, and H. Lu, “Hyaluronidase Enzyme-responsive Targeted Nanoparticles for Effective Delivery of 5-Fluorouracil in Colon Cancer,” *Pharm. Res.*, vol. 35, no. 4, p. 73, Apr. 2018, doi: 10.1007/s11095-017-2302-4.

[175] J. Xiao, A. T. Hara, D. Kim, D. T. Zero, H. Koo, and G. Hwang, “Biofilm three-dimensional architecture influences in situ pH distribution pattern on the human enamel surface,” *Int. J. Oral Sci.*, vol. 9, no. 2, pp. 74–79, Jun. 2017, doi: 10.1038/ijos.2017.8.

[176] M. YAMADA, E. HASEGAWA, and M. KANAMORI, “Purification of Hyaluronidase from Human Placenta,” *The Journal of Biochemistry*, vol. 81, no. 2, pp. 485–494, Feb. 1977, doi: 10.1093/oxfordjournals.jbchem.a131482.

[177] H. Liaqat *et al.*, “pH-Sensitive Hydrogels Fabricated with Hyaluronic Acid as a Polymer for Site-Specific Delivery of Mesalamine,” *ACS Omega*, vol. 9, no. 26, pp. 28827–28840, Jul. 2024, doi: 10.1021/acsomega.4c03240.

[178] O. A. Saputra *et al.*, “Organically surface engineered mesoporous silica nanoparticles control the release of quercetin by pH stimuli,” *Sci. Rep.*, vol. 12, no. 1, p. 20661, Nov. 2022, doi: 10.1038/s41598-022-25095-4.

[179] S. T. Moerz and P. Huber, “pH-Dependent Selective Protein Adsorption into Mesoporous Silica,” *The Journal of Physical Chemistry C*, vol. 119, no. 48, pp. 27072–27079, Dec. 2015, doi: 10.1021/acs.jpcc.5b09606.

[180] N. Chik *et al.*, “Bacterial Adhesion on the Titanium and Stainless-Steel Surfaces Undergone Two Different Treatment Methods: Polishing and Ultrafast Laser Treatment,” *IOP Conf. Ser. Mater. Sci. Eng.*, vol. 358, p. 012034, May 2018, doi: 10.1088/1757-899X/358/1/012034.

[181] C. Du, C. Wang, T. Zhang, and L. Zheng, “Antibacterial Performance of Zr-BMG, Stainless Steel, and Titanium Alloy with Laser-Induced Periodic Surface Structures,” *ACS Appl. Bio Mater.*, vol. 5, no. 1, pp. 272–284, Jan. 2022, doi: 10.1021/acsabm.1c01075.

[182] R. R. Castillo and M. Vallet-Regí, “Recent Advances Toward the Use of Mesoporous Silica Nanoparticles for the Treatment of Bacterial Infections,” *Int. J. Nanomedicine*, vol. Volume 16, pp. 4409–4430, Jun. 2021, doi: 10.2147/IJN.S273064.

[183] M. Mu *et al.*, “Influence of Surface Roughness, Nanostructure, and Wetting on Bacterial Adhesion,” *Langmuir*, vol. 39, no. 15, pp. 5426–5439, Apr. 2023, doi: 10.1021/acs.langmuir.3c00091.

[184] C. L. Romanò, E. De Vecchi, M. Bortolin, I. Morelli, and L. Drago, “Hyaluronic Acid and Its Composites as a Local Antimicrobial/Antiadhesive Barrier,” *J. Bone Jt. Infect.*, vol. 2, no. 1, pp. 63–72, Jan. 2017, doi: 10.7150/jbji.17705.

[185] I. Silvestro *et al.*, “Hyaluronic Acid Reduces Bacterial Fouling and Promotes Fibroblasts’ Adhesion onto Chitosan 2D-Wound Dressings,” *Int. J. Mol. Sci.*, vol. 21, no. 6, p. 2070, Mar. 2020, doi: 10.3390/ijms21062070.

[186] Y. Yuan, M. P. Hays, P. R. Hardwidge, and J. Kim, “Surface characteristics influencing bacterial adhesion to polymeric substrates,” *RSC Adv.*, vol. 7, no. 23, pp. 14254–14261, 2017, doi: 10.1039/C7RA01571B.

[187] C. R. Arciola, D. Campoccia, G. D. Ehrlich, and L. Montanaro, “Biofilm-Based Implant Infections in Orthopaedics,” 2015, pp. 29–46. doi: 10.1007/978-3-319-11038-7_2.

[188] P. Speziale *et al.*, “Structural and functional role of Staphylococcus aureus surface components recognizing adhesive matrix molecules of the host,” *Future Microbiol.*, vol. 4, no. 10, pp. 1337–1352, Dec. 2009, doi: 10.2217/fmb.09.102.

[189] W. L. Hynes and S. L. Walton, “Hyaluronidases of Gram-positive bacteria,” *FEMS Microbiol. Lett.*, vol. 183, no. 2, pp. 201–207, Feb. 2000, doi: 10.1111/j.1574-6968.2000.tb08958.x.

[190] C. Tan *et al.*, “The inoculum effect and band-pass bacterial response to periodic antibiotic treatment,” *Mol. Syst. Biol.*, vol. 8, no. 1, Jan. 2012, doi: 10.1038/msb.2012.49.

[191] K. L. LaPlante and M. J. Rybak, “Impact of High-Inoculum Staphylococcus aureus on the Activities of Nafcillin, Vancomycin, Linezolid, and Daptomycin, Alone and in Combination with Gentamicin, in an In Vitro Pharmacodynamic Model,” *Antimicrob. Agents Chemother.*, vol. 48, no. 12, pp. 4665–4672, Dec. 2004, doi: 10.1128/AAC.48.12.4665-4672.2004.

[192] C. B. Ibberson *et al.*, “Staphylococcus aureus Hyaluronidase Is a CodY-Regulated Virulence Factor,” *Infect. Immun.*, vol. 82, no. 10, pp. 4253–4264, Oct. 2014, doi: 10.1128/IAI.01710-14.

[193] J.-Y. Jiang *et al.*, “A comprehensive review on microbial hyaluronan-degrading enzymes: from virulence factors to biotechnological tools,” *Bioresour. Bioprocess.*, vol. 11, no. 1, p. 114, Dec. 2024, doi: 10.1186/s40643-024-00832-x.

[194] A. Acharya, P. K. Behera, and U. Kleinekathöfer, “Molecular Mechanism of Ciprofloxacin Translocation Through the Major Diffusion Channels of the ESKAPE Pathogens Klebsiella pneumoniae and Enterobacter cloacae,” *J. Phys. Chem. B*, vol. 128, no. 35, pp. 8376–8387, Sep. 2024, doi: 10.1021/acs.jpcb.4c03327.

A
PREPARATION OF BUFFER SOLUTIONS

Phosphate Buffered Saline (0.01M) pH 7.4

0.2 g KCl

8 g NaCl

0.24 g KH_2PO_4

1.44 g Na_2HPO_4

were dissolved in 900 mL of distilled water, after which the solution volume was brought to 1 L and the pH was adjusted to 7.4.

MES Buffer (0.01M) pH 5.5

1.95 g MES acid hydrate

was dissolved in 900 mL of distilled water, after which the solution volume was brought to 1 L and the pH was adjusted to 5.5.

PUBLICATIONS FROM THE THESIS

Conference Papers

1. M. Yolum and S. Önder, “Biyomedikal uygulamalar için enzime duyarlı mezogözenekli silika nanopartikül taşıyıcı sistemlerin geliştirilmesi,” presented at the 29. Ulusal Biyomedikal Bilim ve Teknoloji Sempozyumu, Ankara, Türkiye, Nov. 21–23, 2025, p. 114.

Papers

1. M. Yolum and S. Önder, “Hyaluronidase-responsive MSN–HA coatings for infection-triggered antibiotic delivery on titanium surfaces,” manuscript under review.

Projects

1. Yıldız Technical University Scientific Research Projects Coordinatorship, Graduate Thesis Project no. FYL-2024-6341, “Lokal İlaç Salımında Kullanılabilecek Nanopartikül Esaslı Fonksiyonel Kaplama Geliştirilmesi ve Test Edilmesi”, 2024–2026.